

UC Santa Cruz

UC Santa Cruz Electronic Theses and Dissertations

Title

Mapping Kelp Forests Using Existing and Emerging Remote Sensing Techniques

Permalink

<https://escholarship.org/uc/item/3z3681hn>

Author

McPherson, Meredith L

Publication Date

2021

Peer reviewed|Thesis/dissertation

UNIVERSITY OF CALIFORNIA
SANTA CRUZ

**MAPPING KELP FORESTS USING EXISTING AND EMERGING REMOTE SENSING
TECHNIQUES**

A dissertation submitted in partial satisfaction
of the requirements for the degree of

DOCTOR OF PHILOSOPHY

in

OCEAN SCIENCES

by

Meredith L. McPherson

June 2021

The Dissertation of Meredith L.
McPherson is approved by:

Professor Raphael M. Kudela, chair

Professor Mark H. Carr

John P. Ryan, Ph.D.

Laura Rogers-Bennett, Ph.D.

Quentin Williams
Acting Vice Provost and Dean of Graduate Studies

Copyright © by
Meredith L. McPherson
2021

TABLE OF CONTENTS

LIST OF FIGURES	V
LIST OF TABLES	X
ABSTRACT	XII
DEDICATION	XIII
ACKNOWLEDGMENTS	XIV
INTRODUCTION	1
REFERENCES	4
1. LARGE-SCALE SHIFT IN THE STRUCTURE OF A KELP FOREST ECOSYSTEM CO-OCCURS WITH AN EPIZOOTIC AND MARINE HEATWAVE	
1.1 ABSTRACT.	7
1.2 INTRODUCTION.	8
1.3 RESULTS.	11
1.4 DISCUSSION.	18
1.5 METHODS.	24
1.6 REFERENCES.	29
1.7 SUPPLEMENTAL MATERIAL.	36
1.8 SUPPLEMENTAL REFERENCES.	46
2. KELP PATCH-SPECIFIC CHARACTERISTICS LIMIT DETECTION CAPABILITY OF RAPID SURVEY METHOD FOR DETERMINING CANOPY BIOMASS USING REMOTE SENSING TECHNIQUES	
2.1 ABSTRACT.	48
2.2 INTRODUCTION.	49
2.3 METHODS.	54
2.4 RESULTS.	68
2.5 DISCUSSION.	72
2.6 REFERENCES.	81
2.7 SUPPLEMENTAL MATERIAL.	86
3. UTILIZING A MULTIYEAR DATASET OF UNOCCUPIED AIRCRAFT SYSTEM IMAGERY TO VALIDATE LANDSAT DERIVED GIANT KELP CANOPY	
3.1 ABSTRACT.	92
3.2 INTRODUCTION.	93
3.3 METHODS.	98
3.4 RESULTS.	105

3.5 DISCUSSION.....	113
3.6 CONCLUSIONS.....	118
3.7 REFERENCES.....	121
3.8 SUPPLEMENTAL MATERIAL.....	129
CONCLUSION	132
REFERENCES.....	137

LIST OF FIGURES

FIGURE 1.1 - *Spatial and temporal variability of bull kelp canopy area in northern California from 1985 – 2019. (a) Sonoma and Mendocino county region of study and SST domain (Esri World Imagery – Esri, CGIAR, USGS HERE, Garmin, FAO, METI/NASA, EPA, Earthstar Geographics) and inset with a global map indicating the northern California region with a red star, (b) annual timeseries heatmap of kelp canopy summed within 90 m latitudinal bins. 13*

FIGURE 1.2 - *SST distribution and kelp canopy area in northern California during prominent El Niño and MHW events from 1985 - 2019. Kernel density functions for SST anomalies during (a) the 1997/1998 El Niño, (b) the 2014-2015 NE Pacific MHW event (i.e., ‘blob’ and El Niño), and (c) relatively normal conditions before and after the MHW event (2012/2013 and 2018/2019, respectively). Shaded grey areas (a – c) represent ± 1 SD from the long term mean SST index. Solid black lines (a - c) represent the physiological threshold for bull kelp at 17°C ($\sigma_{1985-2019} = 3.5$) and the NO₃ deplete (NO₃ = 0) threshold ($\sigma_{1985-2019} = 0.48$). (d) Kelp canopy coverage through time with relevant oceanographic and biological events overlaid onto the timeseries as follows: a shaded yellow bar during the 1997/1998 El Niño; a shaded red bar during the 2014/2015 ‘blob’; a shaded orange bar during the overlapping ‘blob’ and 2015/2016 El Niño; a shaded yellow bar during the 2015/2016 El Niño; and a dashed grey line in which SSWD in sunflower stars was first observed in 2013. Annual error estimates (black error bars) for kelp canopy area were determined using the normalized root mean square error (NRMSE) between CDFW aerial flyover surveys and USGS Landsat imagery. 14*

FIGURE 1.3 - *Results of Partial Least Squares Regression analysis for environmental and biological drivers of kelp canopy area from 1985 – 2019. Component 1 partial least squares regression (PLSR) x weights (top row) from environmental indices across 1985 to 2016 (a) and both environmental and biological indices from 2003 to 2016 (b). PLSR models and forecasts using all components overlaid on satellite derived kelp canopy (c,d). See supplementary data for detailed PLSR results (Table SI.1). Predictor variable acronyms are as follows: purple urchin density - ‘Purple Urchin’; seasonal nitrate concentrations - ‘Summer NO₃’ and ‘Spring NO₃’; marine heatwave days - ‘MHW Days’; seasonal sea surface temperature – ‘Summer SST’ and ‘Spring SST’; mean significant wave height – ‘Mean H_s’; Pacific Decadal Oscillation – ‘PDO’; North Pacific Gyre Oscillation – ‘NPGO’; Multivariate El Niño/Southern Oscillation Index – ‘MEI’. See Methods for detailed description of how each environmental variable influence kelp canopy dynamics. 15*

FIGURE 1.4 - *Temporal trends of important environmental and biological drivers of ecosystem change in northern California kelp forests. Standardized indices of (a) bull kelp canopy coverage, MHW days, purple urchin density, and sunflower star density where data is available. Standardized indices overlaid with Ordinary Least Square*

Regression (OLSR) fits (except in 4c 2003 – 2013 where a 2nd degree polynomial LSR is applied) prior to and after the NE Pacific MHW for (b) bull kelp canopy coverage and nitrate concentration, (c) sunflower star density, (d) MHW days, and (e) purple urchin density. See supplementary data for detailed LSR results and error statistics (Figure S1.2 and Table 1.2). 17

FIGURE S1.1 - PLSR models and forecasts using physical drivers (a) and physical and biological drivers (b) overlaid on satellite derived kelp canopy. Forecasted scenarios use environmental variables (MEI, NPGO, PDO, Mean Hs, seasonal SST (spring and summer), MHW days, and seasonal NO₃ (spring and summer) conditions at the climatological mean for 2017 to 2019. For all other years (1985 - 2016 and 2003 - 2016), these variables are the environmentally derived indices. 37

FIGURE S1.2 – Least squares regression (LSR) fits for standardized indices of environmental ((a) bull kelp, (b) spring nitrate, and (d) MHW days) and biological ((c) sunflower star and (e) purple urchin) preceding the NE Pacific MHW and following the NE Pacific MHW. Date ranges depended on data availability for each variable. An ordinary LSR (OLSR) was applied to all variables except the sunflower star’s preceding NE Pacific MHW date range (panel c; 2003 – 2013) where a second degree polynomial LSR was applied. For variable-wise regression statistics see S4. Shading around the regression lines represents the 95% confidence intervals. 38

FIGURE S1.3 - Box and whisker plot for all predictor (environmental and biological) and response (kelp canopy) variables. Variable-wise outliers are defined as datapoints outside 1.5 times the interquartile range (1.5*IQR; black points). Total sample number across the entire variable timeseries is represented by n_i. Sampling frequency (annual, monthly, daily, or hourly) is depicted by the grey boxes near the x-axis. 42

FIGURE S1.4 - Temporal (a) and spatial (b and c) representation of sub-tidal sampling efforts in Sonoma and Mendocino Counties in the northern California, USA region between 2003 and 2018 by California Department of Fish and Wildlife (CDFW) and Reef Check California. 43

FIGURE S1.5 - Correlation matrix of all environmental and biological variables used in the partial least squares regression (PLSR) analysis. The upper panel corner shows the scatter plots Pearson correlation coefficients (r) for each pair-wise relationship. The lower corner shows the kernel density distribution for each pair-wise relationship. The diagonal shows the data distribution for each variable. Strong co-linearity exists between seasonal sea surface temperature (SST) and nitrate (NO₃) conditions. 44

FIGURE S1.6 - Partial least squares regression (PLSR) component- and variable-wise cross-validation results presented as the mean squared error (MSE) for (a) environmental indices (1985 – 2016) and (b) environmental and purple urchins (all indices; 2003 – 2016). 45

FIGURE 2.1 - a) A map of the California coastline illustrating specific areas where survey sites were located in Mendocino County (magenta box) and Monterey County (green box). Each smaller map, outlined with the color corresponding to Mendocino or Monterey, depicts the stitched mosaic of each UAV image (red points), the outline of the kelp bed within that mosaic (white polygon), and the 3600 m² dive site (white square) for each site: b) Noyo Harbor, c) Portuguese Beach, d) Point Pinos, e) Otter Cove, f) Hopkins Marine Station, and g) San Carlos Beach. 57

FIGURE 2.2 - Raster images of MicaSense RedEdge-M scaled near-infrared reflectance (ρ_{NIR}) values for each dive survey site: a) Noyo Harbor (NH), b) Portuguese Beach (PB), c) Point Piños (PP), d) Otter Cove (OC), e) San Carlos Beach (SCB), f) Hopkins Marine Station (HMS). 59

FIGURE 2.3 - Relevant morphometric characteristics of *Nereocystis* and *Macrocystis* adult sporophytes (image credit: Niky Taylor; UCSC). 60

FIGURE 2.4 - The probability distribution of *Nereocystis* bulb diameter for a) Noyo Harbor, b) Portuguese Beach, c) Point Piños. d) Scatter plot of *Nereocystis* canopy biomass against bulb diameter fitted with linear regressions for Alaska (blue line), Mendocino (teal line), Monterey (green line), and all regions combined (black line). e) Scatter plot of *Macrocystis* canopy biomass against frond number fitted with linear regressions for all data from Santa Barbara, CA (blue line), summer data from Santa Barbara (blue dashed line), Monterey, CA (green line), and all regions combined (black line). Regression details listed in Table S2.1. Grey shaded areas represent regression 95% CI. 63

FIGURE 2.5 - Canopy biomass against matchups of MESMA kelp fraction for each site (down) and resolution (across; 0.1 m, 3 m, 5 m, 10 m) for a-d) Noyo Harbor; e-h) Portuguese Beach; i-j) Point Piños; m-p) Otter Cove; q-t) San Carlos Beach; u-x) Hopkins Marine Station with OLS regression (black lines) and 95% confidence intervals (grey shading). See Table 2.4 for regression statistics. Grey shaded areas represent regression 95% CI. 69

FIGURE 2.6 - Genera specific matchups of canopy biomass and MESMA kelp fraction for 30 m resolution data. The relationships include all possible pixel matchups across the three sites for each genus ($n = 12$ matchups per genera). Grey shaded areas represent regression 95% CI. 70

FIGURE 2.7 - Left column: Semi-variogram (spherical model fit) for each station. Right column: Site-specific transect canopy biomass (grey lines) with mean transect canopy biomass (black line) a,f) Noyo Harbor; b,g) Portuguese Beach; c,h) Point Pinos; d,i) Ocean Cove; e,j) San Carlos Beach; f,k) Hopkins Marine Station. 73

FIGURE S2.1 - *Images of morphometric measurements for Macrocyctis and Nereocystis. a) Diver removing whole Macrocyctis sporophyte in situ at the holdfast (Hopkins Marine Life Refuge). b) Macrocyctis sporophyte transport from water to a clean and dry location on land. c) Entire Macrocyctis sporophyte spread across tarp before dividing into 2 m sections. d) Field technicians measuring morphology of each 2 m section of a Macrocyctis sporophyte. E) Nereocystis canopy spread out on clean dock ready to be measured. F) Josie Iselin taking counting Nereocystis blades for morphometric measurement. Photo credit: a) Sara Hamilton (OSU), b-f): Meredith McPherson. 86*

FIGURE S2.2 - *First row: Noyo Harbor; Second row: Portuguese Beach; Third row: Point Pinos; Fourth row: Otter Cove; Fifth row: San Carlos Beach; Sixth row: Hopkins Marine Station. Across columns: 0.1 m, 3 m, 5 m, 10 m, 30 m pixel resolution. 87*

FIGURE S2.3 - *Histograms of pixel kelp fraction for each genera and resolution. Top row: Nereocystis; Bottom row: Macrocyctis. Across columns: 0.1 m, 3 m, 5 m, 10 m, 30 m pixel resolution. 88*

FIGURE 3.1 - *Regional map of the Santa Barbara Channel including the study sites Arroyo Quemado (A) and Mohawk Reef (B) overlaid with historical mean Landsat MESMA kelp fraction from 1984 – 2020. 101*

FIGURE 3.2 - *Example processing steps for comparing sUAS and Landsat imagery to kelp canopy fraction from imagery collected on May 10th, 2018 at Arroyo Quemado. The unmasked stitched sUAS color imagery (A) is masked for land and waves (B) and classified for kelp canopy (C) using a simple band ratio classification approach. The sUAS imagery is degraded to 30 m resolution (D) and compared to 30 m resolution Landsat MESMA kelp fraction (E). A matchup analysis was conducted at the site and pixel scales using the difference between sUAS and Landsat canopy fractions (F) and direct correlation (G). 102*

FIGURE 3.3 - *Differences between environmental conditions (tidal height, wave height, east current velocity, and north current velocity) between the sUAS and Landsat flight times for Arroyo Quemado (A) and Mohawk Reef (B) on all matchup dates through time. Wave height and current velocity difference are shown on the left y-axis. Tidal difference is shown on the right y-axis. The shaded grey area corresponds with the current magnitude case study shown in Figure 3.4 and the dotted black line to the only Arroyo Quemado sUAS flight within that date range (May 10, 2018). Lines connecting data points do not imply a continuous dataset. 106*

FIGURE 3.4 - *(A) Landsat MESMA kelp canopy for each ETM+ or OLI satellite overpass at Arroyo Quemado between January and July 2018 with the corresponding day/time east (E) and (N) current magnitude. The dotted black line represents the day of the only available sUAS and Landsat matchup for this time period (May 10, 2018). The black*

star indicates the sUAS kelp canopy area referenced on the right y-axis scale. (B) Stitched sUAS imagery from Arroyo Quemado on May 10, 2018. (C) Pixel-based difference in kelp canopy fraction between the sUAS and Landsat for the May 10, 2018 matchup. 107

FIGURE 3.5 - Seasonal and Landsat sensor specific kernel density distributions of pixel-based differences between sUAS and Landsat at Arroyo Quemado (A and C) and Mohawk Reef (B and D). 108

FIGURE 3.6 - (A) Predicted sUAS kelp fraction values based on the Reduced Major Axis (RMA) regressions plotted as a function of Landsat MESMA fraction for each matchup date (regression information shown in Table S3.1), regardless of the binary decision tree classification. Regression lines are color coded by the mean Landsat MESMA fraction and overlaid with the results of a general additive model (GAM) for all pixels across all dates/sites ($r^2 = 0.727$, $p < 2e-16$). The grey line represents the 1:1 line between sUAS and Landsat kelp fractions. (B) RMA regression slope values as a function of the mean Landsat MESMA fraction overlaid with a power model fit ($r^2 = 0.638$; RMSE: 1.281). The horizontal grey line represents a regression slope of 1. The vertical grey line indicates the power model's estimated mean Landsat MESMA fraction where RMA regression slope equals 1. 109

FIGURE 3.7 - Site sUAS kelp canopy area plotted as a function of Landsat kelp canopy area for (A) Arroyo Quemado and (B) Mohawk Reef including all pixels regardless of the binary decision tree classification (circles) and only including pixels that were pre-classified as kelp (triangles). Site kelp canopy area through time for (C) Arroyo Quemado and (D) Mohawk Reef for the sUAS (solid line), including all pixels regardless of the binary decision tree classification (dashed line), and only including pixels that were pre-classified as kelp (dotted line). Regression statistics shown in Table S3.2. 111

FIGURE 3.8 - sUAS color imagery (A, D, and G), Landsat MESMA fraction (B, E, and H), and sUAS kelp fraction as a function of Landsat MESMA fraction (C, F, and I) for three different case studies. Top row (A - C): October 6, 2017 Arroyo Quemado. Middle row (D - F): March 18, 2019 Mohawk Reef. Bottom row (G - I): June 16, 2017 Mohawk Reef. 113

FIGURE S3.1 - General additive model (GAM) best fit line for all pixels across all dates/sites ($r^2 = 0.727$, $p < 2e-16$). 131

LIST OF TABLES

TABLE S1.1 - <i>Component-wise PLSR results for each date range (Figure 1.3).</i>	36
TABLE S1.2 - <i>Least squares regression (LSR) fits for standardized indices of environmental (bull kelp, spring nitrate, MHW days) and biological (purple urchin and sunflower star) show in Fig. 1.4 and S3. Date ranges presented for each timeframe (preceding MHW, following MHW, full timeseries) depended on data availability for each variable. Preceding the NE Pacific MHW, the date ranges of 1985 to 2013 and 2003 to 2013 were used for environmental and biological variables, respectively. Following the NE Pacific MHW, date ranges were from 2014 to 2019 and 2014 to 2018 were used for environmental and biological variables, respectively. Full timeseries date ranges were 1985 to 2019 for environmental variables, and 2003 to 2018 for biological variables. Bolded and grey highlighted cells designate statistically significant relationships ($p < 0.05$). Ordinary LSR was used for all trends presented below with the exception of the preceding MHW sunflower star trend, where a second order polynomial LSR was applied (indicated with *).</i>	39
TABLE S1.3 - <i>Index data sources for all environmental (largescale and local-scale) and biological indices. Detailed descriptions of large and local-scale forcings and their influences on kelp dynamics are listed below the table.</i>	40
TABLE 2.1 - <i>Detailed description of each survey location including region (Mendocino County or Monterey Peninsula), kelp genera, dive site coordinates, dive survey date, UAV survey date, and mean tidal height during each UAV survey.</i>	55
TABLE 2.2 - <i>Detailed information of site-specific sporophyte collection including site name, region, kelp genera, latitude/longitude, and collection dates.</i>	61
TABLE 2.3 - <i>ANCOVA results for the effect of region (and seasons for <i>Macrocystis</i>) on the slope and intercepts of the relationship between the dependent variable (bulb diameter or frond count) and canopy biomass. * denotes significance.</i>	62
TABLE 2.4 - <i>ANCOVA results from regression slopes across all sites and resolutions presented in Figure 2.6 and Table S2.2. * denotes significance.</i>	68
TABLE 2.5 - <i>Estimates of the range (a), nugget (η), and sill (C) from semi-variogram analysis on ρ_{NIR} data shown in Figure 2.2. * represents statistical significance.</i>	71
TABLE S2.1 - <i>Spectral characteristics (center wavelengths and full-width at half-max (FWHM) values in nanometer) for each relevant satellite band (blue, green, red, red-edge, and NIR). Within each cell the top value is the band's center wavelength and the bottom value is the band's FWHM. n/a denotes where band information doesn't exist or isn't available.</i>	89

TABLE S2.2 - Results from pairwise Tukey's HSD post-hoc test for location specific *Nereocystis bulb* diameters. * denotes significance. 90

TABLE S2.3 - Regression statistics from Figure 2.6. * represent a significant relationship between MESMA kelp fraction and in situ canopy biomass based on a p-value less than 0.05. 91

TABLE 3.1 - Landsat overflight/sensor and sUAS flight times for each date and site. .100

TABLE S3.1 - RMA regression statistics corresponding to each matchup date across both sites in Figure 3.6. Standard deviations for RMA regression slopes and intercepts are included. 129

TABLE S3.2 - Logarithmic and RMA regression statistics corresponding to Figure 3.7 where sUAS kelp canopy area is plotted as a function of Landsat kelp canopy area for Arroyo Quemado (AQ) and Mohawk Reef (MO). 'All Landsat' indicates that all pixels (regardless of the binary decision tree classification) were included in the calculation of kelp canopy area. 'Classified Landsat' indicates that only pixels identified as kelp via the binary decision tree classification were included in the calculation of kelp canopy area. For AQ 'All Landsat' a logarithmic regression (shown on Figure 3.7) was used to optimize curve fitting. We have also included RMA regression statistics for that category below for comparison and reference to the 'Classified Landsat' RMA regression fits but are not displayed on Figure 3.7 in the main text. Standard deviations for logarithmic coefficients ('Coef') and RMA regression slopes and intercepts are included. 130

ABSTRACT

MAPPING KELP FORESTS USING EXISTING AND EMERGING REMOTE SENSING TECHNIQUES

MEREDITH L. MCPHERSON

Canopy forming kelp species (Order: *Laminariales*), the foundation of productive and species-rich ecosystems along rocky coastlines in temperate and Arctic regions, generate a diversity of provisioning, regulating, and supporting ecosystem services. In the northeast Pacific region, giant kelp (*Macrocystis pyrifera*) and bull kelp (*Nereocystis luetkeana*) are the dominant canopy forming kelps, which can be detected using remote sensing techniques. Historically, fixed-winged-aircraft-based aerial surveys and spaceborne satellites have been used to study canopy forming kelps via remote sensing, but increasingly unoccupied aircraft systems (UASs) are an emerging tool for kelp mapping. The following dissertation utilizes existing and emerging remote sensing techniques to advance the field of kelp remote sensing and provides insight into kelp monitoring and restoration; notably the implementation of ecosystem-based and adaptive management strategies using long-term *in situ* and remote sensing datasets.

To Arda and Olivia

ACKNOWLEDGEMENTS

The research presented in this dissertation would not have been possible without a large community of people who have supported and uplifted me during my time at UC Santa Cruz. I am grateful to my advisor, Raphe Kudela, who has always encouraged me to embrace my independence and follow my personal scientific, research, and outreach goals. My committee members, Mark Carr, Laura Rogers-Bennett, and John Ryan, who represent a variety of backgrounds and perspectives, have all provided enlightening scientific discussions and crucial support through challenging field work situations. I'd also like to acknowledge the support of Tom Bell, who has been a wonderful collaborator from the start of this journey.

Much of what is presented in Chapter 2 would not have been possible without a host of undergraduate student volunteers who committed their entire summer to schlepping kelp and instruments around Monterey and Mendocino, including scientific divers (Logan Grady, Jeannette Peters, and Sara Hamilton) and field volunteers (alphabetically: Dennis Finger, Aimee Foy, Megan Gallagher, Kyle Hughes, Kevin Hum, Josie Iselin, Quinn Letitia, John Mizell, Rich Muller, Brynn O'Hara, and Jezabel Powers). UC Santa Cruz vessel and scuba operation training/support was provided by Dave Benet and Steve Clabuesch. Special collaboration and data collection on the effects of UAVs on sensitive wildlife along the Monterey Peninsula would not have been possible without Karen Grimmer, Sophie De Beukelaer, Herrick Hanks, Teri Nicholson, Jennifer Parkin, Judi Romero, and Bill Standley. I am indebted to Brent Roman and Ben Erwin (Monterey Bay Aquarium Research Institution), Pat Iampietro

(California State University at Monterey Bay), and Andy Lyons and Sean Hogan (Informatics and GIS Statewide Program at UC Agriculture and Natural Resources) for supporting set-up, training, and operation of the UAV and multispectral camera. A very special thanks to Heidi Hirsh (Stanford University), who is just an amazing human being and has been the best teammate I could hope for.

I would like to extend a heartfelt thanks my Ocean Sciences cohort (Kira Mizell, Yang Xiang, Katie Harding, Maria Hamilton, and Bruch Laughlin) and lab mates (Niky Taylor, Henry Houskeeper, Regina Radan, Kendra Negrey, Charlie Martin, and Cori Gibble), who have become wonderful friends and colleagues through my time at UC Santa Cruz. Of course, friends beyond UC Santa Cruz and my family have been the foundation upon which I have relied so heavily. I could not have done it without any of them, but most notably my husband, Arda Akman. In addition to providing emotional support, encouragement, and endless hugs, Arda has a wonderful engineering and scientific mind that challenges me to be a better researcher. I might not be where I am today without his countless hours spent in the lab and field.

Finally, financial support was provided by the Dr. Earl H. Myers and Ethel M. Myers Oceanographic and Marine Biology Trust and the UCSC Department of Ocean Sciences. Vessel support and lodging was provided by Laura Rogers-Bennett's Marine Invertebrate Fisheries and Conservation Laboratory. Funding for the UAV was supported by the Ida Benson-Lynn Ocean Health endowment. Instrumentation and software were supported by the Packard Science and Technology endowment to the Institute of Marine Sciences.

The first chapter of this dissertation includes a reprinted version of previously published work:

McPherson ML, Finger DJI, Houskeeper HF, Bell TW, Carr MH, Rogers-Bennett L, Kudela RM. Large-scale shift in the structure of a kelp forest ecosystem co-occurs with an epizootic and marine heatwave. *Communications Biology*. **4**, 1–9. (2021)

Raphael M. Kudela, Mark H. Carr, and Laura Rogers-Bennett supervised this project and are listed as co-authors. Tom W. Bell, Henry F. Houskeeper, and Dennis J. I. Finger assisted with data science and are also listed as a co-author. The analysis and writing of this manuscript were substantively my own.

The second chapter of this dissertation contains a reprint of submitted work:

McPherson ML, Kudela RM. Kelp patch-specific characteristics limit detection capability of rapid survey method for determining canopy biomass using remote sensing techniques. Submitted to *Frontiers in Environmental Science*: April 2021

Raphael M. Kudela supervised this project and is listed as a co-author, but the analysis and writing of this paper were substantively my own.

INTRODUCTION

Canopy forming kelp species (Order: *Laminariales*) thrive along rocky coastlines in temperate and Arctic regions^{1,2} and are the foundation of productive and species-rich ecosystems that generate a diversity of provisioning, regulating, and supporting ecosystem services³. These services include three-dimensional habitat structure, biodiversity, nutrient cycling, coastline defense, recreational and commercial fisheries, and harvestable biomass⁴. Global rates of kelp forest loss have generally increased over the last 20 years (despite high regional variability) due to a combination of short and long-term anthropogenic influences², such as climate change^{5,6}, increasing frequency and intensity of marine heatwaves⁷⁻¹¹, and overfishing¹². As such, observing and understanding these systems (via both long-term monitoring and targeted studies) is vital to protecting, preserving, and restoring these coastal ecosystems.

In the northeast Pacific region (Aleutians Islands, Alaska to Baja California, Mexico) giant kelp (*Macrocystis pyrifera*) and bull kelp (*Nereocystis luetkeana*) are the dominant canopy forming kelps, which can be detected using remote sensing techniques. Historically, fixed-winged-aircraft-based aerial surveys^{13,14} and spaceborne satellites^{7,15-21} have been used to study canopy forming kelps via remote sensing. Increasingly unmanned aerial vehicles (UAVs) or small unoccupied aircraft systems (sUASs) are emerging as a cost-effective and flexible approach for kelp mapping applications. Together, these platforms provide a powerful suite of tools that have allowed scientists and managers to (1) gain a broader understanding of spatial variability in the environmental and biological processes driving kelp dynamics^{7,17,19},

(2) observe regional and genera-specific patterns of kelp canopy in response to large-scale discrete climatological events^{7,10}, and (3) develop targeted observation strategies for restoration²², aquaculture²³, localized ecosystem events²⁴, and high-frequency temporal observations²⁵.

The following dissertation utilized existing and emerging remote sensing techniques to advance the field of kelp remote sensing. Chapter 1 focuses on exploring northern California historical kelp dynamics and recent response to a large-scale, multi-year marine heatwave using a nearly 35-year timeseries developed from USGS Landsat imagery⁷. This analysis showed that that northern California kelp forests, while temporally dynamic, were historically resilient to fluctuating environmental conditions, even in the absence of key top sea urchin predators. A series of coupled environmental and biological shifts between 2014 and 2016 resulted in the formation of a persistent, altered ecosystem state with low kelp biomass and primary productivity. Chapter 2 investigated methodological approaches and challenges for determining canopy biomass via remote sensing by combining rapid *in situ* diver and UAV surveys. Via this approach, consistently determining canopy biomass from remote sensing at a variety of spatial resolutions was challenged by kelp patch-specific spatial characteristics. Chapter 3 utilized a multi-year dataset of near simultaneous matchups of UAV and Landsat imagery to validate and improve a long-term time-series of kelp canopy area and biomass. High-frequency environmental variability and kelp bed size/biomass were important for driving matchup performance and error, which may influence detection of sparse beds with low canopy expression. Overall, the findings of

this dissertation are applicable to monitoring and restoration strategies, with respect to implementing ecosystem-based management and adaptive management strategies using long-term *in situ* and remote sensing datasets.

References

1. Steneck, R. S. *et al.* Kelp forest ecosystems: biodiversity, stability, resilience and future. *Environ. Conserv.* **29**, 436–459 (2002).
2. Wernberg, T., Krumhansl, K., Filbee-dexter, K. & Pedersen, M. F. Status and Trends for the World's Kelp Forests. in *World Seas: An Environmental Evaluation* 57–78 (Elsevier Ltd., 2019). doi:10.1016/B978-0-12-805052-1.00003-6
3. Schiel, D. R. & Foster, M. S. *The Biology and Ecology of Giant Kelp Forests*. (2015).
4. Teagle, H., Hawkins, S. J., Moore, P. J. & Smale, D. A. The role of kelp species as biogenic habitat formers in coastal marine ecosystems. *J. Exp. Mar. Bio. Ecol.* **492**, 81–98 (2017).
5. Rasher, D. B. *et al.* Keystone predators govern the pathway and pace of climate impacts in a subarctic marine ecosystem. *Science (80-.)*. **369**, 1351–1355 (2020).
6. Wernberg, T. *et al.* Climate-driven regime shift of a temperate marine ecosystem. *Science (80-.)*. **353**, 169–172 (2016).
7. McPherson, M. L. *et al.* Large-scale shift in the structure of a kelp forest ecosystem co-occurs with an epizootic and marine heatwave. *Commun. Biol.* **4**, 1–9 (2021).
8. Oliver, E. C. J. *et al.* The unprecedented 2015/16 Tasman Sea marine heatwave. *Nat. Commun.* **8**, 1–12 (2017).
9. Dexter, K. F., Wernberg, T., Grace, S. P., Thormar, J. & Fredriksen, S. Marine heatwaves and the collapse of marginal North Atlantic kelp forests. *Sci. Rep.* 1–11 (2020). doi:10.1038/s41598-020-70273-x

10. Cavanaugh, K. C. *et al.* Spatial Variability in the Resistance and Resilience of Giant Kelp in Southern and Baja California to a Multiyear Heatwave. *Front. Mar. Sci.* **6**, 1–14 (2019).
11. Straub, S. C. *et al.* Resistance, Extinction, and Everything in Between – The Diverse Responses of Seaweeds to Marine Heatwaves. *Front. Mar. Sci.* **6**, 1–13 (2019).
12. Ling, S. D., Johnson, C. R., Frusher, S. D. & Ridgway, K. R. Overfishing reduces resilience of kelp beds to climate-driven catastrophic phase shift. *Proc. Natl. Acad. Sci.* **106**, (2009).
13. North, W. J., James, D. E. & Jones, L. G. History of kelp beds (*Macrocystis*) in Orange and San Diego Counties, California. *Dev. Hydrobiol.* **85**, 277–283 (1993).
14. Pfister, C. A., Berry, H. D. & Mumford, T. The dynamics of Kelp Forests in the Northeast Pacific Ocean and the relationship with environmental drivers. *J. Ecol.* 1–14 (2017). doi:10.1111/1365-2745.12908
15. Cavanaugh, K. C., Siegel, D. A., Kinlan, B. P. & Reed, D. C. Scaling giant kelp field measurements to regional scales using satellite observations. *Mar. Ecol. Prog. Ser.* **403**, 13–27 (2010).
16. Cavanaugh, K. C., Siegel, D. A., Reed, D. C. & Dennison, P. E. Environmental controls of giant-kelp biomass in the Santa Barbara Channel, California. *Mar. Ecol. Prog. Ser.* **429**, 1–17 (2011).
17. Hamilton, S. L., Bell, T. W., Watson, J. R., Grorun-Colvert, K. A. & Menge, B. A. Remote sensing: generation of long-term kelp bed data sets for evaluation of impacts of climatic variation. *Ecology* **0**, 1–13 (2020).
18. Bell, T. W., Allen, J. G., Cavanaugh, K. C. & Siegel, D. A. Three decades of variability in California’s giant kelp forests from the Landsat satellites. *Remote Sens. Environ.* **238**, (2020).

19. Bell, T. W., Cavanaugh, K. C., Reed, D. C. & Siegel, D. A. Geographical variability in the controls of giant kelp biomass dynamics. *J. Biogeogr.* **42**, 2010–2021 (2015).
20. Nijland, W., Reshitnyk, L. & Rubidge, E. Remote Sensing of Environment Satellite remote sensing of canopy-forming kelp on a complex coastline: A novel procedure using the Landsat image archive. *Remote Sens. Environ.* **220**, 41–50 (2019).
21. Schroeder, S. B., Boyer, L., Juanes, F. & Costa, M. Spatial and temporal persistence of nearshore kelp beds on the west coast of British Columbia, Canada using satellite remote sensing. *Remote Sens. Ecol. Conserv.* 1–17 (2019). doi:10.1002/rse2.142
22. Hohman, R., Hutto, S., Catton, C. A. & Koe, F. *Sonoma-Mendocino Bull Kelp Recovery Plan. Plan for the Greater Farallones National Marine Sanctuary and the California Department of Fish and Wildlife.* (2019).
23. Bell, T. *et al.* The Utility of Satellites and Autonomous Remote Sensing Platforms for Monitoring Offshore Aquaculture Farms: A Case Study for Canopy Forming Kelps. *Front. Mar. Sci.* (2020). doi:10.3389/fmars.2020.520223
24. Thomsen, M. S. *et al.* Local Extinction of Bull Kelp (*Durvillaea* spp.) Due to a Marine Heatwave. *Front. Mar. Sci.* **6**, 1–10 (2019).
25. Cavanaugh, K. C., Cavanaugh, K. C., Bell, T. W. & Hockridge, E. G. An Automated Method for Mapping Giant Kelp Canopy Dynamics from UAV. *Front. Environ. Sci.* **8:587354**, 1–16 (2021).

LARGE-SCALE SHIFT IN THE STRUCTURE OF A KELP FOREST ECOSYSTEM CO-OCCURS WITH AN EPIZOOTIC AND MARINE HEATWAVE

Meredith L. McPherson, Dennis J.I. Finger, Henry F. Houskeeper, Tom W. Bell,
Mark H. Carr, Laura Rogers-Bennett, and Raphael M. Kudela

Abstract

Climate change is responsible for increased frequency, intensity, and duration of extreme events, such as marine heatwaves (MHWs). Within eastern boundary current systems, MHWs have profound impacts on temperature-nutrient dynamics that drive primary productivity. Bull kelp (*Nereocystis luetkeana*) forests, a vital nearshore habitat, experienced unprecedented losses along 350 km of coastline in northern California beginning in 2014 and continuing through 2019. These losses have had devastating consequences to northern California communities, economies, and fisheries. Using a suite of *in situ* and satellite-derived data, we demonstrate that the abrupt ecosystem shift initiated by a multi-year MHW was preceded by declines in keystone predator population densities. We show strong evidence that northern California kelp forests, while temporally dynamic, were historically resilient to fluctuating environmental conditions, even in the absence of key top predators, but that a series of coupled environmental and biological shifts between 2014 and 2016 resulted in the formation of a persistent, altered ecosystem state with low primary productivity. Based on our findings, we recommend the implementation of ecosystem-based and adaptive management strategies, such as (1) monitoring the status of key ecosystem attributes: kelp distribution and abundance, and densities of sea urchins and their predators, (2) developing management responses to threshold levels of these attributes,

and (3) creating quantitative restoration suitability indices for informing kelp restoration efforts.

Introduction

Coastal marine ecosystem response to climate change in the 21st century is predicted to manifest in various ways, including through habitat contraction, species range shifts, and losses of biodiversity and functionality¹. These responses can manifest through both long-term gradual changes and more episodic events^{2,3}. However, it can be difficult to distinguish the impacts of gradual (e.g., increasing mean temperatures) and irregular (e.g., increasing storm frequency) climate-induced shifts from changes in underlying naturally stochastic events (e.g., El Niño Southern Oscillation (ENSO)). One such example is the ocean warming phenomenon of marine heatwaves (MHWs). Global oceanic and atmospheric drivers influence regional frequency, duration, and intensity of MHWs^{4,5}, all of which are increasing^{4,6}. In eastern boundary current ecosystems, such as the California Current, MHWs are highly correlated to changes in nutrient availability given the strong correlation between temperature and nutrients^{7,8} (e.g., anomalously high sea surface temperature (SST), low nitrate concentration [NO₃]). MHWs can have notable impacts on coastal ecosystems, such as seagrass beds⁹, coral reefs¹⁰ and kelp forests¹¹, and especially on the foundation species and ecosystem engineers (e.g., seagrasses, corals, kelps) that define these systems. Furthermore, the specific impacts of climate induced changes to these habitat forming sessile organisms via the coupled impacts of regional non-climate change human

influences and species thermal tolerance, greatly increases their vulnerability relative to mobile species¹².

Canopy forming kelp species (Order: *Laminariales*) thrive along temperate rocky coastlines, and are the foundation of productive and species-rich ecosystems that generate a diversity of provisioning, regulating, and supporting ecosystem services¹³. Despite high regional variation, global rates of kelp forest loss have generally increased over the last 20 years due to a combination of short and long-term anthropogenic influences¹⁴. Furthermore, the influences of ocean warming on kelp forest systems have been observed across nearly every ocean basin¹¹. Intense warming has occurred in localized coastal regions of Western Australia^{15,16}, the Tasman Sea Region¹⁷, New Zealand¹⁸, Baja California^{19,20}, Nova Scotia, Canada²¹, and northern California²². While the direct ecological implications of MHWs on kelp forests are not fully understood, MHWs can alter ecosystem structure and functioning via shifts in kelp community species composition^{15,23,24} leading to dramatic ecosystem shifts from healthy forest to algal turf reefs²⁵ or sea urchin barrens²⁶. These shifts between alternative stable states of these kelp forests often reflect cascading interactions across trophic levels through bottom-up (i.e. environmental influences on kelps) and top-down²⁷⁻²⁹ (i.e. changes in predator control of grazers) processes.

Along the coast of northern California (Figure 1.1a; Mendocino and Sonoma Counties), anomalously warm seawater temperatures persisted from 2014 to 2016 (Figure 1.2b) caused by an ocean warming event (termed ‘the blob’) associated with global climate change and a strong El Niño event³⁰ (collectively referred to as the NE

Pacific MHW). The year prior (2013), the onset of a sea star wasting syndrome (SSWS) epidemic caused dramatic population declines in multiple species of sea stars including the sunflower star, *Pycnopodia helianthoides*, along the entire northeast Pacific coastline (Figure 1.2d)^{22,31}. The sunflower star was the primary predator of sea urchins in northern California since the historic extirpation of sea otters (*Enhydra lutris*)³². Aligned with these events, forests of bull kelp, *Nereocystis luetkeana*, exhibited an unprecedented ecosystem shift from healthy forests to ‘urchin barrens’ devoid of macroalgae along more than 350 km of coastline²². Prior to this regime shift, the forested ecosystem likely persisted because the cool, nutrient-rich waters that fueled kelp production and food availability to urchins^{33,34} was balanced by top-down urchin predation by the sunflower star³⁵.

In contrast to giant kelp, which can live for many years and continuously produce new reproductive and vegetative fronds, bull kelp’s annual life history is limited to the production of a single stipe and its reproductive blades in its lifetime^{36,37}. As such, mechanisms for spore dispersal are limited to a narrow window between the maturity of the kelp and the onset of fall and winter storms, which usually dislodge adult bull kelp from the substrate (except in areas protected from wave energy). These factors lead to high spatial and temporal variability in the distribution and abundance of the surface canopy that can be observed through remote sensing techniques.

Satellite imagery provides a unique perspective on how surface canopy forming kelps respond to both acute climate manifestations and *in situ* biological trends leading to ecosystem phase shifts and can compensate for the scarcity of historical kelp data in

northern California. This dataset precedes the recent influence of the NE Pacific MHW allowing us to explore the contribution of environmental and biological factors on short and long-term trends of kelp canopy coverage. Using a 34-year time series of kelp canopy coverage derived from United States Geological Survey (USGS) Landsat imagery in combination with large-scale, local-scale, and biological drivers, we infer that historically declining predator densities might have laid the groundwork for the observed ecosystem phase shift in northern California initiated by a multi-year MHW. The persistent lack of kelp from 2014 to 2019 does not appear to be the result of unfavorable environmental conditions alone, but by a combination of unfavorable conditions for kelp productivity (related to warm SST and low nutrients) and conditions favorable for the persistence of urchin populations, including recruitment and low rates of mortality stemming from the absence of predators, disease, and starvation. Thus, while fluctuating environmental conditions occurred throughout the past three decades, the combination of abrupt changes in environmental and biological conditions likely hindered the ability of the ecosystem to recover as it had over the past three decades. This work provides context for monitoring biological trends and environmental response in surface canopy forming kelp forest ecosystems globally where satellite monitoring can be applied. These techniques are becoming increasingly important for designing adaptive management strategies to mitigate the impacts of long-term and abrupt environmental stressors.

Results

Northern California bull kelp displayed a dynamic inter-annual pattern of canopy coverage^{38,39} across the 34-year satellite-derived record prior to 2014 (Figure 1.1b). The onset of NE Pacific MHW and prior mass mortality of sunflower stars via SSWS coincided with dramatically reduced kelp canopy area in 2014 (Figure 1.2d and 1.4a). Mean sea surface temperature (SST) anomalies during the MHW event from 2014 to 2015 were approximately 2 standard deviations warmer, with extreme SST anomalies reaching 3 to 4 standard deviations above the long-term mean distribution (Figure 1.2b). Anomalously cool, nutrient-replete conditions ideal for bull kelp growth were observed in 2012 and 2013 (Figure 1.2c), but canopy area fell dramatically in 2014 and has remained suppressed through 2019 even though environmental conditions became more favorable to kelp (Figure 1.1b and 1.2d). The spatial range of bull kelp was also compressed across the last three decades (Figure 1.1b). Specifically, the meridional range of kelp narrowed with complete disappearance within the northern-most region of the study area (north of Fort Bragg) after 2008 and in the southern-most region after 2012. The northern and southern portions of the historical kelp canopy distribution within our study area are regions characterized by sandy sediment⁴⁰ (poor substrate for kelp spore settlement³⁶), resulting in sparser and patchier distribution than the rockier coastline between Fort Bragg and Jenner prior to the NE Pacific MHW. In addition to range reductions, the total loss of canopy area was spatially apparent beginning in 2014 when sparse, patchy conditions began dominating historically dense regions of the coastline (e.g. Point Arena; Figure 1.1b).

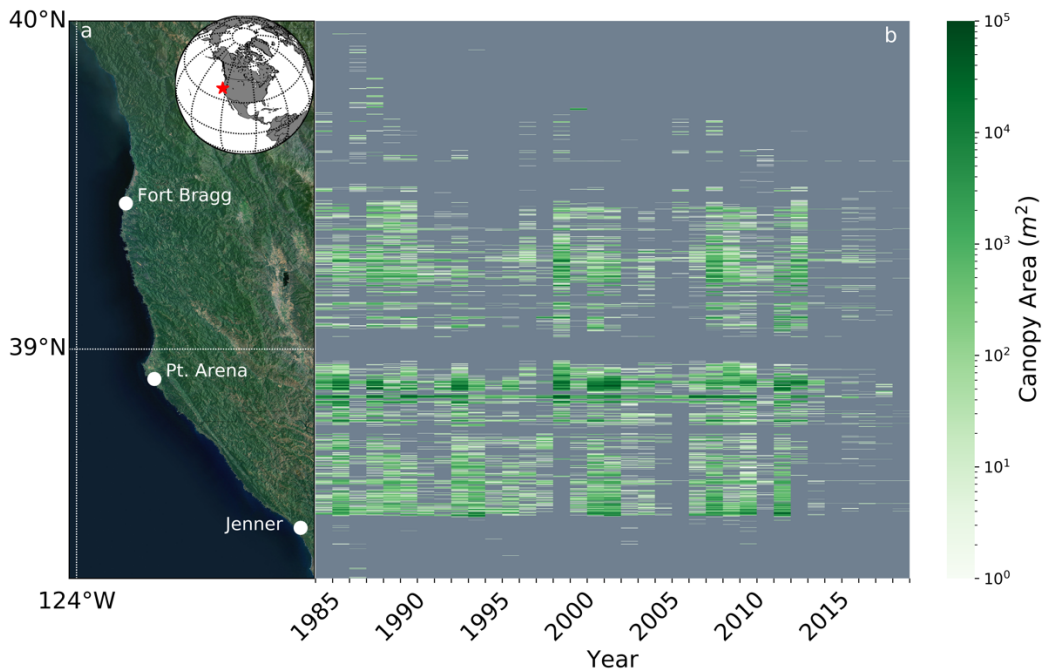


Figure 1.1. **Spatial and temporal variability of bull kelp canopy area in northern California from 1985 – 2019.** (a) Sonoma and Mendocino county region of study and SST domain (Esri World Imagery – Esri, CGIAR, USGS HERE, Garmin, FAO, METI/NASA, EPA, Earthstar Geographics) and inset with a global map indicating the northern California region with a red star, (b) annual timeseries heatmap of kelp canopy summed within 90 m latitudinal bins.

Esri. "World Imagery" [basemap]. Scale Not Given. "World Imagery Map". December 12, 2009. <https://www.arcgis.com/home/item.html?id=10df2279f9684e4a9f6a7f08febac2a9>. (Jan 26, 2021).

Spatial and temporal variability were clearly apparent in the satellite-derived northern California kelp record. Based on results from partial least squares regression (PLSR) analyses, patterns of change in these systems were generally described by co-varying mechanistic drivers of environmental and biological processes (Figure 1.3a and b; Table S1.1) including nitrate (NO_3) availability, SST (relevant to $[\text{NO}_3]$ and physiological temperature thresholds), large-scale ocean-atmospheric forcing (e.g., Multivariate El Niño Southern Oscillation Index (MEI), North Pacific Gyre Oscillation (NPGO), Pacific Decadal Oscillation (PDO)); all which drive local patterns of $[\text{NO}_3]$

and SST), the seasonal timing of swell (significant wave height (H_s), which influences spore dispersal), and grazer (purple sea urchin) abundances.

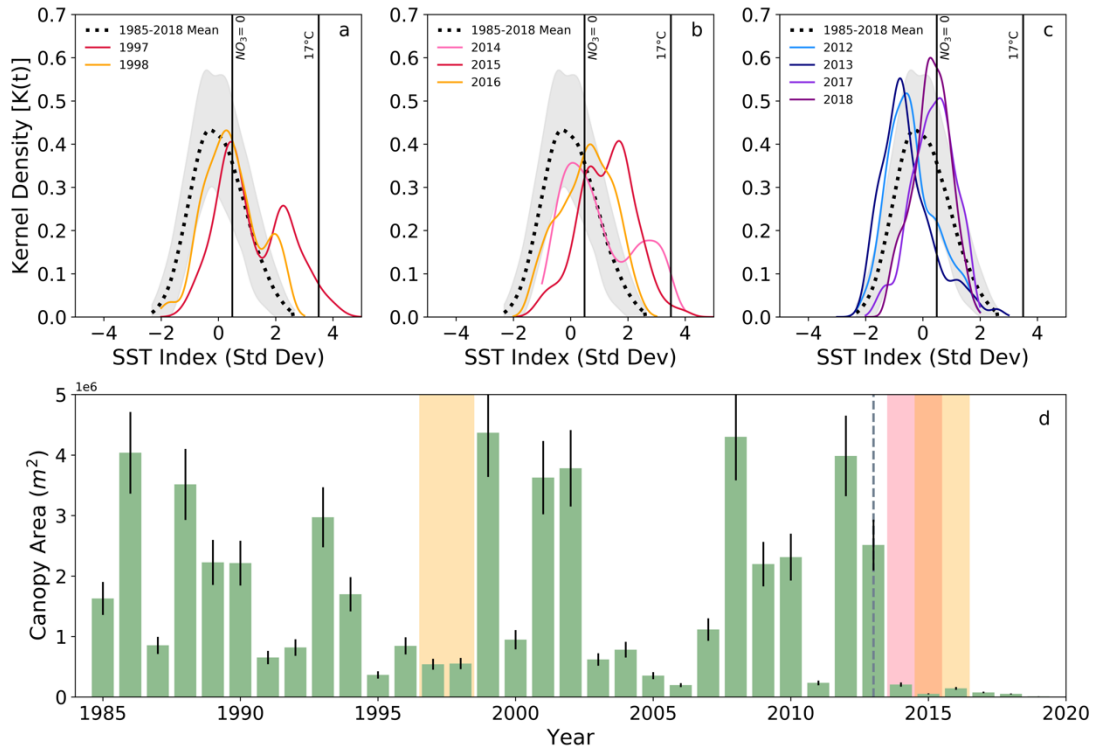


Figure 1.2. **SST distribution and kelp canopy area in northern California during prominent El Niño and MHW events from 1985 - 2019.** Kernel density functions for SST anomalies during (a) the 1997/1998 El Niño, (b) the 2014-2015 NE Pacific MHW event (i.e., ‘blob’ and El Niño), and (c) relatively normal conditions before and after the MHW event (2012/2013 and 2018/2019, respectively). Shaded grey areas (a – c) represent ± 1 SD from the long term mean SST index. Solid black lines (a - c) represent the physiological threshold for bull kelp at $17^\circ C$ ⁶⁶ ($\sigma_{1985-2019} = 3.5$) and the NO_3 deplete ($NO_3 = 0$) threshold ($\sigma_{1985-2019} = 0.48$). (d) Kelp canopy coverage through time with relevant oceanographic and biological events overlaid onto the timeseries as follows: a shaded yellow bar during the 1997/1998 El Niño; a shaded red bar during the 2014/2015 ‘blob’; a shaded orange bar during the overlapping ‘blob’ and 2015/2016 El Niño; a shaded yellow bar during the 2015/2016 El Niño; and a dashed grey line in which SSWD in sunflower stars was first observed in 2013. Annual error estimates (black error bars) for kelp canopy area were determined using the normalized root mean square error (NRMSE) between CDFW aerial flyover surveys and USGS Landsat imagery⁶⁷.

Our results revealed that including grazer dynamics in a predictive model more accurately represented sustained low kelp biomass after environmental perturbations from the NE Pacific MHW than the same predictive model with grazer abundance omitted. Environmental drivers correctly represented bull kelp response to low NO_3

and high SST conditions across the NE Pacific MHW regardless of whether the event was included in the temporal representation of the PLSR model (Figure 1.3c solid black line) and forecast (Figure 1.3c dashed black line) results. Forecasted model results using

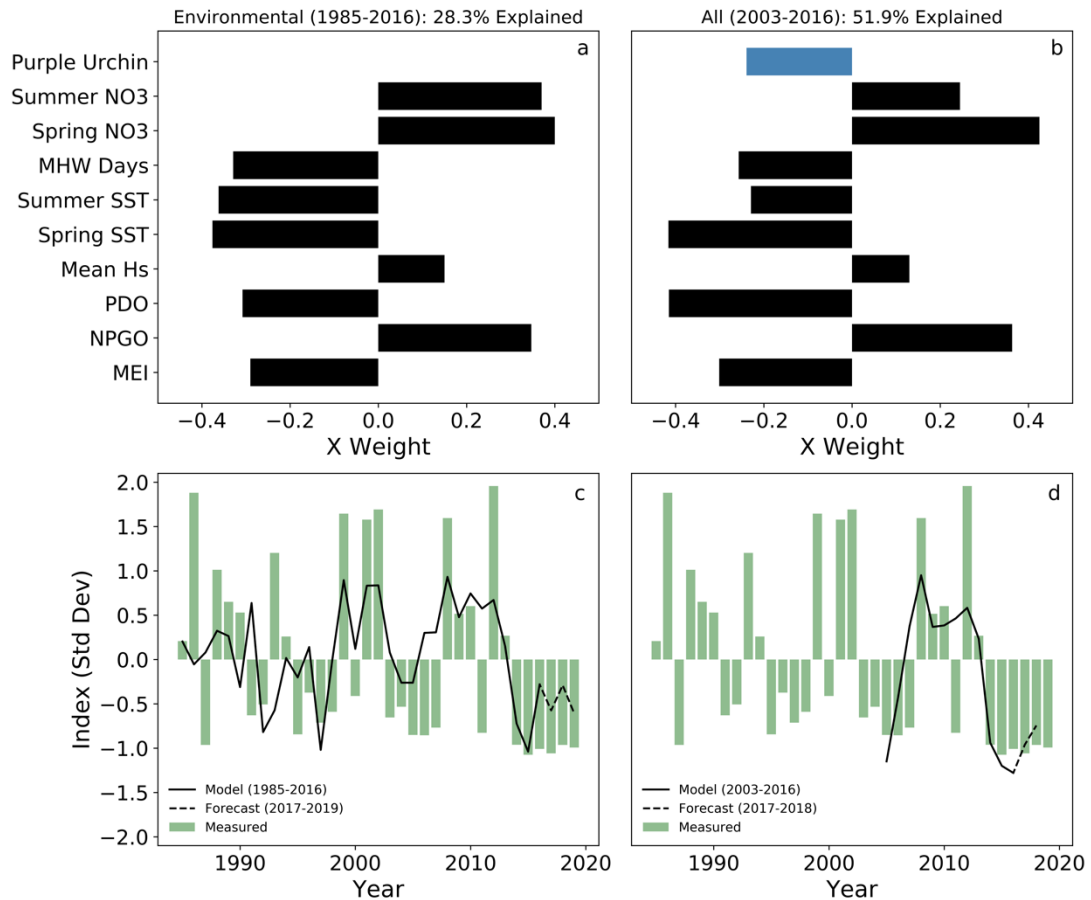


Figure 1.3. Results of Partial Least Squares Regression analysis for environmental and biological drivers of kelp canopy area from 1985 – 2019. Component 1 partial least squares regression (PLSR) x weights (top row) from environmental indices across 1985 to 2016 (a) and both environmental and biological indices from 2003 to 2016 (b). PLSR models and forecasts using all components overlaid on satellite derived kelp canopy (c,d). See supplementary data for detailed PLSR results (Table S1.1). Predictor variable acronyms are as follows: purple urchin density - ‘Purple Urchin’; seasonal nitrate concentrations - ‘Summer NO₃’ and ‘Spring NO₃’; marine heatwave days - ‘MHW Days’; seasonal sea surface temperature - ‘Summer SST’ and ‘Spring SST’; mean significant wave height - ‘Mean H_s’; Pacific Decadal Oscillation - ‘PDO’; North Pacific Gyre Oscillation - ‘NPGO’; Multivariate El Niño/Southern Oscillation Index - ‘MEI’. See Methods for detailed description of how each environmental variable influence kelp canopy dynamics.

only environmental drivers indicated that bull kelp was expected to partially recover in 2017 once SST and NO₃ concentrations rebounded from extreme anomalous conditions (Figure 1.3c). However, full bull kelp recovery in the environmental-only model forecasts may be hindered by NO₃ concentrations that remained below the long-term average after the NE Pacific MHW. Including urchin (grazer) dynamics in the PLSR analysis show that low kelp canopy biomass conditions persist regardless of the anticipated effects of environmental drivers to kelp recovery (Figure 1.3d). Furthermore, simulating a recovery of environmental drivers to the long-term climatological mean across 2017-2019 suggested that high urchin conditions disproportionately suppress kelp relative to environmental drivers (Figure S1.1).

Northern California kelp has historically responded to fluctuations in temperature extremes such as the 1997/1998 El Niño event (depicted in Figure 1.4a by the sharp peak in the 1997 annual number of MHW days) but have been resilient to widespread collapse. The substantial declines (well below the long-term mean) in sunflower stars evident in 2013 (Figure 1.4c; Figure S1.2 and Table S1.2; $m = -0.23 \text{ m}^2 \text{ yr}^{-1}$; $p = 0.01$) set the stage for a system-wide phase shift into an urchin barren state initiated by the NE Pacific MHW event²². Increases in purple urchin densities lagged anomalously low sunflower star densities by one year, spurred by reduced top-down forcing by sunflower stars⁴¹ and a large purple urchin larval recruitment event in 2014⁴² (Figure 1.4). Bull kelp and sunflower stars also exhibited stepwise functions across the

MHW event (Figure 1.4b and 1.4c). Absolute mean densities for both organisms stabilized close to zero, represented by the anomalously low index

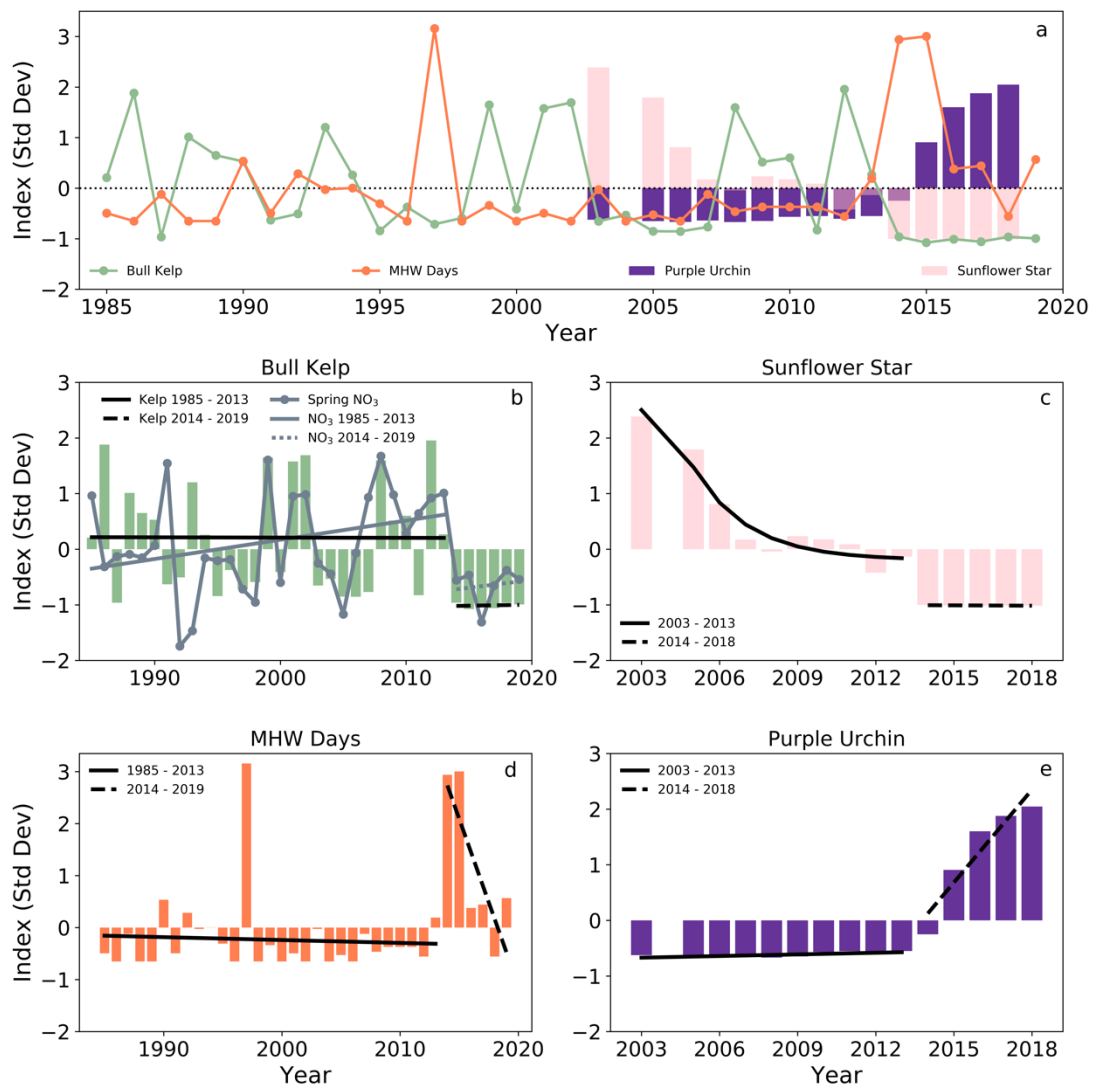


Figure 1.4. **Temporal trends of important environmental and biological drivers of ecosystem change in northern California kelp forests.** Standardized indices of (a) bull kelp canopy coverage, MHW days, purple urchin density, and sunflower star density where data is available. Standardized indices overlaid with Ordinary Least Square Regression (OLSR) fits (except in 4c 2003 – 2013 where a 2nd degree polynomial LSR is applied) prior to and after the NE Pacific MHW for (b) bull kelp canopy coverage and nitrate concentration, (c) sunflower star density, (d) MHW days, and (e) purple urchin density. See supplementary data for detailed LSR results and error statistics (Figure S1.2 and Table S1.2).

values between 2013-2018 for sunflower stars and between 2014-2019 for bull kelp (Figure 1.4c; Figure S1.2 and Table S1.2). Despite temperature anomalies returning to near normal distributions (Figure 1.2c) and spring nitrate concentrations rebounding slightly from minimums observed in 2016 (Figure 1.4b), barren conditions likely persist because of a widespread shift in purple urchin foraging behavior³⁴ (Figure 1.4e; slope = $3.1 \pm 0.67 \text{ m}^{-2} \text{ yr}^{-1}$; $p = 0.02$) and sustained high densities (mean = $14.8 \pm 8.3 \text{ m}^{-2}$) hinder a reversal back to healthy kelp forest state (Figure 1.4e).

Discussion

Northern California kelp forests experienced environmental and biological perturbations that likely resulted from the combined effects of (1) the absence of top-down control on urchin populations during and after the NE Pacific MHW (Figure 1.4c), (2) abrupt and persistent shifts in SST and nutrient conditions across the NE Pacific MHW that were beyond the physiological thresholds of optimum bull kelp growth and reproduction, and (3) an eruption in the population and grazing intensity of the herbivorous purple sea urchin. Previous work on the dynamics of marine and terrestrial ecosystem shifts sheds light on how these transitions in northern California were initiated by environmental events⁴³⁻⁴⁵ and preceded by low ecosystem resilience.

Co-varying environmental parameters, including SST and nitrate concentrations, historically maintained fluctuating yet stable long-term trends of bull kelp conditions in northern California (Figure 1.4d; $p > 0.05$). However, differences in the expression of kelp forest canopy dynamics between two foundational kelp genera across the NE Pacific MHW highlights that the annual life cycle of bull kelp makes

them particularly sensitive to acute stressors³⁶, such as MHWs and prolonged nutrient deplete conditions (Figure 1.2 a-c). This is evidenced by the fact that the stepwise decline in northern California bull kelp canopy area across the NE Pacific MHW was not observed in giant kelp (*Macrocystis pyrifera*) canopy biomass at a regional scale in southern California¹⁹ and northern Baja California^{19,20,24}. These observations suggest that giant kelp responded strongly to the NE Pacific MHW as a function of the genera's physiological temperature threshold and latitudinal gradients in SST magnitudes¹⁹, most likely because they were near their southern range and thermal limit in the northern hemisphere (Baja California, Mexico to Aleutian Islands, AK). In contrast, bull kelp forests in our study area, which lie in the middle of their distribution (Point Conception, CA to Unimak Island, AK), did not experience patchy spatial and temporal recovery after the onset of the NE Pacific MHW but maintained very low biomass conditions between 2014 and 2019, perhaps exacerbated by low propagule pressure resulting from patchy, sparse kelp densities and an annual life history strategy³⁶. Furthermore, sea urchin dynamics differed between northern California and southern/Baja California. Increases in crowned sea urchin density (and decreases in invertebrate species richness) in localized areas of the Baja region indicate enhanced grazing pressure, in addition to temperature stress, may have occurred but not on a regional scale²⁰.

Regional-scale sea urchin larval recruitment dynamics are associated with large-scale environmental drivers and subsequent population dynamics⁴². Anomalously high larval recruitment was observed in Fort Bragg, CA, peaking in 2015 and increased

larval settlement appeared to be correlated with juvenile and adult urchin densities during the NE Pacific MHW. Although there are no reliable *in situ* data available for sea urchin densities prior to 2003 from the northern California region, there are purple urchin settlement data as early as 1990 from Fort Bragg (1990-2016⁴²) and Westport, Pt. Cabrillo, and Pt. Arena (1990-1993⁴⁶). These settlement records show there was anomalously high larval settlement from 1993 to 1994 and 1998. Despite bull kelp canopy area being anomalously low between 1995 and 1998 (Figure 1.4b), there is no evidence of complete kelp forest collapse or ecosystem shift during that period and no way to verify that high juvenile urchin densities coincided with the high larval densities. Furthermore, anomalously low kelp conditions do not always follow or co-occur with sea urchin larval settlement events (e.g. Figure 1.4b 2003 – 2007; Okamoto et al. 2020 Figure 1.3a). Given the positive relationship between SST and larval settlement in northern California⁴² and predictions of more frequent and/or severe MHW⁴⁷, restoration efforts in northern California would benefit from a greater understanding of localized sea urchin population dynamics in that region.

Observed historical declines in predator diversity is reflective of a reduction in ecosystem resilience. The sequence of biological events in northern California, beginning with the extirpation of sea otters in the 1800s, appears to have reduced the resilience of kelp ecosystems across the entire region^{44,48}. Throughout California, a suite of predators (e.g. sunflower stars, sea otters, California Sheephead fish³⁴), and their complementary effects, play an essential role in maintaining stable forested states by enhancing resiliency via size-dependent predation⁴³, even when environmental

perturbations occur. In sea urchin barrens, urchins are starved and lack energetic value to predators with high metabolic rates⁴⁹. Moreover, behaviorally mediated predators often track changes in the distribution of profitable prey, which further complicates implications for recovery. Urchin barrens are characterized by low urchin gonad index; because the gonads are what urchin predators target and consume, urchin barren states potentially limit increased predation of this particular prey⁵⁰. The high urchin densities observed in northern California have induced starvation conditions and reduced nutritional value⁵⁰. Additionally, since the overall ecosystem biodiversity of urchin barrens is severely reduced⁵¹, opportunities for predator (otters, sunflower stars, etc.) recovery is diminished. Ecosystem recovery is further limited by evidence that the effects on prey can lag behind the recovery of a predator⁵².

Despite potential limitations of urchin barrens on predator recovery, reintroduction of sea otter populations into urchin barrens has resulted in phase shifts back to forested states in some locations (e.g. Aleutian Islands²⁶). It is unclear from this analysis what future phase state dynamics will occur with the reintroduction of a top predator given the strong potential that this urchin barren constitutes a kelp forest alternative stable state²⁶. Although we refer to the recent wide-spread kelp forest loss as a phase shift and cannot currently provide proof of a true kelp forest alternative stable state, Filbee-Dexter and Scheibling 2014 argues that in most cases the formation of urchin barrens can be regarded as such. Considering that the dynamics of the wide-spread urchin barren in northern California has similar patterns to other urchin barrens,

hysteresis (discontinuous phase shift) and strong positive feedbacks may maintain the current state for a prolonged period of time.

Whatever mechanisms of system-wide resilience that existed prior to the complete loss of sunflower stars in 2014 were eliminated by its removal^{22,24,29}. Though recovery of other sea star species has been observed across the NE Pacific coastline, the sunflower star remains locally extinct from kelp forest and intertidal ecosystems along the entire region. Evidence suggests that the pathogen associated with SSWS in the sunflower star was not temperature dependent, nor responsible for disease observed in other asteroids throughout the region⁵³. This may explain why recovery for sunflower stars across the region, and in turn kelp forest recovery in northern California, remain absent despite temperature and nutrient conditions recovering slightly in 2017. Furthermore, the clear phase shift observed in other biological and environmental conditions in northern California (Figure 1.4b, d, and e), such as sunflower star populations, began to decline well before the NE Pacific MHW in a negative exponential fashion (Figure 1.4c). This indicates more gradual changes in predator abundances prior to large-scale environmental disturbances. The scarcity of historical community-level data within this ecosystem prior to 2000 further limits hypothesis development and testing of the influence of biological parameters on ecosystem patterns, and highlights the need for continued consistent, long-term *in situ* datasets that cannot be obtained via remote sensing.

Our results indicate a potential return of kelp under a forecasted scenario of mean SST and nitrate conditions, but that a full recovery is suppressed by urchin

herbivory (Figure S1.1). Therefore, it is likely that additional mechanisms beyond a return to mean environmental conditions will be necessary in northern California to reduce urchin population densities to enable a phase shift back to forested conditions. Historically, natural processes such as density-dependent sea urchin disease outbreaks⁵⁴ and exposure to large ocean swell events⁵⁵ induce mass mortality of urchins. In the absence of urchin disease or effective human intervention to reduce grazer densities, the existing widespread extent of urchin barrens may continue long into the future with devastating impacts to forest-associated fisheries.

We show that this persistent multi-year event has not been seen in the region for the observable past. As a result, innovative management strategies will need to be developed to address the broad scale collapse of bull kelp forests in northern California and the loss of the fisheries this system once supported. Furthermore, managers of canopy kelp forest ecosystems around the world should work to prioritize time series measurements of remotely sensed and *in situ* data for biological and environmental parameters before, and even after, ecosystem shifts occur. Long-term time series can be used to quantify historical baselines, set thresholds for monitoring criteria, develop restoration targets, and track ecosystem recovery. Additionally, the implementation of environmental forecasting models⁵⁶ should be used to determine if current and future environmental and/or biological conditions are impeding kelp recovery or the likely persistence of recovered forests. Establishing these adaptive management techniques for perturbed and healthy coastal ecosystems around the globe is crucial for understanding and predicting phase shift dynamics^{57,58} and restoring foundation

species, and the ecosystem services they provide, especially in the face of increasing frequency and intensity of MHWs as a result of climate change.

Methods

Determining kelp canopy coverage - Bull kelp forests are readily identified by multiple existing high spatial resolution satellite and airborne platforms because their floating surface canopies have strong reflectance in the near-infrared, similar to terrestrial vegetation, and are optically distinct from the surrounding water. We utilized kelp's spectral signature to generate a remote timeseries of bull kelp canopy coverage in order to investigate the influence of environmental factors on canopy area across more than three decades (1985 to 2019) of US Geological Survey (USGS) Landsat imagery. Cloud-free Landsat 5, 7, and 8 imagery were collected as close to historical maximum canopy extent as possible (August through early-November) and analyzed using multiple endmember spectral mixture analysis (MESMA)⁵⁹, which is more robust than band ratio methods such as the Normalized Difference Vegetation Index (NDVI), a commonly used algorithm for detecting kelp^{38,60}.

Environmental and biological drivers of bull kelp canopy - Although most kelp decline occurs at small scales driven by local processes³⁸, losses of northern California bull kelp in 2014 occurred across nearly 350 km of continuous coastline (Figure 1.1b). Therefore, the environmental and biological drivers of kelp were investigated in the context of regional scale kelp dynamics that occurred across the NE Pacific MHW (Table S1.3 and Figure S1.3). The large-scale environmental forcings included the Multivariate El Niño/Southern Oscillation Index (MEI), North Pacific Gyre Oscillation (NPGO), and Pacific Decadal Oscillation (PDO). Local-scale environmental forcings

included multiple signatures corresponding with coastal upwelling dynamics, including sea surface temperature (SST) and surface nitrate concentrations (NO_3), and significant wave height (H_s).

The climatology for each index was removed and then the index was standardized to each variable's mean and standard deviation. For environmental indices (1985 to 2019) that were measured at hourly (H_s) and daily frequency (SST and NO_3), data were temporally binned into monthly averages across 1985 to 2019. Standardized indices were calculated by removing the long-term monthly climatology from absolute monthly means and normalizing to the standard deviation. To scale monthly indices to the annual frequency of the kelp index, the monthly climatologically corrected indices were averaged to annual or seasonal values (e.g. spring SST and spring NO_3). The annual frequency of marine heatwave (MHW) days was determined from daily satellite SST measurements based on published methodology from Hobday et al.⁶¹. Sea surface NO_3 concentrations were calculated from SST- NO_3 relationships developed for northern California by Garcia-Reyes et al.⁶² (Table S1.3).

Biological indices, including purple sea urchin (*Strongylocentrotus purpuratus*) and sunflower star (*Pycnopodia helianthoides*) densities, were obtained from California Department of Fish and Wildlife (CDFW; 2003 - 2018) and Reef Check California (2007 – 2018)⁶³ subtidal rocky reef habitat surveys (Figure S1.4). Both organizations conduct annual surveys through the summer and early fall in northern California. Reef Check California utilizes trained citizen scientists to support coastal ecosystem monitoring, management, and to promote stewardship of sustainable kelp

forest communities. Reef Check California surveyed 27 sites in the northern California Sonoma and Mendocino counties between 2007 and 2018 (Figure S1.4) ranging between 7 and 22 sites annually. Each site consisted of 2 depth strata (inshore: 0 – 10 m and offshore: 10 – 20 m) and 6, 60 m² (2 x 30 m) invertebrate and algal transects. Three 60 m² transects were conducted in each depth strata generally parallel to shore. Partial transects densities were calculated when more than 50 individuals of a species were counted along a distance of at least 5 m.

CDFW subtidal surveys occur as part of the agency's kelp ecosystem management program⁶⁴. CDFW surveyed 12 sites in the northern California Sonoma and Mendocino counties between 2003 and 2018 (Figure S1.4) ranging between 2 and 11 sites annually. Random transects were placed within four depth strata (0 – 4.5 m, 4.5 m – 8.3 m, 9 – 13.7 m, and 13.7 – 18.3 m), divided equally within the full depth range (0 –18 m) with 60 m² transects (2 x 30 m). Transect locations were at predetermined random GPS coordinates greater than 70 m apart and generally parallel to shore. At each site 15–55 transects were surveyed, with equal numbers of transects per depth stratum. All organisms were counted and recorded within the transect area regardless of density distribution.

Annual densities for the entire study region were determined by taking the mean of all 60 m² transects conducted by Reef Check California and CDFW. Standardized indices were calculated by removing the long-term annual climatology from absolute annual means and normalizing to the standard deviation.

Statistics and Reproducibility: Determining the drivers of bull kelp canopy coverage -

Following determination of maximum annual kelp canopy coverage, a partial least squares regression⁶⁵ (PLSR) was used to investigate the temporal response of kelp canopy coverage in northern California (Mendocino and Sonoma Counties; Figure 1.1a) to large- and local-scale oceanographic and biological processes. PLSR combines principle component analysis (PCA) and multiple linear regression to maximize covariance between the predictor and response variables. This method works particularly well where (1) strong collinearity occurs between predictor variables (Figure S1.5) and (2) a relatively low number of observations would otherwise reduce model performance⁶⁵. Many of the variables used in this study present strong multicollinearity (Figure S1.5) especially between seasonal SST, seasonal NO₃ and PDO.

PLSR analysis was conducted using the PLSRegression function in the Python 3.7 sklearn.cross_decomposition machine learning statistical module. Using a k-fold cross-validation technique, environmental variables were selected by calculating the mean squared error (MSE) and determining the optimal configuration via the lowest MSE (Figure S1.6a). The cross-validation showed that the number of predictor variables had little influence on the performance of the environmental-only indices' first component (Figure S1.6a). Therefore, a one component, 9 variable configuration was selected. Although a two component, 4 variable configuration was optimal for environmental and biological indices combined (Figure S1.6b), the study's goal was to compare how the 'environmental-only' model results changed when adding biological

forcing (purple urchins). As a result, a one component, 10 variable configuration was selected.

After determining and modeling important drivers of kelp canopy area, a least squares regression (LSR) approach was utilized to understand significant and insignificant temporal changes in relevant biological and environmental indices (kelp canopy area, spring NO₃, MHW Days, sunflower star density, and purple urchin density) across the entire timeseries, prior to (pre-2014) the NE Pacific MHW, and following (post-2013) the NE Pacific MHW. For all indices, except the pre-2014 sunflower star index (which was optimized to a polynomial LSR), ordinary LSRs were fit to data. This simple correlative approach was valuable for understanding how these relevant variables changed on both long and short-term timescales with relevance to dramatic declines in kelp canopy coverage. Trendline error (Figure S1.2) and regression statistics (Table S1.2; slope, r^2 , and p -value) are presented in the Supplementary material.

Acknowledgments

We thank Reef Check California Program for contribution of subtidal survey data and the many volunteers who devote their time and energy to citizen science efforts. M.H. Carr received support from the National Science Foundation (OCE-1538582).

References

1. Bindoff, N. L. *et al.* Changing Ocean, Marine Ecosystems, and Dependent Communities. in *IPCC Special Report on the Ocean and Cryosphere in a Changing Climate* (eds. Pörtner, H.-O. et al.) 447–588 (2019).
2. Collins, M. *et al.* Extremes, Abrupt Changes and Managing Risks. in *IPCC Special Report on the Ocean and Cryosphere in a Changing Climate* (eds. Pörtner, H.-O. et al.) 589–656 (2019).
3. Hoegh-Guldberg *et al.* The Ocean. in *Climate Change 2014: Impacts, Adaptation, and Vulnerability. Part B: Regional Aspects. Contribution of Working Group II to the Fifth Assessment Report of the Intergovernmental Panel on Climate Change* (eds. Barros, V. R. et al.) 1655–1731 (Cambridge University Press, 2014).
4. Laufkotter, C., Zscheischler, J. & Frolicher, T. L. High-impact marine heatwaves attributable to human-induced global warming. *Science (80-)*. **369**, 1621–1625 (2020).
5. Holbrook, N. J. *et al.* A global assessment of marine heatwaves and their drivers. *Nat. Commun.* **10**, 1–13 (2019).
6. Oliver, E. C. J. *et al.* Longer and more frequent marine heatwaves over the past century. *Nat. Commun.* **9**, 1–12 (2018).
7. Carr, M. & Kearns, E. J. Production regimes in four Eastern Boundary Current systems. *Deep. Res. Part II* **50**, 3199–3221 (2003).
8. Castro, C. G. *et al.* Introduction to ‘ The 1997 – 8 El Nino Atlas of oceanographic conditions along the west coast of North America (23°N – 50°N)’’. *Prog. Oceanogr.* **54**, 503–511 (2002).
9. Kendrick, G. A. *et al.* A Systematic Review of How Multiple Stressors From an Extreme Event Drove Ecosystem-Wide Loss of Resilience in an Iconic Seagrass Community. *Front. Mar. Sci.* **6**, 1–15 (2019).

10. Nohaïc, M. Le *et al.* Marine heatwave causes unprecedented regional mass bleaching of thermally resistant corals in northwestern Australia. *Sci. Rep.* **7**, 1–11 (2017).
11. Smale, D. A. Impacts of ocean warming on kelp forest ecosystems. *New Phytol.* **225**, 1447–1454 (2020).
12. Smale, D. A. *et al.* Marine heatwaves threaten global biodiversity and the provision of ecosystem services. *Nat. Clim. Chang.* **9**, 306–312 (2019).
13. Schiel, D. R. & Foster, M. S. *The Biology and Ecology of Giant Kelp Forests.* (2015).
14. Wernberg, T., Krumhansl, K., Filbee-dexter, K. & Pedersen, M. F. Status and Trends for the World’s Kelp Forests. in *World Seas: An Environmental Evaluation* 57–78 (Elsevier Ltd., 2019). doi:10.1016/B978-0-12-805052-1.00003-6
15. Wernberg, T. *et al.* An extreme climatic event alters marine ecosystem structure in a global biodiversity hotspot. *Nat. Clim. Chang.* **3**, 78–82 (2012).
16. Wernberg, T. *et al.* Climate-driven regime shift of a temperate marine ecosystem. *Science* (80-.). **353**, 169–172 (2016).
17. Oliver, E. C. J. *et al.* The unprecedented 2015/16 Tasman Sea marine heatwave. *Nat. Commun.* **8**, 1–12 (2017).
18. Thomsen, M. S. *et al.* Local Extinction of Bull Kelp (*Durvillaea* spp.) Due to a Marine Heatwave. *Front. Mar. Sci.* **6**, 1–10 (2019).
19. Cavanaugh, K. C. *et al.* Spatial Variability in the Resistance and Resilience of Giant Kelp in Southern and Baja California to a Multiyear Heatwave. *Front. Mar. Sci.* **6**, 1–14 (2019).

20. Arafeh-dalmau, N., Montaña-moctezuma, G., Martínez, J. A. & Smale, D. A. Extreme Marine Heatwaves Alter Kelp Forest Community Near Its Equatorward Distribution Limit. *Front. Mar. Sci.* **6**, 1–18 (2019).
21. Filbee-Dexter, K., Feehan, C. J. & Scheibling, R. E. Large-scale degradation of a kelp ecosystem in an ocean warming hotspot. **543**, 141–152 (2016).
22. Rogers-Bennett, L. & Catton, C. A. Marine heat wave and multiple stressors tip bull kelp forest to sea urchin barrens. *Sci. Rep.* **9**, 1–9 (2019).
23. Sanford, E., Sones, J. L., García-reyes, M., Goddard, J. H. R. & Largier, J. L. Widespread shifts in the coastal biota of northern California during the 2014–2016 marine heatwaves. *Sci. Reportscientific Reports* **9**, 1–14 (2019).
24. Beas-luna, R. *et al.* Geographic variation in responses of kelp forest communities of the California Current to recent climatic changes. *Glob. Chang. Biol.* 1–17 (2020). doi:10.1111/gcb.15273
25. Filbee-Dexter, K. & Wernberg, T. Rise of Turfs : A New Battlefield for Globally Declining Kelp Forests. *Bioscience* **68**, 64–76 (2018).
26. Filbee-Dexter, K. & Scheibling, R. E. Sea urchin barrens as alternative stable states of collapsed kelp ecosystems. *Mar. Ecol. Prog. Ser.* **495**, 1–25 (2014).
27. Ling, S. D., Johnson, C. R., Frusher, S. D. & Ridgway, K. R. Overfishing reduces resilience of kelp beds to climate-driven catastrophic phase shift. *Proc. Natl. Acad. Sci.* **106**, (2009).
28. Estes, J. A., Tinker, M. T., Williams, T. M. & Doak, D. F. Killer Whale Predation on Sea Otters Linking Oceanic and Nearshore Ecosystems. *Science (80-)*. **282**, 473–477 (1998).
29. Hamilton, S. L. & Caselle, J. E. Exploitation and recovery of a sea urchin

- predator has implications for the resilience of southern California kelp forests. *Proc. R. Soc. B* **282**, (2014).
30. Jacox, M. G. *et al.* Forcing of Multiyear Extreme Ocean Temperatures that Impacted California Current Living Marine Resources in 2016. *Bull. Am. Meteorol. Soc.* **99**, 27–33 (2018).
 31. Montecino-latorre, D. *et al.* Devastating Transboundary Impacts of Sea Star Wasting Disease on Subtidal Asteroids. *PLoS One* **11**, 1–21 (2016).
 32. Eisaguirre, J. M., Davis, K., Carlson, P. M., Gaines, S. D. & Caselle, J. E. Trophic redundancy and predator size class structure drive differences in kelp forest ecosystem dynamics. *Ecology* **101**, 1–11 (2020).
 33. Harrold, C. & Reed, D. C. Food Availability, Sea Urchin Grazing, and Kelp Forest Community Structure. *Ecology* **66**, 1160–1169 (1985).
 34. Cowen, R. K. The effect of sheephead (*Semicossyphus pulcher*) predation on red sea urchin (*Strongylocentrotus franciscanus*) populations: an experimental analysis. *Oecologia* **58**, 249–255 (1983).
 35. Burt, J. M. *et al.* Sudden collapse of a mesopredator reveals its complementary role in mediating rocky reef regime shifts. *Proc. R. Soc. B* **285**, (2018).
 36. Springer, Y. P., Hays, C., Carr, M. H. & Mackey, M. R. Toward ecosystem-based management of marine macroalgae—the bull kelp, *Nereocystis luetkeana*. *Oceanogr. Mar. Biol. Annu. Rev.* **48**, 1–42 (2010).
 37. Springer, Y., Hays, C., Carr, M., Mackey, M. & Bloeser, J. Ecology and management of the bull kelp, *Nereocystis luetkeana*: A synthesis with recommendations for future research. 48 (2006).
 38. Bell, T. W., Allen, J. G., Cavanaugh, K. C. & Siegel, D. A. Three decades of variability in California’s giant kelp forests from the Landsat satellites. *Remote Sens. Environ.* **238**, (2020).

39. Pfister, C. A., Berry, H. D. & Mumford, T. The dynamics of Kelp Forests in the Northeast Pacific Ocean and the relationship with environmental drivers. *J. Ecol.* 1–14 (2017). doi:10.1111/1365-2745.12908
40. Griggs, G. B. & Hein, J. R. Sources, Dispersal, and Clay Mineral Composition of Fine-Grained Sediment off Central and Northern California. *J. Geol.* **88**, 541–566 (1979).
41. Harvell, C. D., Caldwell, J. M., Burt, J. M., Bosley, K. & Keller, A. Disease epidemic and a marine heat wave are associated with the continental-scale collapse of a pivotal predator (*Pycnopodia helianthoides*). *Sci. Adv.* **5**, 1–9 (2019).
42. Okamoto, D. K., Schroeter, S. C. & Reed, D. C. Effects of ocean climate on spatiotemporal variation in sea urchin settlement and recruitment. *Limnol. Oceanogr.* 1–16 (2020). doi:10.1002/lno.11440
43. Burt, J. M. *et al.* Sudden collapse of a mesopredator reveals its complementary role in mediating rocky reef regime shifts. *Proc. R. Soc. B* **285**, (2018).
44. Estes, J. A., Burdin, A. & Doak, D. F. Sea otters, kelp forests, and the extinction of Steller’s sea cow. *Proc. Natl. Acad. Sci.* **113**, 880–885 (2016).
45. Scheffer, M., Carpenter, S., Foley, J. A., Folke, C. & Walker, B. Catastrophic shifts in ecosystems. *Nature* **413**, 591–596 (2001).
46. Ebert, T. A., Schroeter, S. C., Dixon, J. D. & Kalvass, P. Settlement patterns of red and purple sea urchins (*Strongylocentrotus franciscanus* and *Strongylocentrotus purpuraceus*). *Mar. Ecol. Prog. Ser.* **111**, 41–52 (1994).
47. Frölicher, T. L., Fischer, E. M. & Gruber, N. Marine heatwaves under global warming. *Nature* **560**, 360–366 (2018).

48. Steneck, R. S. *et al.* Kelp forest ecosystems: biodiversity, stability, resilience and future. *Environ. Conserv.* **29**, 436–459 (2002).
49. Smith, J. G. *et al.* Behavioral responses across a mosaic of ecosystem states restructure a sea otter-urchin trophic cascade. *Proc. Natl. Acad. Sci.* (2021).
50. Eurich, J. G., Selden, R. L. & Warner, R. R. California spiny lobster preference for urchins from kelp forests: implications for urchin barren persistence. *Mar. Ecol. Prog. Ser.* **498**, 217–225 (2014).
51. Graham, M. H. Effects of Local Deforestation on the Diversity and Structure of Southern California Giant Kelp Forest Food Webs. *Ecosystems* **7**, 341–357 (2004).
52. Babcock, R. C. *et al.* Decadal trends in marine reserves reveal differential rates of change in direct and indirect effects. *Proc. Natl. Acad. Sci.* **107**, 18256–18261 (2010).
53. Hewson, I., Bistolas, K. S. I., Cardé, E. M. Q. & Button, J. B. Investigating the Complex Association Between Viral Ecology , Environment , and Northeast Pacific. *Front. Mar. Sci.* **5**, (2018).
54. Pearse, J. S. & Hines, A. H. Expansion of a Central California Kelp Forest Following the Mass Mortality of Sea Urchins. **91**, 83–91 (1979).
55. Ebeling, A. W., Laur, D. R., Rowley, R. J. & Barbara, S. Severe storm disturbances and reversal of community structure in a southern California kelp forest. *Mar. Biol.* **294**, 287–294 (1985).
56. Martínez, B. *et al.* Distribution models predict large contractions of forming seaweeds in response to ocean warming. *Divers. Distrib.* **24**, 1350–1366 (2018).
57. DeYoung, B. *et al.* Regime shifts in marine ecosystems: detection, prediction and management. *Trends Ecol. Evol.* **23**, 402–409 (2008).
58. Crépin, A., Biggs, R., Polasky, S., Troell, M. & Zeeuw, A. De. Regime shifts

and management. *Ecol. Econ.* **84**, 15–22 (2012).

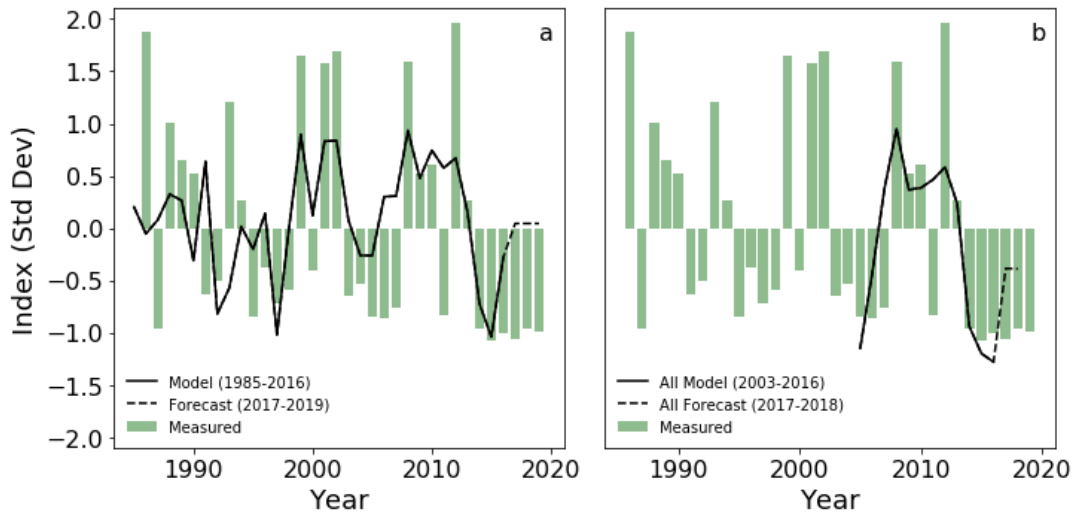
59. Roberts, D. A. *et al.* Mapping chaparral in the Santa Monica Mountains using multiple endmember spectral mixture models. *Remote Sens. Environ.* **65**, 267–279 (1998).
60. Cavanaugh, K. C., Siegel, D. A., Reed, D. C. & Dennison, P. E. Environmental controls of giant-kelp biomass in the Santa Barbara Channel, California. *Mar. Ecol. Prog. Ser.* **429**, 1–17 (2011).
61. Hobday, A. J. *et al.* A hierarchical approach to defining marine heatwaves. *Prog. Oceanogr.* **141**, 227–238 (2016).
62. García-Reyes, M., Larmgier, J. L. & Sydeman, W. J. Progress in Oceanography Synoptic-scale upwelling indices and predictions of phyto- and zooplankton populations. *Prog. Oceanogr.* **120**, 177–188 (2014).
63. McHugh, T., Abbott, D. & Freiwald, J. Phase shift from kelp forest to urchin barren along California’s North Coast. in *Western Society of Naturalists* (2018).
64. Rogers-Bennett, L., Kashiwada, J. V., Taniguchi, I. K., Kawana, S. K. & Catton, C. A. Using density-based fishery management strategies to respond to mass mortality events. *J. Shellfish Res.* **38**, 1–11 (2019).
65. Carrascal, L. M. & Galva, I. Partial least squares regression as an alternative to current regression methods used in ecology. *Oikos* **118**, 681–690 (2009).
66. Vadas, R. L. Ecological implications of culture studies on *nereocystis luetkeana*. *J. Phycol.* **8**, 196–203 (1972).
67. Finger, D. J. I., Mcpherson, M. L., Houskeeper, H. F. & Kudela, R. M. Mapping bull kelp canopy in northern California using Landsat to enable long-term monitoring. *Remote Sens. Environ.* **254**, 112243 (2021).

Supplemental Material

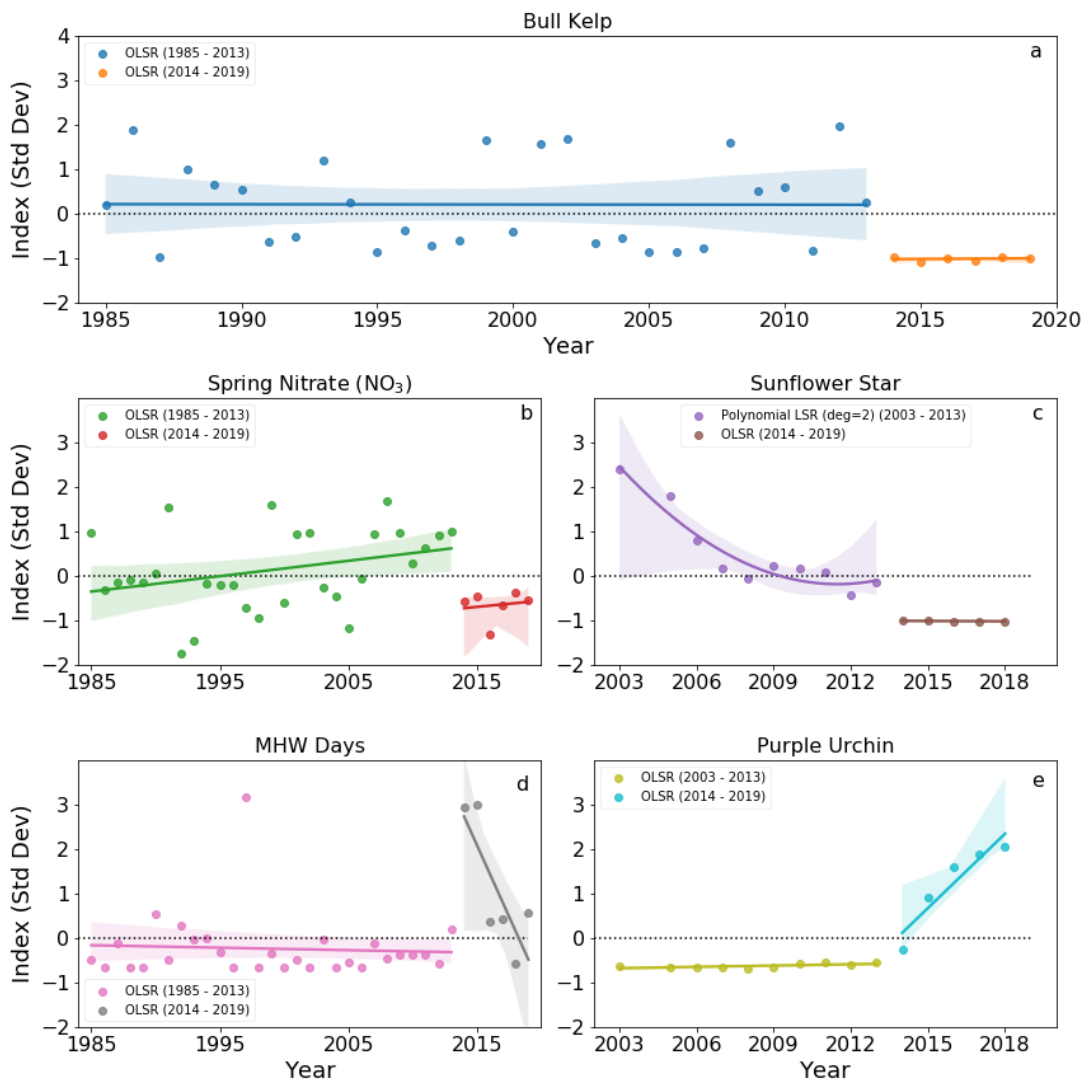
Supplementary Table 1 (Table S1.1) – Component-wise PLSR results for each date range (Figure 1.3).

	Full Timeseries	Preceding MHW	Recent Decade	With Biological Forcings
Date Range	1985 – 2016	1985 – 2013	2003 – 2016	2003 - 2016
Component 1 r^2	0.303	0.224	0.517	0.498

Supplementary Figure 1 (Figure S1.1) – PLSR models and forecasts using physical drivers (a) and physical and biological drivers (b) overlaid on satellite derived kelp canopy. Forecasted scenarios use environmental variables (MEI, NPGO, PDO, Mean Hs, seasonal SST (spring and summer), MHW days, and seasonal NO₃ (spring and summer) conditions at the climatological mean for 2017 to 2019. For all other years (1985 - 2016 and 2003 - 2016), these variables are the environmentally derived indices.



Supplementary Figure 2 (Figure S1.2) – Least squares regression (LSR) fits for standardized indices of environmental ((a) bull kelp, (b) spring nitrate, and (d) MHW days) and biological ((c) sunflower star and (e) purple urchin) preceding the NE Pacific MHW and following the NE Pacific MHW. Date ranges depended on data availability for each variable. An ordinary LSR (OLSR) was applied to all variables except the sunflower star’s preceding NE Pacific MHW date range (panel c; 2003 – 2013) where a second degree polynomial LSR was applied. For variable-wise regression statistics see S4. Shading around the regression lines represents the 95% confidence intervals.



Supplementary Table 2 (Table S1.2) - Least squares regression (LSR) fits for standardized indices of environmental (bull kelp, spring nitrate, MHW days) and biological (purple urchin and sunflower star) show in Figure 1.4 and Figure S1.3. Date ranges presented for each timeframe (preceding MHW, following MHW, full timeseries) depended on data availability for each variable. Preceding the NE Pacific MHW, the date ranges of 1985 to 2013 and 2003 to 2013 were used for environmental and biological variables, respectively. Following the NE Pacific MHW, date ranges were from 2014 to 2019 and 2014 to 2018 were used for environmental and biological variables, respectively. Full timeseries date ranges were 1985 to 2019 for environmental variables, and 2003 to 2018 for biological variables. Bolded and grey highlighted cells designate statistically significant relationships ($p < 0.05$). Ordinary LSR was used for all trends presented below with the exception of the preceding MHW sunflower star trend, where a second order polynomial LSR was applied (indicated with *).

Index	Preceding MHW (1985 – 2013 or 2003 – 2013)			Following MHW (2014 – 2019 or 2014 -2018)			Full Timeseries (1985 – 2019 or 2003 to 2018)		
	slope	r ²	p-value	slope	r ²	p-value	slope	r ²	p-value
Bull kelp	-4.6x10 ⁻⁴	1.6x10 ⁻⁵	0.98	3.7x10 ⁻³	2.1x10 ⁻²	0.78	- 3.0x10 ⁻²	9.2x10 ⁻²	7.7x10 ⁻²
Spring nitrate	3.5 x10 ⁻²	0.11	8.6x10 ⁻²	2.8x10 ⁻²	0.024	0.77	6.4x10 ⁻⁴	5.4x10 ⁻⁵	0.97
MHW days	-5.5x10 ⁻³	4.2x10 ⁻³	0.74	-0.64	0.66	5.03x10⁻²	2.7x10 ⁻²	7.4x10 ⁻²	0.11
Purple urchin	9.8x10⁻³	0.46	3.03x10⁻²	0.56	0.88	1.8x10⁻²	0.25	0.64	3.1x10⁻⁴
Sunflower star	*-0.21	*0.84	*1.3x10⁻⁶	-2.1x10 ⁻²	0.72	6.8x10 ⁻²	-0.21	0.84	1.3x10⁻⁶

Supplementary Table 3 (Table S1.3) – Index data sources for all environmental (largescale and local-scale) and biological indices. Detailed descriptions of large and local-scale forcings and their influences on kelp dynamics are listed below the table.

Response Variable	Predictor Variables		
	1985 – 2019		2003 - 2018
Kelp Index	Largescale Indices	Local-scale Indices	Biological Indices
USGS Landsat derived canopy area - https://earthexplorer.usgs.gov	<p>NPGO - http://www.o3d.org/npgo/</p> <p>PDO - http://research.jiso.washington.edu/pdo/</p> <p>MEI - https://www.esrl.noaa.gov/psd/enso/mei/</p>	<p>SST - https://www.ncei.noaa.gov/erddap/griddap/ncdc_oisst_v2_avhrr_by_time_zlev_lat_lon.html</p> <p>MHW Days - Hobday et al. 2016²</p> <p>[NO₃] - Garcia-Reyes et al. 2014³</p> <p>H_s - https://www.ndbc.noaa.gov/ - station 46013</p>	Purple urchin and Sunflower star densities - http://data.reefcheck.us/ ¹ and California Department of Fish and Wildlife (L.R.B)

SST Index –SST conditions effect the distribution (physiological temperature threshold), gametophyte maturation⁴, and the seasonal growth rates⁵.

NO₃ Index – Nitrate conditions fuel growth seasonally. Growth rates are primarily high in the spring and early summer due to the availability of nutrient rich water brought to the surface by seasonal upwelling. Growth rates are generally low in the summer due to limited nitrate conditions ^{5,6}.

H_s Index – Bull kelp are an annual algal species and in exposed regions, such as the northern California coast, are typically removed by strong wave forces during fall and winter storms. Therefore, seasonal and annual trends in significant wave height influence canopy distribution ⁶.

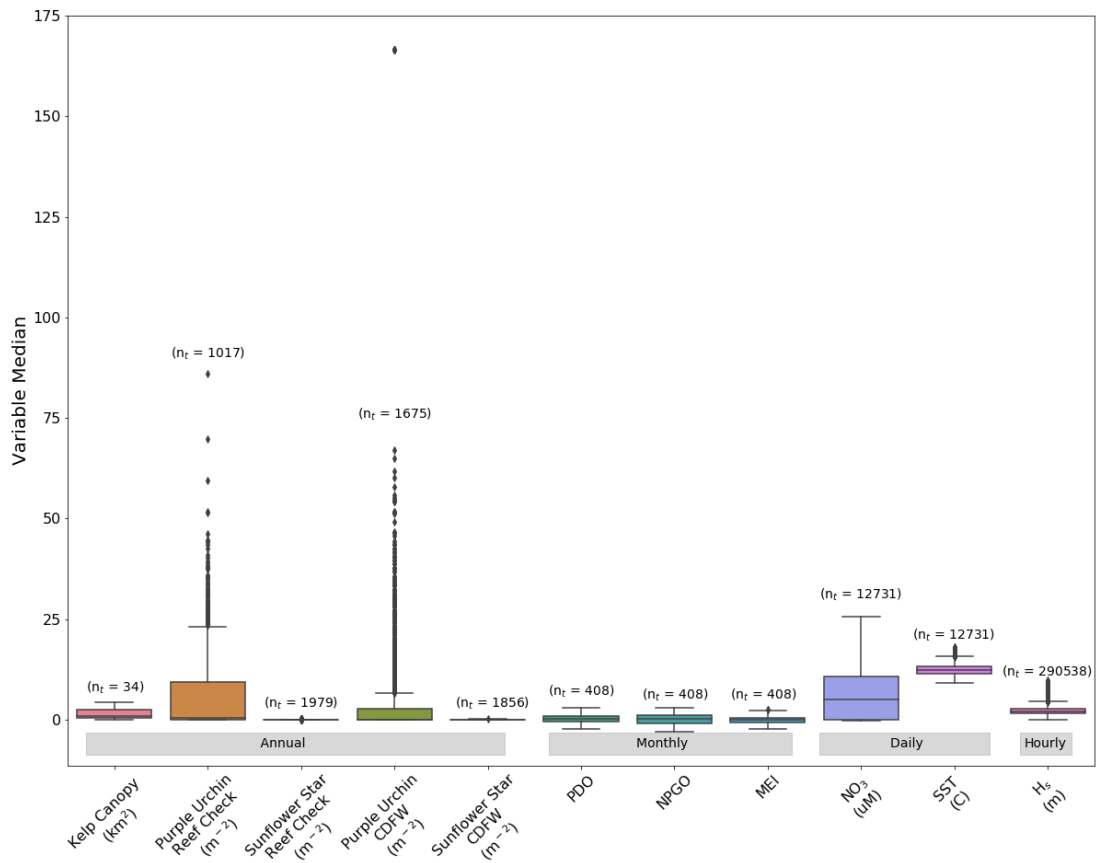
MEI Index – the Multivariate El Niño/Southern Oscillation (ENSO) Index (MEI.v2) is indicative of global climate disruptions and derived from five different variables (sea level pressure, sea surface temperature, zonal and meridional components of the surface wind, and outgoing longwave radiation). Disruptions to oceanographic conditions via ENSO patterns influence SST, NO₃, and wave height conditions (H_s). Studies have found ENSO to be an important driver of kelp dynamics across the globe⁷⁻¹¹.

NPGO Index – the North Pacific Gyre Oscillation is an oceanic climate index derived from the second mode of sea surface height variability in the northeast Pacific and influences sea surface nutrient

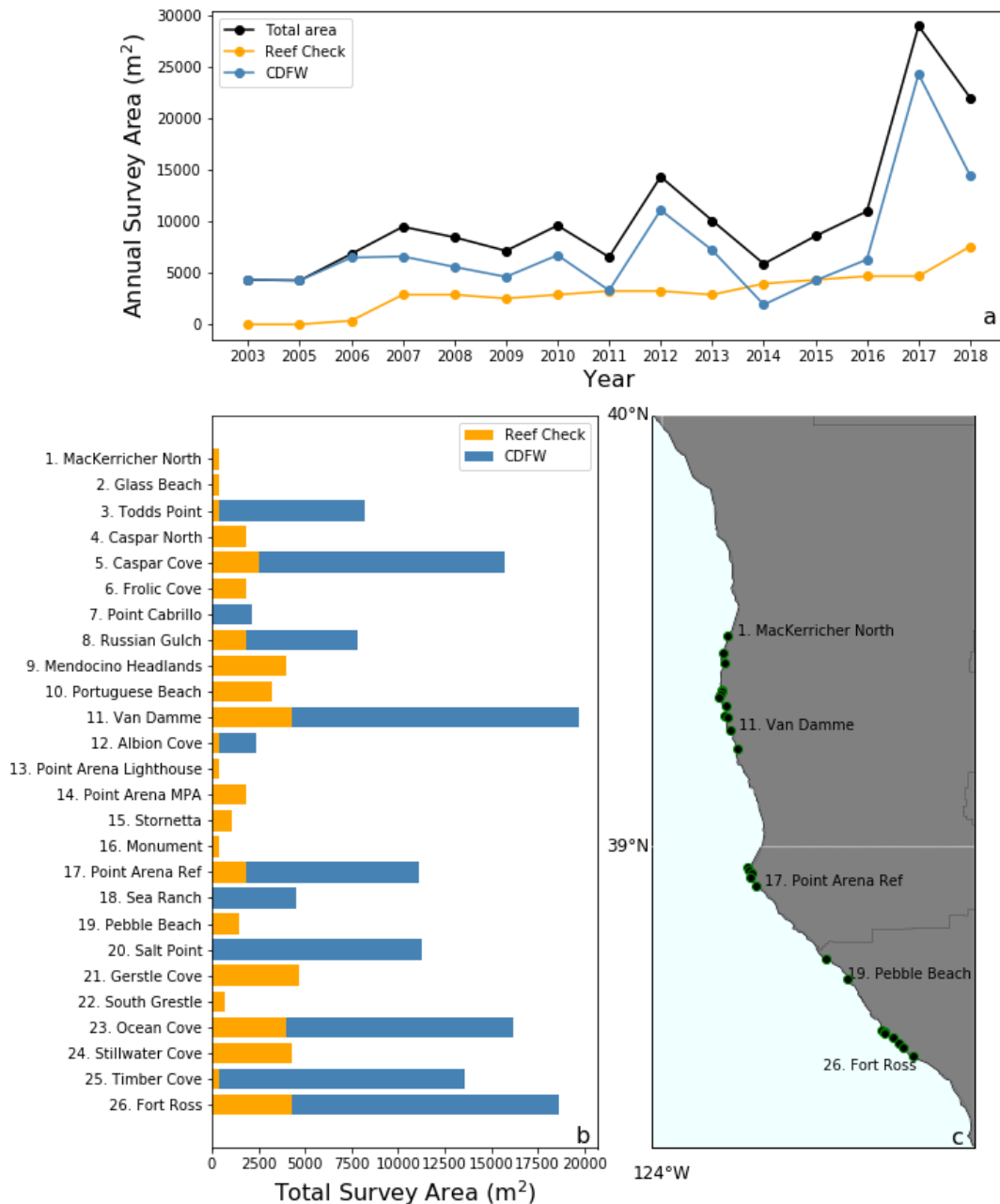
dynamics in the North Pacific Gyre and California Current. Many studies in the NE Pacific have found NPGO to be an important driver of regional kelp dynamics^{10,12,13}.

PDO Index – the Pacific Decadal Oscillation index is derived from the first mode of sea surface temperature variability in the north Pacific poleward of 20°N. Many studies in the NE Pacific have found PDO to be an important driver of regional kelp dynamics^{10,12,13}.

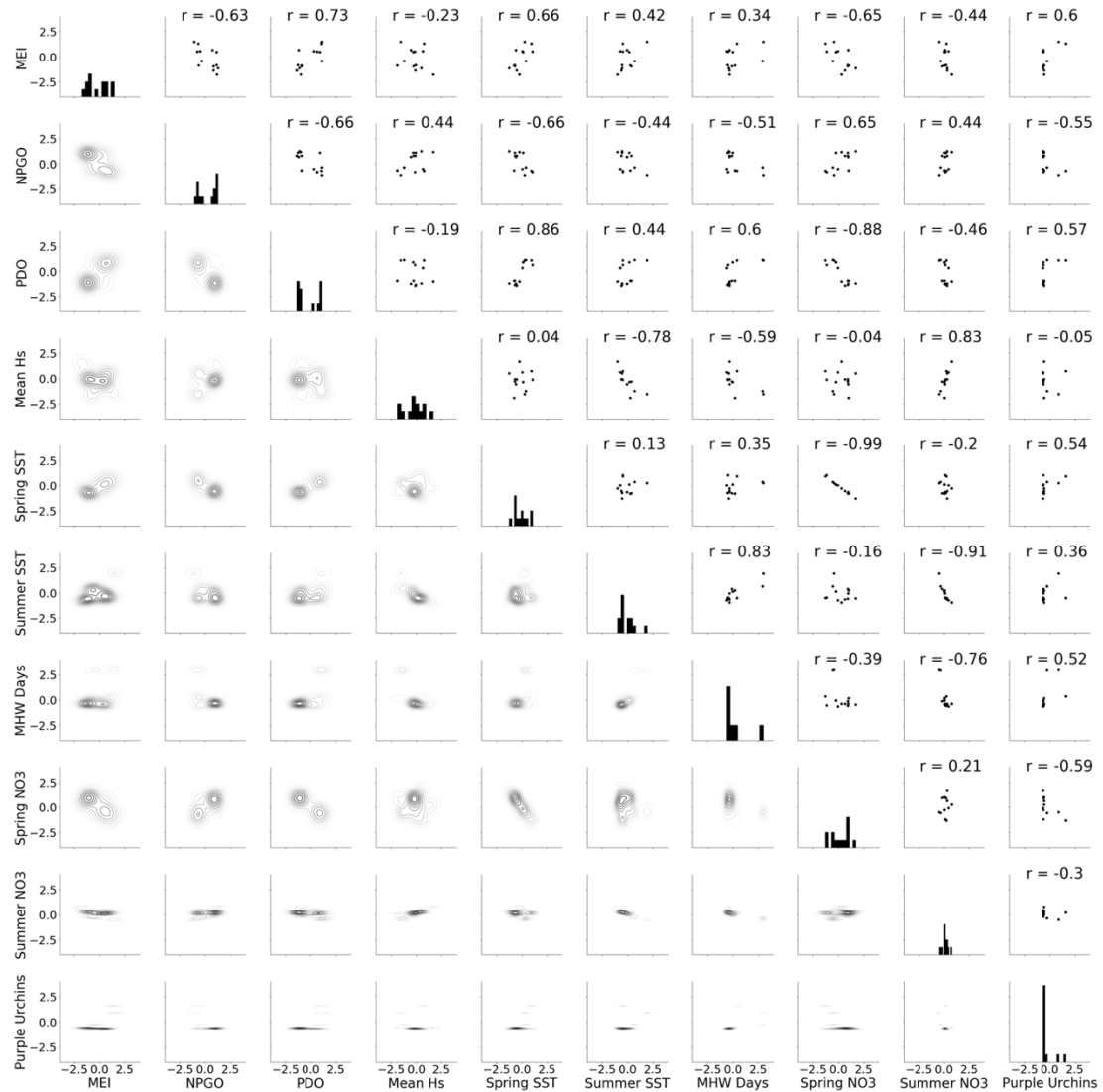
Supplementary Figure 3 (Figure S1.3) – Box and whisker plot for all predictor (environmental and biological) and response (kelp canopy) variables. Variable-wise outliers are defined as datapoints outside 1.5 times the interquartile range ($1.5 \cdot IQR$; black points). Total sample number across the entire variable timeseries is represented by n_t . Sampling frequency (annual, monthly, daily, or hourly) is depicted by the grey boxes near the x-axis.



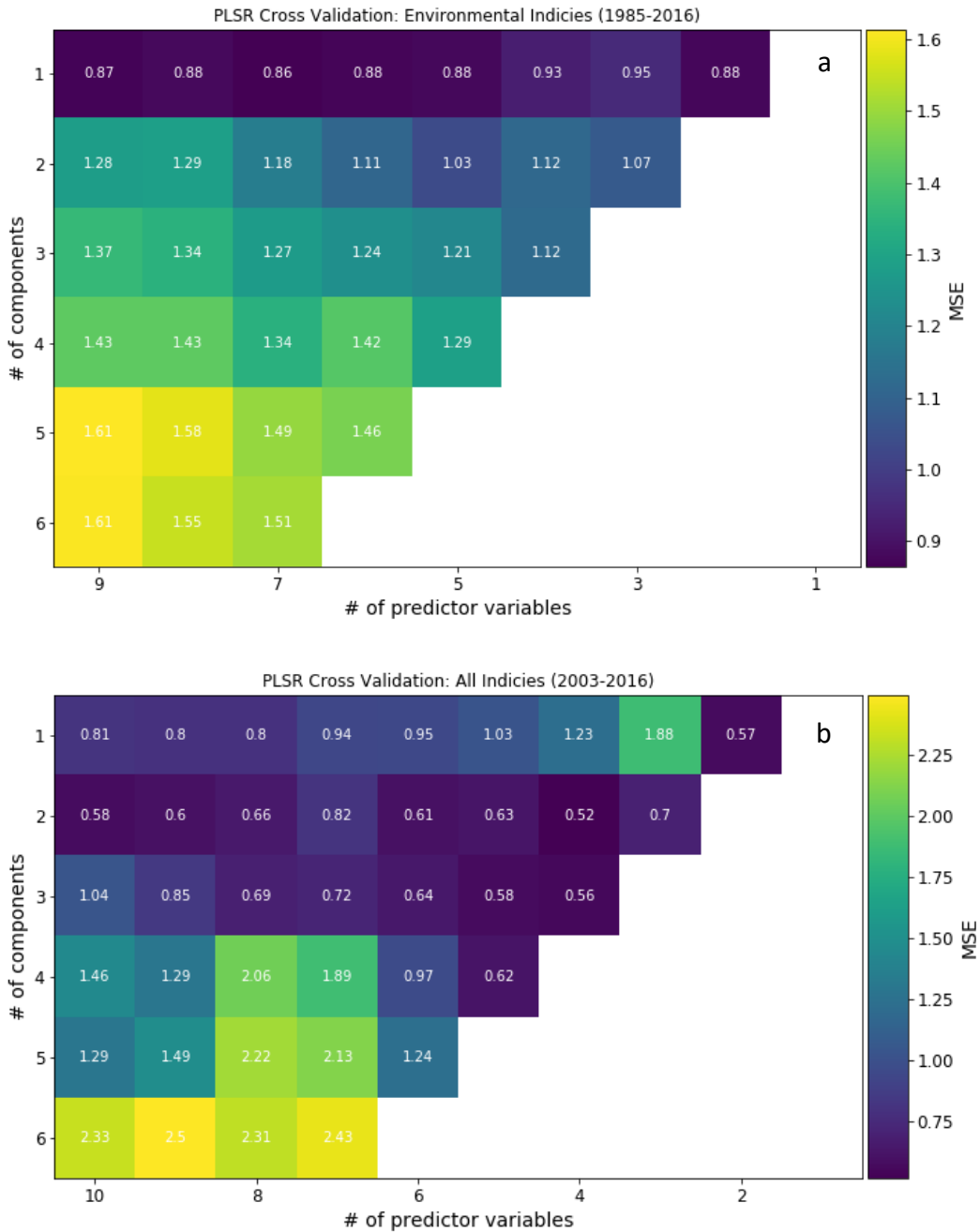
Supplementary Figure 4 (Figure S1.4) – Temporal (a) and spatial (b and c) representation of sub-tidal sampling efforts in Sonoma and Mendocino Counties in the northern California, USA region between 2003 and 2018 by California Department of Fish and Wildlife (CDFW) and Reef Check California.



Supplementary Figure 5 (Figure S1.5) – Correlation matrix of all environmental and biological variables used in the partial least squares regression (PLSR) analysis. The upper panel corner shows the scatter plots Pearson correlation coefficients (r) for each pair-wise relationship. The lower corner shows the kernel density distribution for each pair-wise relationship. The diagonal shows the data distribution for each variable. Strong co-linearity exists between seasonal sea surface temperature (SST) and nitrate (NO_3) conditions.



Supplementary Figure 6 (Figure S1.6)– Partial least squares regression (PLSR) component- and variable-wise cross-validation results presented as the mean squared error (MSE) for (a) environmental indices (1985 – 2016) and (b) environmental and purple urchins (all indices; 2003 – 2016).



Supplemental References

1. McHugh, T., Abbott, D. & Freiwald, J. Phase shift from kelp forest to urchin barren along California's North Coast. in *Western Society of Naturalists* (2018).
2. Hobday, A. J. *et al.* A hierarchical approach to defining marine heatwaves. *Prog. Oceanogr.* **141**, 227–238 (2016).
3. García-reyes, M., Largier, J. L. & Sydeman, W. J. Progress in Oceanography Synoptic-scale upwelling indices and predictions of phyto- and zooplankton populations. *Prog. Oceanogr.* **120**, 177–188 (2014).
4. Vadas, R. L. Ecological implications of culture studies on *nereocystis luetkeana*. *J. Phycol.* **8**, 196–203 (1972).
5. Wheeler, W. N., Smith, R. G. & Srivastava, L. M. Seasonal Photosynthetic Performance of *Nereocystis-Luetkeana*. *Can. J. Bot. Can. Bot.* **62**, 664–670 (1984).
6. Springer, Y., Hays, C., Carr, M., Mackey, M. & Bloeser, J. Ecology and management of the bull kelp, *Nereocystis luetkeana*: A synthesis with recommendations for future research. 48 (2006).
7. Tegner, M. J. M. & Dayton, P. K. P. El Nino effects on southern California kelp forest communities. *Adv. Ecol. Res.* **17**, 243–279 (1987).
8. Friedlander, A. M. *et al.* Kelp forests at the end of the earth : 45 years later. *PLoS One* **15**, 1–23 (2020).
9. Tally, L. ., Pickard, G. L., Emery, W. J. & Swift, J. H. *Descriptive Physical Oceanography: An Introduction.* (Elsevier Ltd., 2011).
10. Cavanaugh, K. C., Siegel, D. A., Reed, D. C. & Dennison, P. E. Environmental controls of giant-kelp biomass in the Santa Barbara Channel, California. *Mar.*

KELP PATCH-SPECIFIC CHARACTERISTICS LIMIT DETECTION CAPABILITY OF RAPID SURVEY METHOD FOR DETERMINING CANOPY BIOMASS USING REMOTE SENSING TECHNIQUES

Meredith L. McPherson and Raphael M. Kudela

Abstract

Restoration and cultivation of kelp forests is a potential tool for both habitat protection and carbon sequestration in response to global climate change. However, accurate estimates of biomass are required to determine carbon export and burial rates. Remote sensing data are advantageous for deriving region-specific estimates of carbon pools and quantifying regional and global rates of carbon sequestration by canopy-forming kelp. However, development and validation of these metrics is lacking in the scientific literature because most remote observation of kelp utilizes canopy area rather than biomass. This study attempted to close that gap by exploring and validating sub-regional differences in canopy biomass estimates. Kelp sporophytes were collected and measured for morphometric characteristics and genera-specific allometry to canopy biomass. Kelp density was measured using a rapid *in situ* diver survey approach and coupled with unmanned aerial vehicle (UAV) imagery to quantify kelp canopy biomass at a range of pixel spatial resolutions (ground sampling distance). We successfully determined kelp canopy biomass from UAV imagery at 33% of the survey sites, but consistently determining canopy biomass from remote sensing at a variety of spatial resolutions was challenged by kelp patch-specific spatial characteristics. The morphologies of bull kelp in Monterey were significantly different than other regions measured, which means that sub-regional differences should be considered when

making estimates of canopy biomass using remote sensing. Although the use of kelp canopy area in both scientific and monitoring applications continues to be relevant for a wide range of applications, further work is required to understand differences in canopy biomass at the regional and sub-regional scale. As such, we recommend implementing long-term monitoring programs across the northeast Pacific region and beyond to validate remote sensing derived biomass estimates beyond the small number of existing well-characterized sites.

Introduction

Kelp forests are highly productive and diverse nearshore systems that thrive in temperate and Arctic regions (Steneck et al., 2002). Spanning approximately 25% of the world's coastlines (Wernberg et al., 2019), these biogenic habitats support a range of goods and services of ecological (three-dimensional habitat structure, biodiversity, nutrient cycling, etc.) and economic (coastline defense, recreational and commercial fisheries, harvestable biomass) value (Teagle et al., 2017). Kelp forests are also threatened by the influence of anthropogenic factors such as climate change (Wernberg et al., 2016; Rasher et al., 2020), increasing frequency and intensity of marine heatwaves (Oliver et al., 2017; Cavanaugh et al., 2019; Straub et al., 2019; Dexter et al., 2020; McPherson et al., 2021), and overfishing (Ling et al., 2009). Managers have recently begun promoting restoration, protection, and cultivation of kelp forests as a potential tool for carbon sequestration and ocean acidification amelioration in response to global climate change (Phillips et al., 2018; Macreadie et al., 2019; Crowfoot et al., 2020).

Ecol. Prog. Ser. **429**, 1–17 (2011).

11. Schiel, D. R. & Foster, M. S. *The Biology and Ecology of Giant Kelp Forests*. (2015).
12. Hamilton, S. L., Caselle, J. E. & Hamilton, S. L. Exploitation and recovery of a sea urchin predator has implications for the resilience of southern California kelp forests. *Proc. R. Soc. B* **282**, (2014).
13. Pfister, C. A., Berry, H. D. & Mumford, T. The dynamics of Kelp Forests in the Northeast Pacific Ocean and the relationship with environmental drivers. *J. Ecol.* 1–14 (2017). doi:10.1111/1365-2745.12908

aerial vehicles (UAVs). Historically, the most common kelp mapping approaches have evaluated kelp canopy area rather than biomass because (1) many mapping campaigns are conducted by state natural resource departments that prioritize canopy extent as a metric for kelp as a harvestable and managed natural resource (e.g. California Department of Fish and Wildlife (CDFW), Oregon Department of Fish and Wildlife (ODFW), Washington Department of Natural Resources (WDNR), Alaska Department of Fish and Game, etc.), and (2) species- or region-specific relationships between pixel spectral characteristics and biomass have not been widely developed nor validated. While there is significant value in monitoring kelp canopy area, quantifying rates of primary productivity and carbon sequestration at scales from 10s to 100s km will continue to be limited unless estimates of region and genera-specific biomasses can be derived from remote sensing data. As such, understanding and accurately quantifying canopy biomass parameters at a variety of spatial scales (local, regional, and global) has significant value to scientists and managers.

Studies reporting validation of remote sensing derived estimates of biomass are limited but effective resources to build upon. Stekoll et al. (2006) created the first remote estimates of kelp canopy biomass for *Nereocystis* and *Allaria fistulosa* in southeast Alaska using high spatial resolution (0.5 – 2 m) multispectral (4 band) airborne data and rapid ground truthing techniques in 2002 and 2003. Canopy coverage estimated using normalized difference $[(\rho_{nir} - \rho_{blue})/(\rho_{nir} + \rho_{blue})]$ was validated to biomass by measuring *in situ* density counts and sub-bulb diameter in 16 m² surface quadrats. Cavanaugh et al. (2010, 2011) found a strong correlation between spectral

To date, few studies have explored rates of carbon export and burial from macroalgal habitats (Krause-Jensen and Duarte, 2016; Ortega et al., 2019) and none have explored regional or genera-specific rates, but a global assessment by Krause-Jensen and Duarte (2016) approximate burial rates at 173 TgC yr⁻¹ in coastal and deep sea sediments. These studies are limited by the uncertainties in estimates of total macroalgal extent and the quantity of macroalgal derived carbon (source, export, and burial; Krause-Jensen and Duarte, 2016). Although species distribution models (SDMs) have been used to estimate spatial distribution of non-surface canopy forming kelp biomass (Gorman et al., 2013; van Son et al., 2020), remote sensing and satellite derived data are advantageous for deriving region-specific estimates of carbon pools (biomass) and for quantifying regional and global scale canopy-forming kelp carbon sequestration rates. Furthermore, satellites are more capable of high frequency temporal measurements than *in situ* surveys. This is important because kelp forests and macroalgal habitats are spatially and temporally dynamic (Dayton et al., 1999), where distribution, canopy expression, and biomass are driven by both (1) environmental conditions such as temperature, nutrient availability, and physical disturbance (waves and swell) and (2) patch-level biological and physical factors such as grazing, spore dispersal, and substrate type.

In the northeast Pacific region (Aleutians Islands, Alaska to Baja California, Mexico) giant kelp (*Macrocystis pyrifera*) and bull kelp (*Nereocystis luetkeana*) are the dominant canopy forming kelps and are easily observed with remote sensing techniques, such as plane-based aerial surveys, spaceborne satellites, and unmanned

band information and canopy biomass using 10 m and 30 m spatial resolutions for southern California *Macrocystis* along the Santa Barbara coast (using both normalized difference vegetation index (NDVI) and multiple endmember spectral mixture analysis (MESMA)). This was aided by long-term subtidal monitoring of *Macrocystis* biomass (Rassweiler et al., 2008) within permanent approximately 1600 m² plots. Subsequently, the relationship between MESMA derived pixel kelp fraction and Santa Barbara *Macrocystis* canopy biomass has been used to make regional estimates of canopy biomass from Baja California, Mexico to Año Nuevo, California using USGS Landsat imagery across more than 30 years (Bell et al., 2015; Cavanaugh et al., 2019; Bell et al., 2020b). Despite the robust nature of the satellite-derived canopy biomass for the Santa Barbara coastal sites, there may be significant sub-regional differences in sporophyte morphology and allometry affecting the broader regional validity of this relationship.

In addition to the applicability of biomass predictions, there is increasing motivation to apply higher spatial resolution (<30 m) imagery, to kelp mapping efforts in regions where complex shoreline topography exists (Nijland et al., 2019) and significant kelp canopy declines have occurred (McPherson et al., 2021). To date, a range of platforms with varying spatial resolutions have been applied to kelp mapping efforts (Schroeder et al., 2019). Multispectral USGS Landsat imagery (30 m spatial resolution) has been widely used because of the large temporal and spatial scales at which data are freely available (Cavanaugh et al., 2010, 2011; Bell et al., 2015, 2020b; Young et al., 2015; Beas-luna et al., 2020; Friedlander et al., 2020; McPherson et al.,

2021). Studies comparing the suite of sensors (Landsat 5, 7, and 8) to higher spatial resolution imagery (e.g. CDFW/ODFW aerial survey data, Digital Globe World View-2 imagery) have found that though false positives (water pixels mis-identified as kelp) by Landsat are uncommon, the sensor often misses pixels containing less than 20% kelp (Hamilton et al., 2020; Finger et al., 2021). Furthermore, the difference between relatively high (~ 2 m) and moderate (30 m) spatial resolution is pronounced when canopy coverage is low (Finger et al. 2021; kelp reflectance signals are lower than Landsat's detection capabilities) or coastline features (large tidal range and complex topography) limit detection of fringing kelp beds within a 30 m buffer to the shore (Nijland et al., 2019). Mora-soto et al. (2020) and Huovinen et al. (2020) were the first studies to use European Space Agency (ESA) Sentinel-2 (10 m) imagery to map *Macrocystis*. The creation of a global kelp map by Moro-Soto et al. (2020) was validated against previously surveyed or observed beds, but the approach was not effective at detecting bed sizes < 1 hectare (10,000 m²).

Increasingly, scientists and managers are using UAV platforms to customize and validate kelp mapping efforts. UAVs offer flexibility for studying kelp beds at local, and potentially regional, scales and have applicability in offshore aquaculture (Bell et al., 2020a), satellite remote sensing validation (Bell et al., 2020a; Mora-Soto et al., 2020), and may supplement expensive aerial surveys by resource management/monitoring efforts (Hohman et al., 2019) in some places, despite tradeoffs in the total area covered using UAVs versus other platforms and logistical challenges. Other tradeoffs include local scale variability; Cavanaugh (2020) illustrated the

significance of tidal height and current velocity on changes in kelp canopy area, but the effect was variable across sites. Furthermore, there is potential for quantifying fine-scale physiological and biological metrics using UAVs given sufficient understanding of patch dynamics and the influence of local physical and environmental factors.

Due to the limited validation of biomass across regions and genera, and the wide range of remote sensing data available at a variety of spatial resolutions, we developed a rapid survey approach to determine kelp canopy biomass at a range of spatial resolutions using a UAV. Due to the high spatial resolution of UAV imagery, data can be modified to represent a variety of spatial resolutions by binning to simulate various remote sensing platforms. The aim of this study was to understand the influence of (1) regional differences in allometric relationships for biomass prediction, and (2) complex patch characteristics and spatial resolution on characterizing and determining canopy biomass via remote sensing.

Methods

Survey locations – Six sites along the California coastline were selected for *in situ* diver and remote sensing surveys in July and August 2019 (Figure 2.1; Table 2.1). The length of time between conducting the dive and UAV surveys for sites did not exceed 30 days. Three of the sites consisted of pure *Nereocystis*, two in Mendocino County in northern California and one along the northeastern side of the Monterey Peninsula (Figure 2.1a-

d). The other three consisted of pure *Macrocystis* along the northeastern side of the Monterey Peninsula in central California (Figure 2.1a, e-f). Site locations were chosen based on accessibility to kelp beds, protection from large swell, collection and transport of kelp to shore, and ease of accessibility for UAV flight operations.

Table 2.1. Detailed description of each survey location including region (Mendocino County or Monterey Peninsula), kelp genera, dive site coordinates, dive survey date, UAV survey date, and mean tidal height during each UAV survey.

Site Name	Site Region	Kelp genera	Location	Dive Survey Date	UAV Survey Date	UAV survey tidal height (m)
Noyo Harbor (NH)	Mendocino County	<i>Nereocystis</i>	39.42880 -123.81016	August 7, 2019	August 8, 2019	0.766
Portuguese Beach (PB)	Mendocino County	<i>Nereocystis</i>	39.30283 -123.802	August 8, 2019	August 8, 2019	1.716
Point Piños (PP)	Monterey Peninsula	<i>Nereocystis</i>	36.629691, -121.91903	August 14 and 28, 2019	September 12, 2019	1.337
Otter Cove (OC)	Monterey Peninsula	<i>Macrocystis</i>	36.639664, -121.92801	July 26, 2019	July 2, 2019	1.098
San Carlos Beach (SCB)	Monterey Peninsula	<i>Macrocystis</i>	36.61268 -121.89496	July 22, 2019	July 3, 2019	0.143
Hopkins Marine Station (HMS)	Monterey Peninsula	<i>Macrocystis</i>	36.62162 -121.90198	July 10, 2019	July 5, 2019	0.976

Field surveys of kelp density and biomass – *In situ* surveys were used to develop spatially resolved estimates of canopy biomass for *Nereocystis* and *Macrocystis* across six sites via 1) assessment of subtidal stipe (frond) density and 2) sporophyte collection and morphometric measurement of genera-specific allometry. Results from field-based data were applied in a matchup analysis to pixel-based results from UAV surveys.

Subtidal surveys were designed to rapidly assess stipe density across many kelp beds without employing labor and time-intensive techniques used at permanent sites for biomass estimation by other organizations, such as the SBC LTER in Santa Barbara,

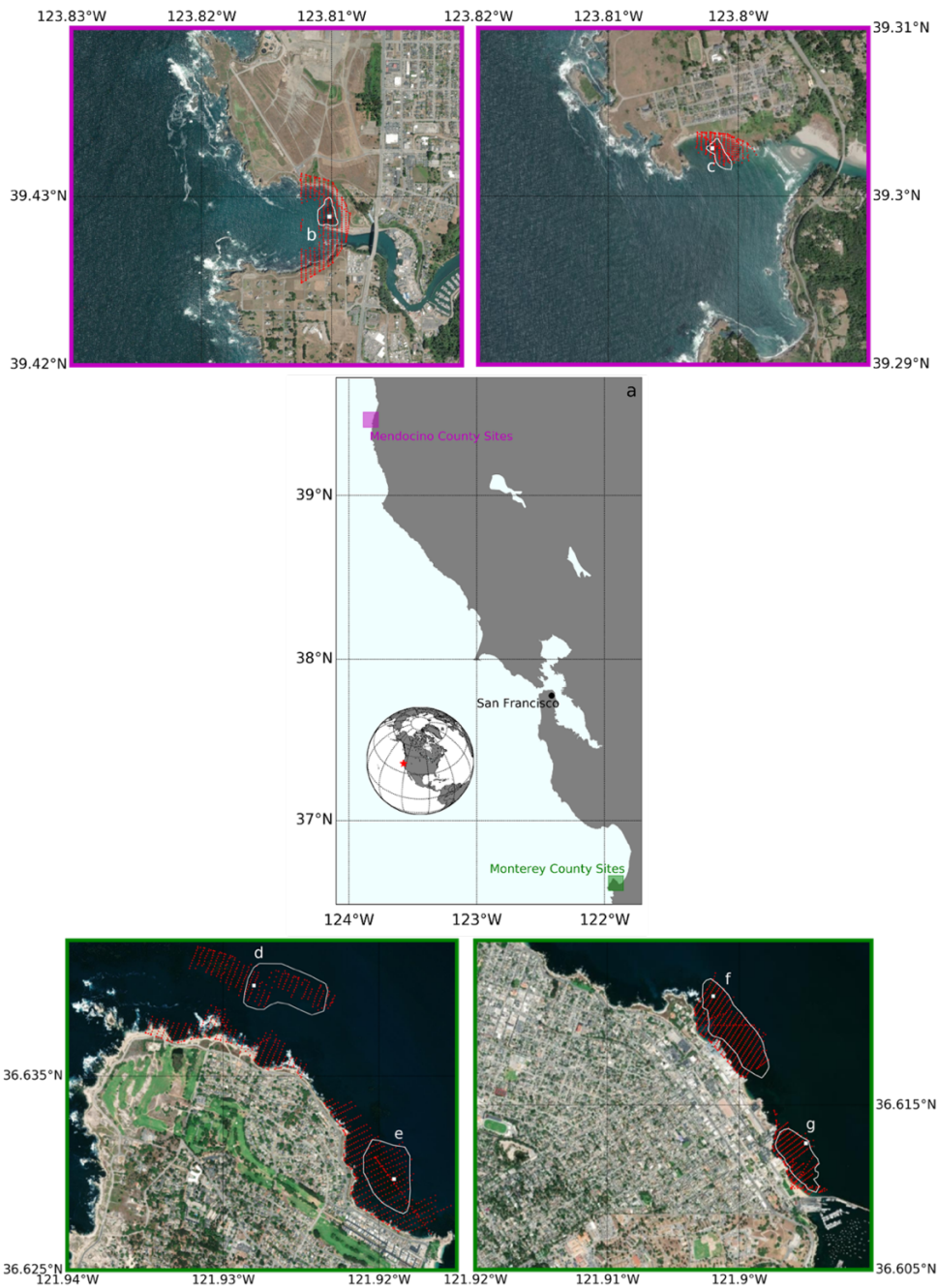


Figure 2.1. a) A map of the California coastline illustrating specific areas where survey sites were located in Mendocino County (magenta box) and Monterey County (green box). Each smaller map, outlined with the color corresponding to Mendocino or Monterey, depicts the stitched mosaic of each UAV image (red points), the outline of the kelp bed within that mosaic (white polygon), and the 3600 m² dive site (white square) for each site: b) Noyo Harbor, c) Portuguese Beach, d) Point Pinos, e) Otter Cove, f) Hopkins Marine Station, and g) San Carlos Beach.

CA. Dive sites consisted of 3600 m² square plots surveyed in a bicycle spoke configuration (Figure 2.1b-g white points and Figure 2.2). At five of the six sites (Portuguese Beach, Point Piños, Otter Cove, San Carlos Beach, and Hopkins Marine Station; Figure 2.2b-f), eight separate transects were conducted. At Noyo Harbor (Figure 2.2a), only 4 of the 8 transects were conducted because ocean conditions limited dive operations. Point Piños was surveyed across two separate days (Table 2.1) because ocean conditions limited dive operations after the first 4 transects were conducted on August 14, 2019.

Survey teams consisted of two divers. One navigated each compass heading (30°, 60°, 120°, 150°, 210°, 240°, 300°, and 330°) and reeled out the transect tape to 40 meters, while the other counted stipes (fronds) within a two-meter swath along the transect tape. Stipe (frond) counts were recorded for every five-meter interval (area = 10 m²), which we have termed the ‘transect interval’. Each individual transect began at the five-meter mark to avoid overlap of stipe (frond) counts at the center of the bicycle spoke. As a result, each complete dive survey consisted of a series of 4 or 8, 70 m² transects or a total dive survey area of 280 m² (Noyo Harbor) or 560 m² (Portuguese Beach, Point Piños, Otter Cove, San Carlos Beach, and Hopkins Marine Station).

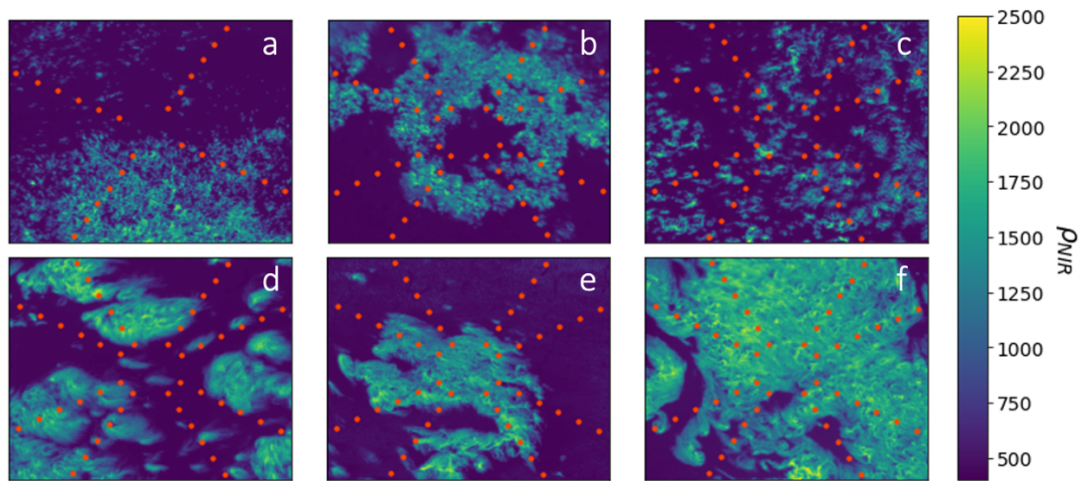


Figure 2.2. Raster images of MicaSense RedEdge-M scaled near-infrared reflectance (ρ_{NIR}) values for each dive survey site: a) Noyo Harbor (NH), b) Portuguese Beach (PB), c) Point Piños (PP), d) Otter Cove (OC), e) San Carlos Beach (SCB), f) Hopkins Marine Station (HMS).

Adult sporophytes (Figure 2.3), defined as the mature stage of the *Nereocystis* and *Macrocystis* diploid lifecycles, were indiscriminately collected for morphometric measurement and canopy biomass determination across multiple locations in central and northern California (Table 2.2) in 2018 and 2019, including five of the six dive sites surveyed in 2019 (Noyo Harbor, Point Piños, Otter Cove, Hopkins Marine Station, and San Carlos Beach). Specifically, we measured morphology at 4 sites for *Macrocystis* (total of 11 sporophytes) in 2019 and 6 sites for *Nereocystis* (total of 86 sporophytes) in 2018 and 2019 (Table 2.2). Divers removed sporophytes from the substrate manually by cutting the primary stipe just above the holdfast (Figure 2.3), brought them to the surface and then to shore where morphometric measurements were conducted on a clean surface (Figure S2.1b-f). When tissue hydration could not be maintained using fresh seawater, a portable pop-up tent was used to shade samples (Figure S2.1c and d).

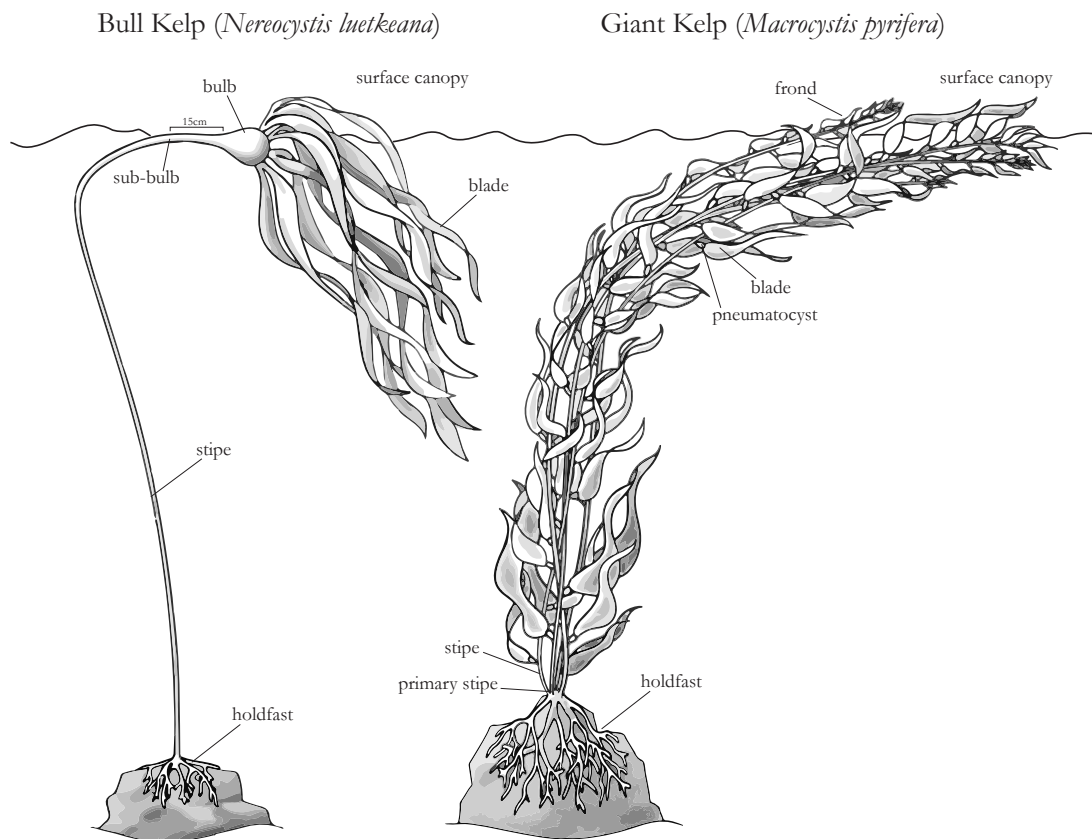


Figure 2.3. Relevant morphometric characteristics of *Nereocystis* and *Macrocystis* adult sporophytes (image credit: Niky Taylor; UCSC).

Nereocystis morphometric measurements were made for stipe length and width, bulb diameter, sub-bulb diameter (15 cm below the base of the bulb), longest blade length/width, longest blade weight, number of blades, canopy weight (top 1 m of stipe including all the blade biomass), stipe weight, and total plant weight (Figure 2.4d; n = 86). Central and northern California data from 2018 and 2019 were combined with data collected on the western coastline of Prince of Wales Island, Alaska in 2018 (Pearson et al. 2019; Figure 2.4d; n = 55).

Table 2.2. Detailed information of site-specific sporophyte collection including site name, region, kelp genera, latitude/longitude, and collection dates.

Site Name	Site Region	Kelp genera	Location	Collection Date(s) - # of sporophytes
Casper Cove	Mendocino County	<i>Nereocystis</i>	39.36218 -123.81973	Sept. 17, 2018 – 10
Albion Cove	Mendocino County	<i>Nereocystis</i>	39.22754 -123.77197	Sept. 18, 2018 – 15
Bodega Marine Lab	Sonoma County	<i>Nereocystis</i>	38.31094 -123.07061	Sept. 25, 2018 – 17
Noyo Harbor	Mendocino County	<i>Nereocystis</i>	39.42865 -123.81221	Sept. 19, 2018 – 12 Aug. 7, 2019 – 22
Point Piños	Monterey Peninsula	<i>Nereocystis</i>	36.64104 -121.93052	Aug. 28, 2019 – 10
Hopkins Marine Station	Monterey Peninsula	<i>Macrocystis</i>	36.62162 -121.90198	July 8, 2019 – 2 July 10, 2019 – 1 July 17, 2019 – 1
San Carlos Beach	Monterey Peninsula	<i>Macrocystis</i>	36.61266 -121.89496	July 22, 2019 – 1 July 31, 2019 – 1
Ocean Cove	Monterey Peninsula	<i>Macrocystis</i>	36.62969 -121.91903	July 26, 2019 – 1 Aug. 8, 2019 – 1 Aug. 26, 2019 – 1
Steamer Lane	Santa Cruz	<i>Macrocystis</i>	36.95174 -121.02295	Aug. 16, 2019 – 2

Macrocystis sporophytes were divided into 2 sections, the sub-surface canopy and surface canopy (Figure 2.3). The surface canopy was determined by measuring the depth of the holdfast prior to collection. Within each section, morphometric measurements were made for total tissue weight and number of fronds. Central California *Macrocystis* data were combined with SBC LTER measurements of canopy biomass and frond counts from 2002 and 2003 (Nelson et al. 2021; Figure 2.4e; n = 36). For both genera, lengths were measured to the nearest mm using a diver transect

tape and weights were measured to the nearest 0.01 kg using a portable electronic balance.

Table 2.3. ANCOVA results for the effect of region (and seasons for *Macrocystis*) on the slope and intercepts of the relationship between the dependent variable (bulb diameter or frond count) and canopy biomass. * denotes significance.

Genera	Group	Degrees of freedom (df)	F	p-value	Effect size
<i>Nereocystis</i>	Location	2	11.6	*2.3 x 10 ⁻⁵	0.15
<i>Nereocystis</i>	Bulb Diameter (cm)	1	84.7	*5.3 x 10 ⁻¹⁶	0.38
<i>Macrocystis</i>	Location	2	2.6	8.5 x 10 ⁻²	0.074
<i>Macrocystis</i>	Sporophyte frond	1	44.6	*6.9 x 10 ⁻⁹	0.41

Sub-bulb diameter was the strongest predictor of both whole *Nereocystis* and canopy biomass ($r^2 = 0.56$ and 0.44 , respectively), and was consistent with Stekoll et al. (2006) for bull kelp in Alaska. Bulb diameter was the second strongest predictor of whole *Nereocystis* and canopy biomass ($r^2 = 0.51$ and 0.43) and was used in this study to estimate *in situ* canopy biomass from subtidal counts of stipe density because bulb diameter could be quickly measured by divers or from a boat at the surface of the kelp canopy.

At each *Nereocystis* dive site measurements of bulb diameter were indiscriminately measured within the 3600 m² dive survey plot. Both sites displayed a gaussian probability distribution of diameters (Figure 2.4a-c). Though the range of bulb diameter at Point Piños (Figure 2.4c; 7.06 ± 0.96 ; $n = 148$) was slightly larger than Noyo Harbor (Figure 2.4a; 6.50 ± 0.76 ; $n = 80$) and Portuguese Beach (Figure 2.4b; 6.44 ± 0.64 ; $n = 79$), their means and standard deviations were similar.

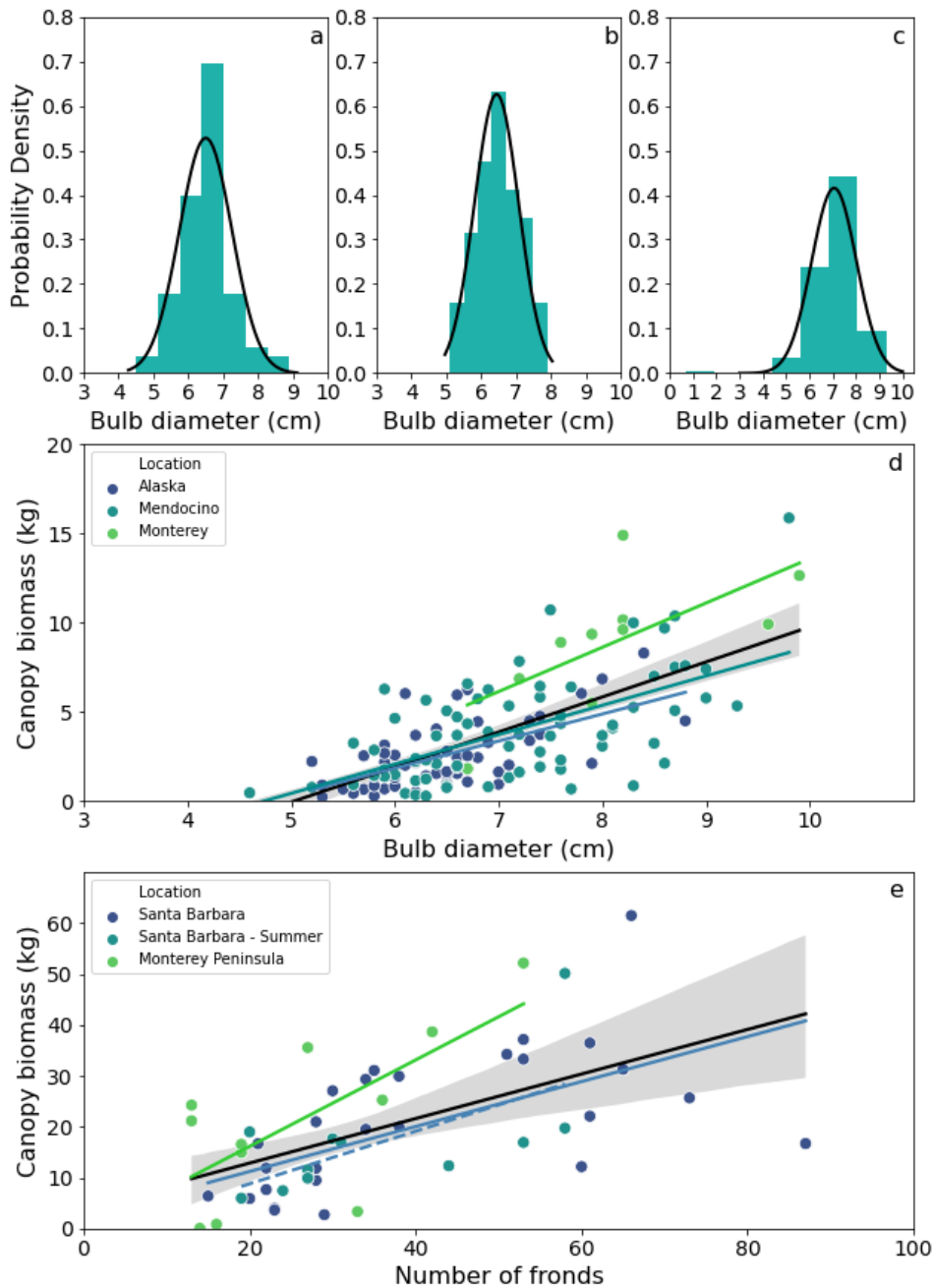


Figure 2.4. The probability distribution of *Nereocystis* bulb diameter for a) Noyo Harbor, b) Portuguese Beach, c) Point Piños. d) Scatter plot of *Nereocystis* canopy biomass against bulb diameter fitted with linear regressions for Alaska (blue line), Mendocino (teal line), Monterey (green line), and all regions combined (black line). e) Scatter plot of *Macrocystis* canopy biomass against frond number fitted with linear regressions for all data from Santa Barbara, CA (blue line), summer data from Santa Barbara (blue dashed line), Monterey, CA (green line), and all regions combined (black line). Regression details listed in Table S2.1. Grey shaded areas represent regression 95% CI.

The mean bulb diameter was then used to determine the mean canopy biomass per sporophyte at each dive site using the relationships developed in Figure 2.4d. The total biomass for each transect interval (10 m²) was determined by taking the product of the stipe counts within each transect interval and the site-specific mean canopy biomass per sporophyte.

At each *Macrocystis* dive site the total canopy biomass per transect interval was determined with the relationship developed for the Monterey Peninsula (Figure 2.4e) using the total number of fronds counted within each transect interval to calculate the corresponding canopy biomass. For both *Nereocystis* and *Macrocystis* allometric relationships presented in Figure 2.4, an ANCOVA and post-hoc Tukey Test was run using the Python 3.1 *pingouin* statistics module (Vallat 2018) to determine the effect of region (and season) on the slope and intercepts of the relationship between the dependent variable (bulb diameter or frond count) and canopy biomass.

UAV data acquisition and processing – High resolution multispectral imagery were obtained at each site (Table 2.1) using a DJI Matrice 100 quadcopter mounted with a MicaSense RedEdge-M. The RedEdge-M simultaneously captures data in five spectral bands, the blue (475 nm), green (560 nm), red (668 nm), red-edge (717 nm), and near-infrared (NIR; 840 nm) (See Table S2.1 for FWHM). The RedEdge-M was equipped with a downwelling light sensor (DLS) for all flights. To calibrate reflectance for each flight, we imaged a spectral calibration panel with known reflectance before, during, and after each flight. Our along-track overlap between consecutive images was 80% and side-track overlap between consecutive flight lines was 75%. Sun glint can distort

the reflectance of pixels when imagery is collected when the sun is at or close to zenith (90°). To avoid glint contamination, we conducted flights at or close to optimal sun angle (~45°).

RedEdge-M imagery was processed in the photogrammetric software Pix4D Mapper (Pix4D, 1008 Prilly, Switzerland). Raw images with pixel values in digital numbers (DN) were converted to radiance ($\text{W}/\text{m}^2/\text{nm}/\text{sr}$) using a built-in radiometric calibration. Radiance was then converted to reflectance and mosaicked into orthomosaics. The stitched orthomosaics for each spectral band were exported as GeoTIFFs. Individual band orthomosaics were then merged and subset to the appropriate dive site coordinates (Table 2.1) using the Python 3.1 functions *gdal_translate* and *gdalwarp* (GDAL/OGR Contributors 2021), respectively. UAV imagery from each site was binned to 5 different spatial resolutions (0.1 m, 3 m, 5 m, 10 m, and 30 m) using the Python 3.1 function *gdalwarp* and average interpolation as the resampling method. The 3, 5, 10, and 30 m spatial resolutions were chosen for this analysis because of the availability of existing and historical satellite imagery at these four resolutions and their applicability to kelp monitoring. The relevant sensors include PlanetScope (3 m), Planet RapidEye (5 m), ESA Sentinel-2 (10 m), and Landsat (30 m) of which the relevant wavelengths for detecting kelp are described in Table S2.1.

Pixel based kelp detection - Multiple Endmember Spectral Mixture Analysis (MESMA) was used to determine the fractional coverage of kelp within each imaged pixel. MESMA was originally developed for terrestrial systems by Roberts et al. (1998). MESMA calculates the spectral similarity of a given pixel to one or more

reference spectra, termed endmembers. This method has been applied in *Macrocystis* and *Nereocystis* systems using a two-endmember model (kelp and water) for 30 m resolution USGS Landsat 7 and Landsat 8 imagery with specific endmembers developed for each kelp genera and sensor (Cavanaugh et al., 2011; Bell et al., 2015, 2020a; Hamilton et al., 2020; Finger et al., 2021; McPherson et al., 2021). We used endmember average root mean square error (EAR) analysis (Dennison and Roberts, 2003) to determine a single kelp endmember that best represented the entire RedEdge-M library of *Macrocystis* and *Nereocystis* kelp spectra.

Matchup analysis between UAV and diver-based data – A matchup analysis was conducted to compare *in situ* derived canopy biomasses to MESMA derived kelp fractions at 5 different spatial resolutions (0.1 m, 3 m, 5 m, 10 m, and 30 m). This analysis was used to determine the influence of pixel resolution on canopy biomass detection via a pixel's MESMA kelp fraction. For resolutions less than 30 m, where a single pixel overlapped with no more than one transect interval location per pixel, a matchup was defined as all pixels whose center points fell within a 5 m radius to the center of the transect interval. All pixels that fell within the radius were averaged, resulting in a single mean kelp fraction per transect interval location. For 30 m resolution imagery, a matchup was defined as the average of all canopy biomass values within a single pixel resulting in a single mean canopy biomass per 30 m pixel kelp fraction. An ANCOVA was run using the Python 3.1 pinguin statistics module to determine the effect of pixel resolution (covariate) and site (covariate) on the slope of

the relationship between MESMA kelp fraction and canopy biomass (dependent variable).

Semi-variogram analysis – A geostatistical approach was used to model kelp patch spatial autocorrelation by calculating the semi-variance of each dive site’s MicaSense RedEdge-M NIR reflectance (ρ_{NIR}) at 10 cm pixel resolution (Figure 2.2). We used the Python 3.1 Variogram and DirectionalVariogram classes within the SciKit-GStat (skgstat) module to determine the semi-variance (γ), which can be described as half of the measured variance between pairs of values separated by an increasing lag distance between pixels (h):

$$\gamma(h) = \frac{1}{2N(h)} * \sum_{i=1}^{N(h)} (\rho_{NIR}(x_i) - \rho_{NIR}(x_{i+h}))^2 \quad Eq. (1)$$

where ρ_{NIR} are the observations at locations x_i and x_i+h and $N(h)$ is the number of point pairs at that lag. Semi-variance parameters were estimated by fitting spherical models to the empirical semivariograms:

$$\gamma = \eta + C * (1.5 * \frac{h}{r} - 0.5 * \frac{h^3}{\alpha}) \quad Eq. (2)$$

where η is the nugget, C is the sill, and α is the range. The η describes the total unresolved variability, or noise, while C describes the total resolved variability. The α describes the distance at which the semi-variance reaches a maximum and, therefore, the distance of spatial autocorrelation. Spherical models are ideal when the increase in semi-variance is steep or being estimated within a small region (such as the 60 m length scale of this study). Because some kelp beds exhibit anisotropy, we first calculated and modeled the directional (north-south and east-west) semi-variance of each site.

Anisotropy was manually determined by comparing the sill (C), nugget (η), and range (α) for each site's directional semi-variograms. Since α indicates autocorrelation, and therefore patch-size, we used significant α differences between north-south and east-west to determine anisotropy at each individual site. While differences in C were observed, the differences in α between the directional semi-variances were small. As such we concluded that the survey sites used in this study are relatively isotropic.

Results

Region-specific differences in morphology were detected for *Nereocystis* (Figure 2.4d), but not *Macrocystis* (Figure 2.4e). ANCOVA results indicated that there were significant differences between *Nereocystis* bulb diameters measured across different locations (Alaska, Mendocino County, and the Monterey Peninsula). Post-hoc Tukey Tests (Table 2.2) revealed that the morphology of Monterey Peninsula *Nereocystis* (Figure 2.4d; green lines) were significantly different from the morphology of *Nereocystis* in Alaska and Mendocino. Conversely, ANCOVA results indicated that there was not a significant difference between canopy biomass characteristics for *Macrocystis* allometry (Monterey Peninsula and Santa Barbara).

Table 2.4. ANCOVA results from regression slopes across all sites and resolutions presented in Figure 2.5 and Table S2.2. * denotes significance.

Group	Degrees of freedom (df)	F	p -value	Effect size
Site	5	100.8	* 5.1×10^{-12}	9.7×10^{-1}
Pixel Resolution	1	2.2×10^{-2}	8.7×10^{-1}	1.7×10^{-4}

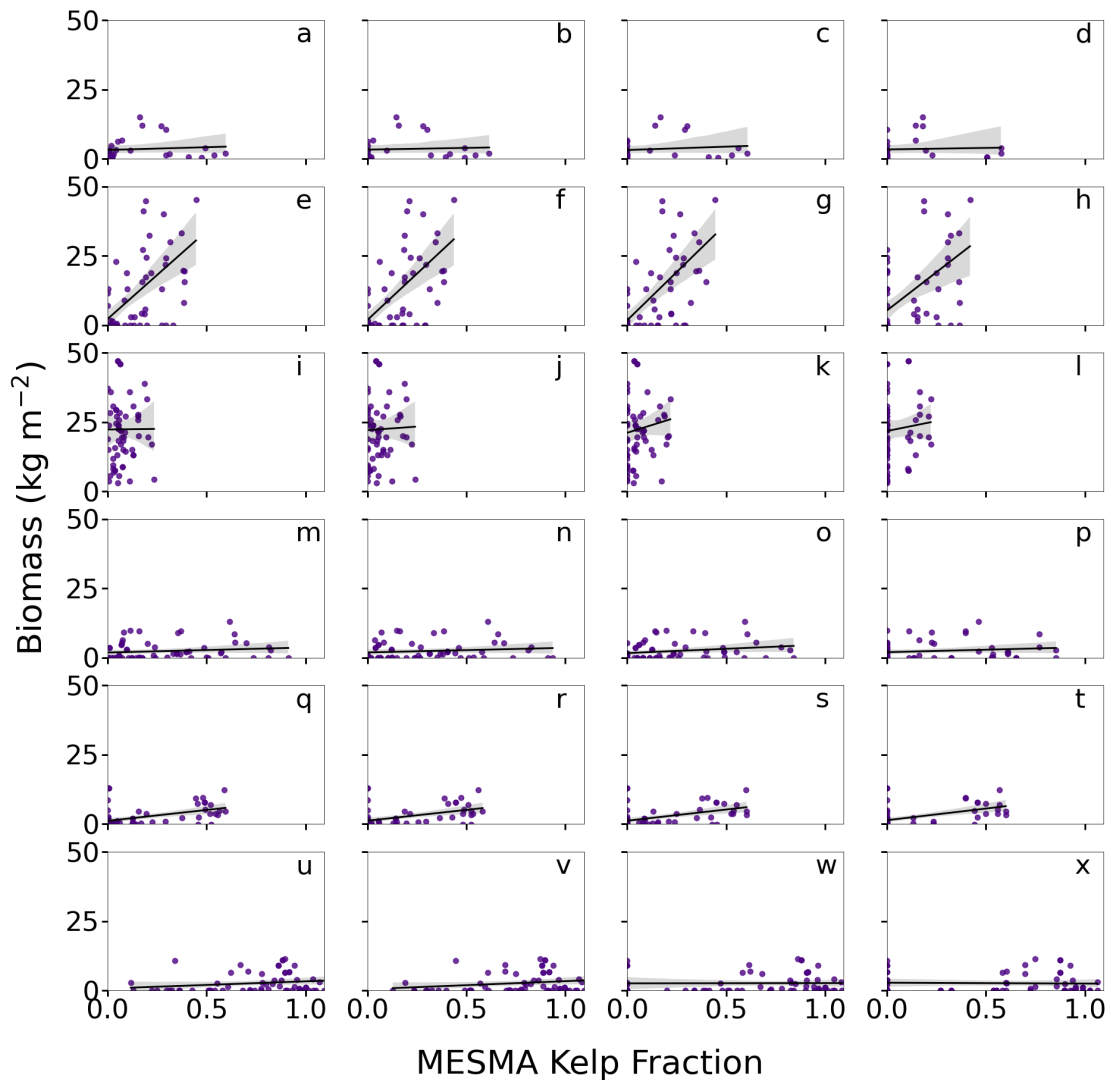


Figure 2.5. Canopy biomass against matchups of MESMA kelp fraction for each site (down) and resolution (across; 0.1 m, 3 m, 5 m, 10 m) for a-d) Noyo Harbor; e-h) Portuguese Beach; i-j) Point Piños; m-p) Otter Cove; q-t) San Carlos Beach; u-x) Hopkins Marine Station with OLS regression (black lines) and 95% confidence intervals (grey shading). See Table 2.4 for regression statistics. Grey shaded areas represent regression 95% CI.

Across all six central and northern California study locations, site characteristics dominated the relationship between MESMA kelp fraction and canopy biomass (Figure 2.5; Table 2. Table 2.4; Table S2.3). A strong predictive relationship between canopy biomass and kelp fraction was observed at two of the study sites,

Portuguese Beach (*Nereocystis*; Figure 2.5e-h) and San Carlos Beach (*Macrocystis*; Figure 2.5q-t), for 0.1 m, 3 m, 5 m, and 10 m pixel resolutions (Table S2.3).

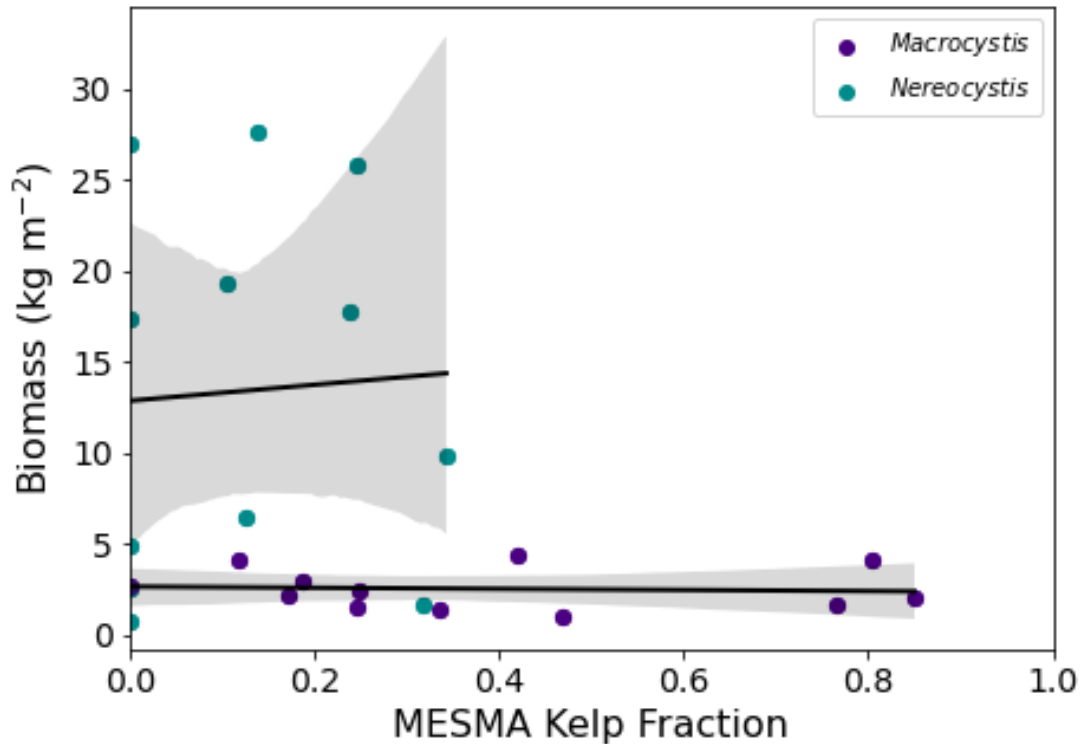


Figure 2.6. Genera specific matchups of canopy biomass and MESMA kelp fraction for 30 m resolution data. The relationships include all possible pixel matchups across the three sites for each genus ($n = 12$ matchups per genera). Grey shaded areas represent regression 95% CI.

No significant relationship was observed for 30 m resolution relationships between MESMA kelp fraction and canopy biomass for *Nereocystis* or *Macrocystis* combined across all six sites (Figure 2.6). Both measured canopy biomass and mean kelp fraction values ranged significantly across sites (Figure 2.5). Portuguese Beach (Figure 2.5e-h) had the largest range in canopy biomass (0 – 63.3 kg m⁻²) and Point Piños exhibited the smallest range in kelp fraction (0 – 0.25). Conversely, Hopkins Marine Station (Figure 2.5p-t) had the smallest range in canopy biomass (1.7 – 9.7 kg m⁻²), and the largest range in kelp fraction (0 – 1.04). ANCOVA results (Table 2.4) of the effect of pixel

resolution and site characteristics on the slope of the relationship between canopy biomass and kelp fraction (Figure 2.5; Table S2.3) indicate that site characteristics drove the variability in regression slope across the survey sites (p -value = 5.1×10^{-12}), rather than the pixel resolution (p -value = 8.7×10^{-1}).

Table 2.5. Estimates of the range (a), nugget (η), and sill (C) from semi-variogram analysis on ρ_{NIR} data shown in Figure 2.2. * represents statistical significance.

Site	Range – a (m)	Nugget - η	Sill – C	Slope of <i>in situ</i> biomass (kg m ⁻² /m)	p -value of <i>in situ</i> biomass slope
NH	>60	3.5×10^{-13}	6170.5	-3.4×10^{-3}	9.1×10^{-1}
PB	17.9	0.99	987.0	-4.4×10^{-1}	* 9.97×10^{-3}
PP	33.9	0.99	26.0	-9.9×10^{-2}	3.7×10^{-1}
OC	>60	0.99	1827.0	4.8×10^{-3}	8.5×10^{-1}
SCB	34.2	0.99	6311.8	-9.6×10^{-2}	* 1.3×10^{-2}
HMS	>60	0.99	1229.7	4.3×10^{-2}	5.5×10^{-2}

Distinct spatial patterns existed in the canopy structure across the survey sites (Figure 2.7a-f; Table 2.5). Unlike Noyo Harbor (Figure 2.7a) and Hopkins Marine Station and (Figure 2.7f), a clear negative exponential trend emerged for Portuguese Beach (Figure 2.7b) and San Carlos Beach (Figure 2.7c). The range (a ; Table 2.5), which represented the distance at which pixel ρ_{NIR} values no longer displayed autocorrelation, for the two sites were 17.9 m and 34.2 m, respectively. Ranges from Noyo Harbor, Otter Cove, and Hopkins Marine Station were > 60 m, beyond the spatial scale of the survey site. There did not appear to be any trend in the images unresolved variability (η) or resolved variability (C) across the four sites (Table 2.5). The spatial structure observed within the canopy via ρ_{NIR} was mirrored in the *in situ* along-transect canopy biomass

measurements (Figure 2.7e-g). The along-transect view of each individual transect (grey) and mean of all transects (black) show spatial structure in the *in situ* biomasses for Portuguese Beach (Figure 2.7g) and San Carlos Beach (Figure 2.7j) where the slope of the mean along-transect biomass values was significant for these two sites (Table 2.5). The Point Piños kelp bed appeared to be an exception to the pattern observed across the other sites. Although there was no significant pattern observed in the slope of the *in situ* biomass, a was 33.9 m.

Discussion

Regional and site-specific validation of remote sensing derived canopy biomass estimates for *Nereocystis* and *Macrocystis* is noticeably lacking from the scientific literature. We showed the limitations of applying a single relationship derived from one location to disparate sites and that reliable, consistent quantification of biomass is difficult and highly dependent on specific patch characteristics and spatial variability across sites. These factors influenced the ability to make accurate assessments of canopy biomass across a range of spatial resolutions appropriate for detecting kelp canopy using remote sensing (Figure 2.5; Figure 2.7; Table 2.3 -2. Table 2.5; Table S2.2).

Significant regional differences in allometric relationships for canopy biomass existed between Monterey *Nereocystis* and other regions investigated (Figure 2.4). Though there were no observed differences in the relationship between Santa Barbara *Macrocystis* canopy biomass and frond count when considering seasonal effects (Figure 2.4e), the relationship for Monterey *Macrocystis*, which were all measured in summer 2019, exhibited a different slope than Santa Barbara. Seasonal differences in

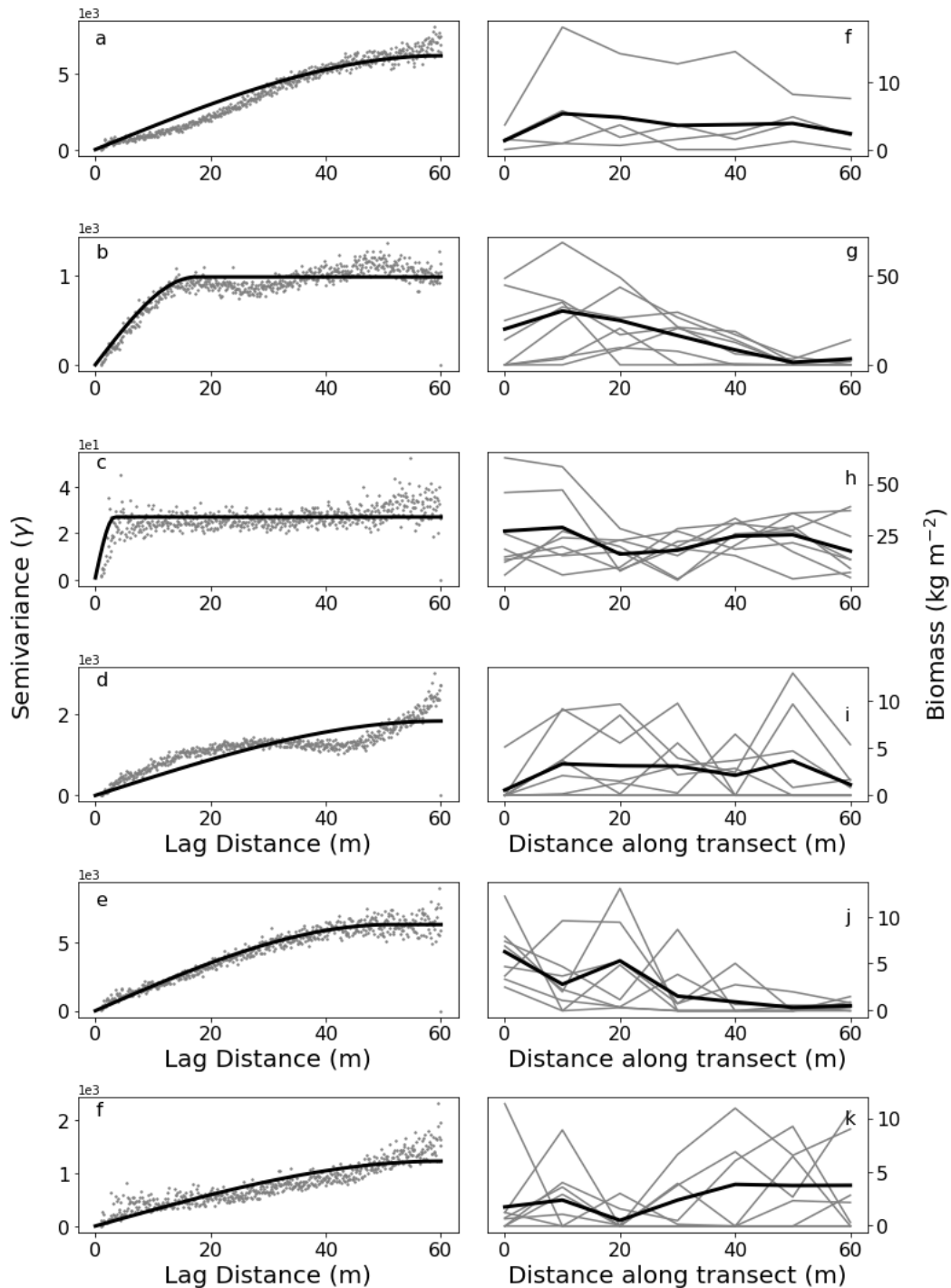


Figure 2.7. Left column: Semi-variogram (spherical model fit) for each station. Right column: Site-specific transect canopy biomass (grey lines) with mean transect canopy biomass (black line) a,f) Noyo Harbor; b,g) Portuguese Beach; c,h) Point Pinos; d,i) Ocean Cove; e,j) San Carlos Beach; f,k) Hopkins Marine Station.

kelp canopy expression patterns may be driving small differences between canopy biomass and frond count as a result of physical and environmental drivers between Santa Barbara and central California (Bell et al., 2020b). While differences between regions are small, it is important to recognize these differences and take them into account when making canopy biomass estimates via remote sensing platforms across large spatial domains.

The *in situ* diver survey approach developed in this study was similar to methodology for Landsat derived *Macrocystis* canopy biomass (Rassweiler et al., 2008; Cavanaugh et al., 2011) and aerial survey derived Alaska *Nereocystis* biomass (Stekoll et al. 2006) in that disparate kelp beds were measured to quantify canopy biomass and then associated with spectral characteristics of kelp canopy. However, the goal of this *in situ* survey design was to rapidly assess as many large sites (3600 m²) as possible by only collecting stipe (frond) counts within each 5-m section of the transect. The bicycle spoke pattern allowed us to have 8 transects of reasonable length (35 m) within each survey site. By assessing a large area, we could then compare *in situ* measurements of canopy biomass to a range of pixel spatial resolutions. Ultimately, this particular survey approach shed light on (1) the influence of patch dynamics and characteristics on determining canopy biomass, and (2) the significant advantages of site-specific long-term monitoring for determining canopy biomass. Neither the SBC LTER or Stekoll et al. (2006) sampling approaches considered the influence of patch dynamics or spatial resolution on remote sensing derived canopy biomass estimates.

Semi-variance patterns (Figure 2.7) indicated that if a kelp patch was larger than the spatial area of the dive survey (i.e. a break down in autocorrelation did not occur within the survey area; $a > 60$ m), we were limited in our ability to develop a robust working relationship between canopy biomass and kelp fraction using this dive survey method. If the kelp patch was smaller than the spatial area of the dive survey (i.e., pixel autocorrelation broke down within the dive survey area; $a < 60$), we were able to identify a relationship between canopy biomass and kelp fraction. This pattern in the semi-variance results described sites with a distinct kelp patch surrounded by water. Biomass at these sites also had a strong correlation with MESMA kelp fraction pixel matchups. Out of the six sites, Portuguese Beach (Figure 2.2b; Figure 2.5e-h; Figure 2.7b,g) and San Carlos Beach (Figure 2.2e; Figure 2.5q-t; Figure 2.7d,i) were clear examples of this pattern, exhibiting dense, relatively homogenous stipe (frond) counts inside the kelp bed and a relatively homogenous absence of stipes (fronds) outside of the kelp bed. This indicates a potential mismatch between diver survey results and remote sensing because surveying large patches is quantified best by satellite remote sensing but isn't feasible for *in situ* surveys.

Patterns of canopy expression also appear to be important when using MESMA kelp fraction to quantify canopy biomass. Hopkins Marine Station exhibited the biggest range in MESMA kelp fraction (Figure 2.5u-x), while mean tidal height during the UAV survey was ~1 m (Table 1.1). Where kelp was present, high MESMA fractions indicated very dense canopy coverage. However, dive surveys didn't capture this range in canopy biomasses, likely because the sporophyte distribution at the bottom was

relatively sparse and patchy leading to an under representation of the canopy characteristics. Conversely, Point Piños exhibited the smallest range in MESMA kelp fraction values and the highest range in canopy biomass values (Figure 2.5i-l), while mean tidal height during the UAV survey was ~1.3 m (Table 1.1). High kelp canopy biomass was not captured in the UAV imagery despite being measured in late summer (early September) when *Nereocystis* canopy maxima occurs. This may have occurred because even though sporophyte distribution was dense and relatively homogenous across the survey site, (1) the depth of the site (~30 m) limited some sporophytes from reaching the surface, and (2) specific characteristics of *Nereocystis* canopy expression.

Despite SBC LTER's robust prediction of Santa Barbara *Macrocystis* canopy biomass estimates from 30 m Landsat (Cavanaugh et al., 2011; Bell et al., 2020b), we had little success developing a significant relationship between MESMA kelp fraction and canopy biomass for binned 30 m resolution UAV imagery. This is likely due, in part, to the spatial and canopy characteristics of the kelp beds sampled in this study, the limited *in situ* and UAV sampling, and environmental variability influencing surface expression of the canopy. In general, the *Nereocystis* canopy spectral signature was low at 30 m resolution across all three sites and, as a result, MESMA kelp fractions of zero were common even if kelp canopy was detected at higher spatial resolutions (Figure S2.2). The poor relationship observed for *Macrocystis* at 30 m resolution may be a result of the inability to accurately capture enough variability in patchy biomass coverage at the benthos (2, 70 m² transects) to represent surface canopy expression across the entire 900 m² pixel using diver surveys.

In general, MESMA kelp fraction values observed across all three *Nereocystis* sites were lower than the *Macrocystis* sites (Figure S2.3). This influenced (1) the general patterns observed between the two genera's predictive relationships between MESMA kelp fraction and canopy biomass predictions and (2) the ability to accurately determine canopy biomass. Patterns may be attributed to each genera's canopy structure/morphology, and local tide/current conditions of the stations sampled (Jensen et al., 1980; Koehl, 1984; Schroeder et al., 2019). *Nereocystis* has a single gas-filled stipe and pneumatocyst (Figure 2.3). The blades (length \cong 1 m), which can number up to the hundreds, are concentrated at the top of the sporophyte and do not float on the water surface without sufficient tidal and current forcing. As a result, much of the biomass in the canopy is not floating on the water surface at our study sites and, therefore, the spectral signature of the kelp canopy observed from a remote sensing platform is relatively low. This results in a narrower range of MESMA kelp fractions, while canopy biomasses range significantly depending on the density of *Nereocystis* sporophytes.

In contrast to *Nereocystis*, the morphological characteristics of *Macrocystis* tended to underrepresent canopy biomass. *Macrocystis* blades grow along the entire frond from the base to the growing tip (meristem). More of the canopy biomass is floating because the base of each *Macrocystis* blade (length \cong 30 cm) contains a single pneumatocyst. Additionally, a single *Macrocystis* sporophyte can contain up to ~100 fronds clustered together (Figure 2.3; Figure S2.1a). Therefore, dense floating canopies of *Macrocystis* fronds can form, often with many fronds laying on top of each other at

the surface. Since the distribution of individual sporophytes at the substrate are often sparse and non-homogenously distributed across a kelp patch, disparities can develop between diver counts of fronds and the expression of the surface canopy, and an under-representation of canopy biomass relative to MESMA kelp fraction.

Patterns in environmental and biological drivers of kelp canopy coverage/biomass have been widely studied in the NE Pacific region, and more specifically in California and Oregon, using remote sensing techniques. However, few studies have investigated regional patterns and validation of canopy biomass derived via remote sensing. In this study, we shed light on limitations and challenges in determining and validating remotely derived kelp canopy biomass for *Macrocystis* and *Nereocystis* in central and northern California and, based on our findings, recommend implementation of long-term monitoring programs, such as those used by the SBC LTER, across the region for both *Macrocystis* and *Nereocystis*. It is also clear from this study that, while significantly time and energy intensive, additional work across different regions and sites is required to fully understand the legitimacy of applying allometric relationships developed at one kelp bed to an entire region or, even nearby kelp beds. If regional differences are small, and the errors in applying those methods to different regions are acceptable (as they appear to be for Monterey) broad remote sensing biomass estimates may still be useful. If a greater understanding of regional patterns and differences among kelp canopy biomass is achieved, rates of physiological metrics, such as NPP, and carbon sequestration can be robustly quantified. However, the challenges presented here reinforce the use of kelp canopy area in both scientific

and monitoring applications, especially in cases where biomass is not of primary importance.

Acknowledgements

Many thanks to the all the people who made this work possible, including Heidi Hirsh (Stanford University), scientific divers (Logan Grady, Jeannette Peters, and Sara Hamilton), field volunteers (alphabetically: Dennis Finger, Aimee Foy, Megan Gallagher, Kyle Hughes, Kevin Hum, Josie Iselin, Quinn Letitia, John Mizell, Rich Muller, Brynn O'Hara, and Jezabel Powers), and sensitive wildlife monitors (Herrick Hanks, Teri Nicholson, Jennifer Parkin, Judi Romero, and Bill Standley). Helpful feedback on this manuscript was provided by Tom Bell (University of California Santa Barbara/Woods Hole Oceanographic Institute) and Niky Taylor (University of California Santa Cruz). Financial support was provided by the Dr. Earl H. Myers and Ethel M. Myers Oceanographic and Marine Biology Trust and the UCSC Department of Ocean Sciences. Vessel support and lodging was provided by Laura Rogers-Bennett's Marine Invertebrate Fisheries and Conservation Laboratory. Funding for the UAV was supported by the Ida Benson-Lynn Ocean Health endowment. The MicaSense RedEdge-M and Pix4D software was supported by the Packard Science and Technology endowment to the Institute of Marine Sciences.

References

- Beas-luna, R., Micheli, F., Woodson, C. B., Carr, M., Malone, D., Torre, J., et al. (2020). Geographic variation in responses of kelp forest communities of the California Current to recent climatic changes. *Glob. Chang. Biol.*, 1–17. doi:10.1111/gcb.15273.
- Bell, T., Nidzieko, N. J., Siegel, D. A., Miller, R. J., Cavanaugh, K. C., Nelson, N. B., et al. (2020a). The Utility of Satellites and Autonomous Remote Sensing Platforms for Monitoring Offshore Aquaculture Farms: A Case Study for Canopy Forming Kelps. *Front. Mar. Sci.* doi:10.3389/fmars.2020.520223.
- Bell, T. W., Allen, J. G., Cavanaugh, K. C., and Siegel, D. A. (2020b). Three decades of variability in California's giant kelp forests from the Landsat satellites. *Remote Sens. Environ.* 238. doi:10.1016/j.rse.2018.06.039.
- Bell, T. W., Cavanaugh, K. C., and Siegel, D. A. (2015). Remote monitoring of giant kelp biomass and physiological condition: An evaluation of the potential for the Hyperspectral Infrared Imager (HypIRI) mission. *Remote Sens. Environ.* 167, 218–228. doi:10.1016/j.rse.2015.05.003.
- Cavanaugh, K. C., Cavanaugh, K. C., Bell, T. W., and Hockridge, E. G. (2021). An Automated Method for Mapping Giant Kelp Canopy Dynamics from UAV. *Front. Environ. Sci.* 8:587354, 1–16. doi:10.3389/fenvs.2020.587354.
- Cavanaugh, K. C., Reed, D. C., Bell, T. W., Castorani, M. C. N., Beas-luna, R., and Barrett, N. S. (2019). Spatial Variability in the Resistance and Resilience of Giant Kelp in Southern and Baja California to a Multiyear Heatwave. *Front. Mar. Sci.* 6, 1–14. doi:10.3389/fmars.2019.00413.
- Cavanaugh, K. C., Siegel, D. A., Kinlan, B. P., and Reed, D. C. (2010). Scaling giant kelp field measurements to regional scales using satellite observations. *Mar. Ecol. Prog. Ser.* 403, 13–27. doi:10.3354/meps08467.
- Cavanaugh, K. C., Siegel, D. A., Reed, D. C., and Dennison, P. E. (2011). Environmental controls of giant-kelp biomass in the Santa Barbara Channel, California. *Mar. Ecol. Prog. Ser.* 429, 1–17. doi:10.3354/meps09141.

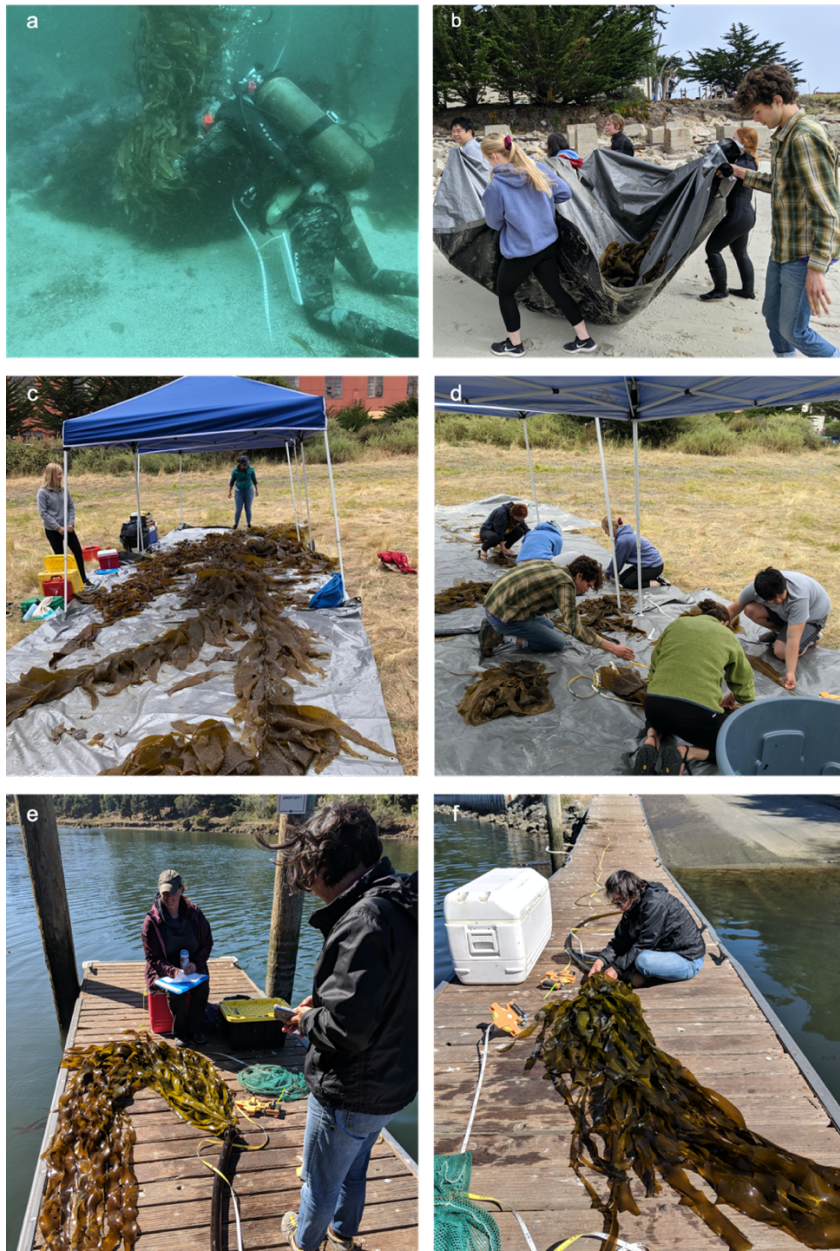
- Crowfoot, W., Allen, B., Blumenfeld, J., Stone, M., Diamond, J., Yee, B., et al. (2020). Strategic Plan Strategic Plan to Protect California's Coast and Ocean 2020-2025. Available at: <http://www.afpe.org.uk/physical-education/wp-content/uploads/afPE-Strategic-Plan-2016-2020.pdf>.
- Dayton, P. K., Tegner, M. J., Edwards, P. B., and Riser, K. L. (1999). TEMPORAL AND SPATIAL SCALES OF KELP DEMOGRAPHY: THE ROLE OF OCEANOGRAPHIC CLIMATE. *Ecol. Monogr.* 69, 219–250.
- Dennison, P. E., and Roberts, D. A. (2003). Endmember selection for multiple endmember spectral mixture analysis using endmember average RMSE. *Remote Sens. Environ.* 87, 123–135. doi:10.1016/S0034-4257(03)00135-4.
- Dexter, K. F., Wernberg, T., Grace, S. P., Thormar, J., and Fredriksen, S. (2020). Marine heatwaves and the collapse of marginal North Atlantic kelp forests. *Sci. Rep.*, 1–11. doi:10.1038/s41598-020-70273-x.
- Finger, D. J. I., McPherson, M. L., Houskeeper, H. F., and Kudela, R. M. (2021). Mapping bull kelp canopy in northern California using Landsat to enable long-term monitoring. *Remote Sens. Environ.* 254, 112243. doi:10.1016/j.rse.2020.112243.
- Friedlander, A. M., Ballesteros, E., Bell, T. W., Caselle, J. E., Campagna, C., Goodell, W., et al. (2020). Kelp forests at the end of the earth: 45 years later. *PLoS One* 15, 1–23. doi:10.1371/journal.pone.0229259.
- Gorman, D., Bajjouk, T., Populus, J., Vasquez, M., and Ehrhold, A. (2013). Modeling kelp forest distribution and biomass along temperate rocky coastlines. *Mar. Biol.* 160, 309–325. doi:10.1007/s00227-012-2089-0.
- Hamilton, S. L., Bell, T. W., Watson, J. R., Grorun-Colvert, K. A., and Menge, B. A. (2020). Remote sensing: generation of long-term kelp bed data sets for evaluation of impacts of climatic variation. *Ecology* 0, 1–13. doi:10.1002/ecy.3031.

- Hohman, R., Hutto, S., Catton, C. A., and Koe, F. (2019). Sonoma-Mendocino Bull Kelp Recovery Plan. Plan for the Greater Farallones National Marine Sanctuary and the California Department of Fish and Wildlife. San Francisco, CA.
- Huovinen, P., Ramirez, J., Palacios, M., and Gomez, I. (2020). Satellite-derived mapping of kelp distribution and water optics in the glacier impacted Yendegaia Fjord (Beagle Channel, Southern Chilean Patagonia). *Sci. Total Environ.* 703.
- Jensen, J. R., Estes, J. E., and Tinney, L. (1980). Remote sensing techniques for kelp surveys. *Photogramm. Eng. Remote Sens.* 46, 743–755.
- Koehl, M. A. R. (1984). How do benthic organisms withstand moving water? *Integr. Comp. Biol.* 24, 57–70. doi:10.1093/icb/24.1.57.
- Krause-Jensen, D., and Duarte, C. M. (2016). Substantial role of macroalgae in marine carbon sequestration. *Nat. Geosci.* 9, 737–742. doi:10.1038/ngeo2790.
- Ling, S. D., Johnson, C. R., Frusher, S. D., and Ridgway, K. R. (2009). Overfishing reduces resilience of kelp beds to climate-driven catastrophic phase shift. *Proc. Natl. Acad. Sci.* 106.
- Macreadie, P. I., Anton, A., Raven, J. A., Beaumont, Nicola, Connolly, R. M., Friess, D., et al. (2019). The future of Blue Carbon science. *Nat. Commun.* 10, 1–13. doi:10.1038/s41467-019-11693-w.
- McPherson, M. L., Finger, D. J. I., Houskeeper, H. F., Bell, T. W., Carr, M. H., Rogers-Bennett, L., et al. (2021). Large-scale shift in the structure of a kelp forest ecosystem co-occurs with an epizootic and marine heatwave. *Commun. Biol.* 4, 1–9. doi:10.1038/s42003-021-01827-6.
- Mora-Soto, A., Palacios, M., Macaya, E. C., Gomez, I., Huovinen, P., Perez-Matus, A., et al. (2020). A High-Resolution Global Map of Giant Kelp (*Macrocystis pyrifera*) Forests and Intertidal Green. *Remote Sens.* 12, 1–20.
- Nijland, W., Reshitnyk, L., and Rubidge, E. (2019). Remote Sensing of Environment

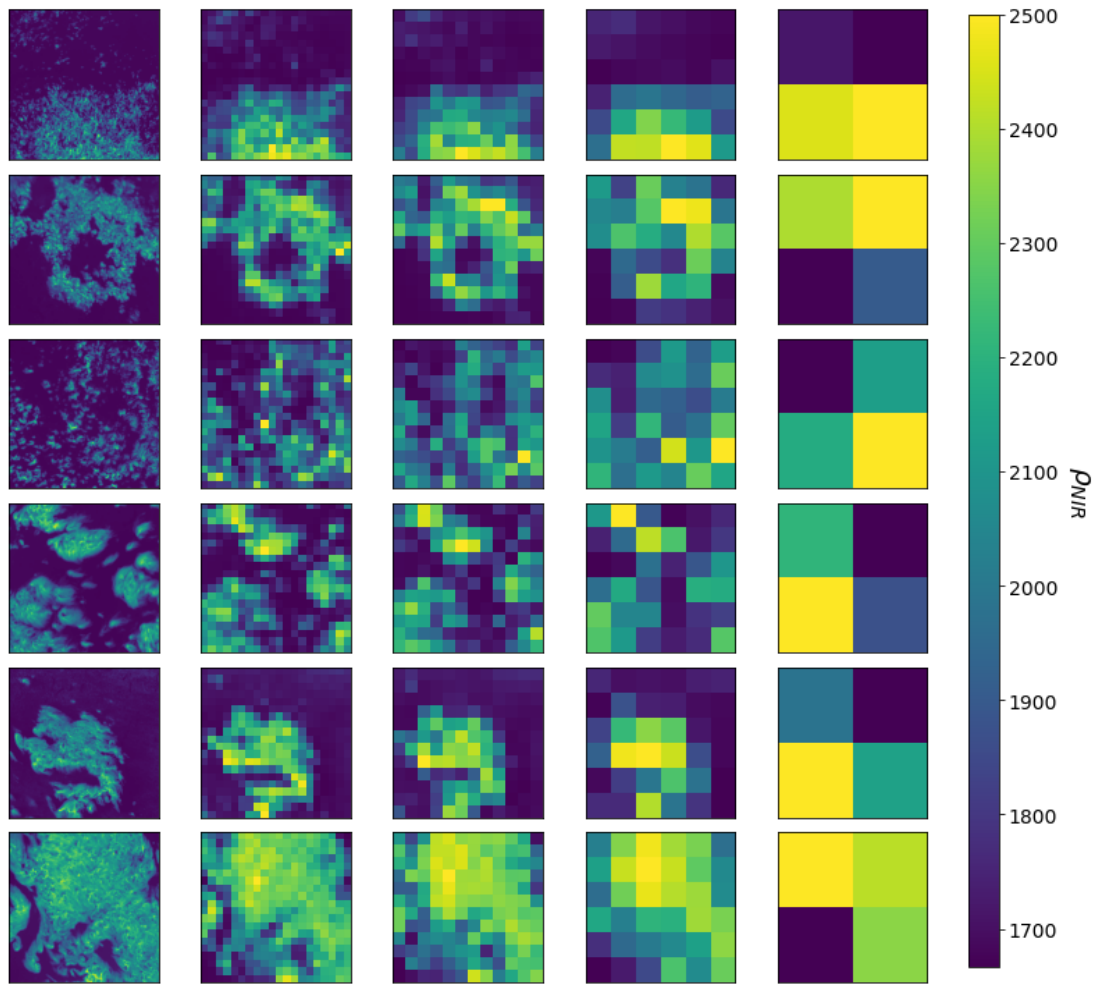
- Satellite remote sensing of canopy-forming kelp on a complex coastline: A novel procedure using the Landsat image archive. *Remote Sens. Environ.* 220, 41–50. doi:10.1016/j.rse.2018.10.032.
- Oliver, E. C. J., Benthuisen, J. A., Bindoff, N. L., Hobday, A. J., Holbrook, N. J., Mundy, C. N., et al. (2017). The unprecedented 2015/16 Tasman Sea marine heatwave. *Nat. Commun.* 8, 1–12. doi:10.1038/ncomms16101.
- Ortega, A., Geraldi, N. R., Alam, I., Kamau, A. A., Acinas, S. G., Logares, R., et al. (2019). Important contribution of macroalgae to oceanic carbon sequestration. *Nat. Geosci.* 12. doi:10.1038/s41561-019-0421-8.
- Phillips, J., Berry, W., Carter, H., Sievanen, L., Whiteman, L., and Chornesky, Li. (2018). State of California Ocean Acidification Action Plan.
- Rasher, D. B., Steneck, R. S., Halfar, J., Kroeker, K. J., Ries, J. B., Tinker, M. T., et al. (2020). Keystone predators govern the pathway and pace of climate impacts in a subarctic marine ecosystem. *Science*. 369, 1351–1355. doi:10.1126/SCIENCE.AAV7515.
- Rassweiler, A., Arkema, K. ., Reed, D. C., Zimmerman, R. ., and Brzenzinski, M. A. (2008). Data Papers. *Ecology* 89, 2068.
- Roberts, D. A., Gardner, M., Church, R., Ustin, S., Scheer, G., and Green, R. O. (1998). Mapping chaparral in the Santa Monica Mountains using multiple endmember spectral mixture models. *Remote Sens. Environ.* 65, 267–279. doi:10.1016/S0034-4257(98)00037-6.
- Schroeder, S. B., Dupont, C., Boyer, L., Juanes, F., and Costa, M. (2019). Passive remote sensing technology for mapping bull kelp (*Nereocystis luetkeana*): A review of techniques and regional case study. *Glob. Ecol. Conserv.* 19, e00683. doi:10.1016/j.gecco.2019.e00683.
- Stekoll, M. S., Deysher, L. E., and Hess, M. (2006). A remote sensing approach to estimating harvestable kelp biomass. *J. Appl. Phycol.* 18, 323–334. doi:10.1007/s10811-006-9029-7.

- Steneck, R. S., Graham, M. H., Bourque, B. J., Corbett, D., Erlandson, J. M., Estes, J. a., et al. (2002). Kelp forest ecosystems: biodiversity, stability, resilience and future. *Environ. Conserv.* 29, 436–459. doi:10.1017/S0376892902000322.
- Straub, S. C., Wernberg, T., Thomsen, M. S., Moore, P. J., Burrows, M. T., Harvey, B. P., et al. (2019). Resistance, Extinction, and Everything in Between – The Diverse Responses of Seaweeds to Marine Heatwaves. *Front. Mar. Sci.* 6, 1–13. doi:10.3389/fmars.2019.00763.
- Teagle, H., Hawkins, S. J., Moore, P. J., and Smale, D. A. (2017). The role of kelp species as biogenic habitat formers in coastal marine ecosystems. *J. Exp. Mar. Bio. Ecol.* 492, 81–98. doi:10.1016/j.jembe.2017.01.017.
- van Son, T. C., Nikolioudakis, N., Steen, H., Albretsen, J., Furevik, B. R., Elvenes, S., et al. (2020). Achieving Reliable Estimates of the Spatial Distribution of Kelp Biomass. *Front. Mar. Sci.* 7, 1–13. doi:10.3389/fmars.2020.00107.
- Wernberg, T., Bennett, S., Babcock, R. C., Bettignies, T. De, Cure, K., Depczynski, M., et al. (2016). Climate-driven regime shift of a temperate marine ecosystem. *Science (80-.).* 353, 169–172.
- Wernberg, T., Krumhansl, K., Filbee-dexter, K., and Pedersen, M. F. (2019). “Status and Trends for the World’s Kelp Forests,” in *World Seas: An Environmental Evaluation* (Elsevier Ltd.), 57–78. doi:10.1016/B978-0-12-805052-1.00003-6.
- Young, M. A., Cavanaugh, K. C., Bell, T. W., Raimondi, P. T., Edwards, C. A., Drake, P. T., et al. (2015). Environmental controls on spatial patterns in the long-term persistence of giant kelp in central California. *Ecology* 86, 45–60. doi:10.1890/15-0267.1.

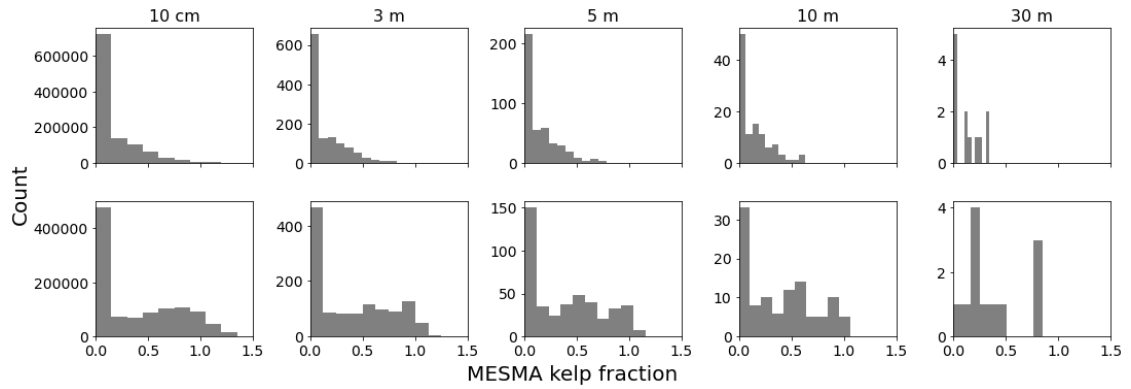
Supplemental Material



Supplemental Figure 1 (Figure S2.1). Images of morphometric measurements for *Macrocyctis* and *Nereocystis*. a) Diver removing whole *Macrocyctis* sporophyte in situ at the holdfast (Hopkins Marine Life Refuge). b) *Macrocyctis* sporophyte transport from water to a clean and dry location on land. c) Entire *Macrocyctis* sporophyte spread across tarp before dividing into 2 m sections. d) Field technicians measuring morphology of each 2 m section of a *Macrocyctis* sporophyte. E) *Nereocystis* canopy spread out on clean dock ready to be measured. F) Josie Iselin taking counting *Nereocystis* blades for morphometric measurement. Photo credit: a) Sara Hamilton (OSU), b-f): Meredith McPherson.



Supplemental Figure 2 (Figure S2.2). First row: Noyo Harbor; Second row: Portuguese Beach; Third row: Point Pinos; Fourth row: Otter Cove; Fifth row: San Carlos Beach; Sixth row: Hopkins Marine Station. Across columns: 0.1 m, 3 m, 5 m, 10 m, 30 m pixel resolution.



Supplemental Figure 3 (Figure S2.3). Histograms of pixel kelp fraction for each genera and resolution. Top row: *Nereocystis*; Bottom row: *Macrocystis*. Across columns: 0.1 m, 3 m, 5 m, 10 m, 30 m pixel resolution.

Supplemental Table 1 (Table S2.1). Spectral characteristics (center wavelengths and full-width at half-max (FWHM) values in nanometer) for each relevant satellite band (blue, green, red, red-edge, and NIR). Within each cell the top value is the band's center wavelength and the bottom value is the band's FWHM. n/a denotes where band information doesn't exist or isn't available.

Band	MicaSense RedEdge-M	PlanetScope	Planet RapidEye	ESA Sentinel-2	USGS Landsat
Blue	475 32	485 n/a	475 n/a	492 66	480 60
Green	560 27	545 n/a	555 n/a	560 36	561 57
Red	668 14	630 n/a	660 n/a	665 31	655 38
Red-Edge	717 12	n/a	710 n/a	n/a	n/a
NIR	842 57	820 n/a	805 n/a	833 106	865 28

Supplemental Table 2 (Table S2.2). Results from pairwise Tukey's HSD post-hoc test for location specific *Nereocystis* bulb diameters. * denotes significance.

Location A	Location B	Mean (A)	Mean (B)	Std. Error	<i>p</i>-value
Alaska	Mendocino	2.56	3.90	0.467	0.012
Alaska	Monterey	2.56	8.97	0.905	*0.001
Mendocino	Monterey	3.90	8.97	0.889	*0.001

Supplemental Table 3 (Table S2.3). Regression statistics from Figure 2.5. * represent a significant relationship between MESMA kelp fraction and in situ canopy biomass based on a p-value less than 0.05.

Station	Spatial Resolution (m)	n	Slope (m)	Intercept (b)	Standard Error (SE)	p-value
Noyo Harbor (NH)	0.1	28	1.99	3.19	4.15	>0.05
	3	28	1.24	3.31	3.89	>0.05
	5	28	2.40	3.18	3.92	>0.05
	10	28	1.11	3.38	4.19	>0.05
Portuguese Beach (PB)	0.1	56	63.35	2.23	12.86	*8.3 x 10 ⁻⁶
	3	56	64.64	1.87	12.53	*2.1 x 10 ⁻⁶
	5	56	69.55	1.75	11.99	*3.6 x 10 ⁻⁷
	10	56	55.27	5.29	11.83	*2.03 x 10 ⁻⁶
Point Piños (PP)	0.1	56	5.14	22.10	26.55	>0.05
	3	56	22.29	21.16	26.19	>0.05
	5	56	14.41	21.79	23.61	>0.05
	10	56	1.80	1.89	1.63	>0.05
Otter Cove (OC)	0.1	56	1.80	1.89	1.63	>0.05
	3	56	1.68	1.92	1.59	>0.05
	5	56	3.08	1.68	1.71	>0.05
	10	56	1.79	2.01	1.51	>0.05
San Carlos Beach (SCB)	0.1	56	7.87	1.16	1.86	*8.01 x 10 ⁻⁵
	3	56	7.81	1.21	1.96	*1.8 x 10 ⁻⁴
	5	56	8.07	1.21	1.93	*9.2 x 10 ⁻⁵
	10	56	8.41	1.39	1.83	*2.2 x 10 ⁻⁵
Hopkins Marine Station (HMS)	0.1	56	2.60	0.67	1.74	>0.05
	3	56	2.88	0.44	1.77	>0.05
	5	56	0.09	2.54	1.31	>0.05
	10	56	-0.31	2.77	1.15	>0.05

UTILIZING A MULTIYEAR DATASET OF UNOCCUPIED AIRCRAFT SYSTEM IMAGERY TO VALIDATE LANDSAT DERIVED GIANT KELP CANOPY

Meredith L. McPherson and Tom W. Bell

Abstract

Long-term and large-scale monitoring of marine, freshwater, and terrestrial systems are crucial for detecting changes and drivers of ecosystems. This is especially true as climate change alters the environmental conditions that maintain a given ecosystem's function and stability. Traditionally, satellites have been used for large-scale monitoring approaches because they can make observations at spatial scales from 10s to 100s of kms. Small unoccupied aircraft systems (sUAS) have recently emerged as a valuable remote sensing tool in environmental biology because they are logistically flexible. Though these platforms provide the opportunity to observe an area quickly and on demand, they lack the spatio-temporal resolution that satellites provide. However, because of their flexibility and the high spatial resolution, sUASs reduce challenges associated with validation and ground-truthing of satellite imagery. They have significant potential to help improve and better understand variability in important long-term satellite derived timeseries. Utilizing a unique four-year dataset of near-simultaneous matchups of sUAS color imagery and Landsat multispectral data, we investigated specific methodological behavior and results from an automated classification and spectral unmixing approach developed for a multi-decade timeseries of giant kelp canopy with the goal of continued improvement to the dataset. Specifically, validating areal estimates and the detection of processes influencing pixel-scale variability. We focused on three specific aspects that influence estimates of kelp

canopy at the pixel and kelp bed scale, including spatio-temporal variability in ocean conditions, and the spectral unmixing and classification of kelp versus seawater. Though this study was designed to reduce temporal offsets, and therefore environmental variability, we observed the impacts of current velocity on kelp canopy fraction between matchups and in a seasonal timeseries of Landsat. Specific kelp bed features, such as seasonal changes in bed size and canopy density/biomass were important for driving matchup performance and error. We found that pre-classification of kelp and seawater is necessary from a quality control perspective because MESMA can be noisy across Landsat sensors, but that it resulted in higher uncertainty of kelp canopy from sparse kelp beds. Therefore, we can expect more error in Landsat MESMA estimates when observing low canopy biomass or fringing kelp bed conditions that result in low pixel canopy fractions. Overall, this study provides broader context for validation approaches to satellite derived timeseries by utilizing a unique multiyear dataset and exploring pixel and patch-scale uncertainties. We recommend considering particular use cases where methodological caveats may influence data products, especially with respect to restoration programs and metapopulation studies.

Introduction

Development and maintenance of long-term timeseries is crucial for detecting changes and drivers of ecosystem status and health in marine, freshwater, and terrestrial systems. These datasets allow us to understand ecosystem baselines and dynamics, and are particularly relevant as climate change alters the environmental conditions that have historically maintained a given ecosystem's function and stability (Doney et al., 2012;

Collins et al., 2019). Many long-term studies often focus on investigating dynamics of ecosystems with context to environmental conditions, discrete disturbances, or known associations with other organisms at specific spatial scales (Stenseth et al., 2002; Mackas et al., 2012; Mieszkowska et al., 2014; Hermosilla et al., 2018). While long-term *in situ* monitoring at small spatial scales has value, particularly for organismal level interactions and dynamics, observations at large spatial scales (10 km to 100 km), using spaceborne sensors, can help describe local- to global-scale trends.

Large-scale monitoring of ecosystems generally utilizes observations of foundational primary producers (e.g. phytoplankton, seagrasses, grasslands, tree canopies, and floating algae). Distinct or defined spectral signatures of these foundational species allow for large temporal and spatial monitoring using remote sensing methods. Ocean color timeseries from across more than 40 years (1978 - *present*) at ~ kilometer scale resolution have been utilized to study phytoplankton ecology at regional to global scales (Alvain et al., 2005; Behrenfeld et al., 2005; Ryan et al., 2009; Kahru et al., 2012), and led to an increased understanding of the role of the surface oceans in carbon cycling (Westberry et al., 2008). However, there are limitations to these datasets for coastal marine and inland freshwater systems that require higher spatial resolution and signal to noise-ratios (Kudela et al., 2019), and improved atmospheric correction than are available from legacy satellite platforms such as SeaWiFS and MODIS. In terrestrial ecosystems, the availability of 30 m resolution imagery from USGS Landsat across more than 30 years (1982 - *present*) has aided in detecting land disturbances (Fraser et al., 2011; Margono et al., 2012; Masek

et al., 2013), determining land use/cover (Nguyen et al., 2020), and mapping global distribution of mangroves (Giri et al., 2011). Landsat has also been advantageous for studying canopy forming kelps, which have a spectral signature that is similar to terrestrial vegetation (high reflectance in the near infrared band) and are relatively bright compared to the surrounding water. Because these systems grow in a narrow band along the coastline (< 1 km), observations are limited to relatively high spatial resolution satellites (10 - 30 m; Cavanaugh et al., 2011).

Small unoccupied aircraft systems (sUAS) have emerged as the newest application for scientific data collection via remote sensing and are becoming increasingly popular in environmental biology (Nowak et al., 2019). These platforms are more flexible than satellites with respect to their ability to observe an area at high spatial resolution quickly and on demand using a range of sensors from simple, low-cost color cameras (Larrinaga and Brotons, 2019) to complex, high-cost hyperspectral imagers (Banerjee et al., 2020; Bell et al., 2020a). These platforms have been used to make event-based observations (i.e. detecting noxious flowering plants; Müllerová et al., 2017), monitor restoration efforts (i.e. tidal marsh restoration; Haskins et al., 2021), monitor harmful algal blooms and water quality (Kislik and Dronova, 2018; Cheng et al., 2020), map ecologically sensitive marine habitats (i.e. seagrass meadows; Ventura et al., 2018), derive forestry inventory (Wu et al., 2021), etc. Furthermore, because there is a need for rapid and easily accessible approaches to ground-truthing in remote sensing studies, many sUAS approaches combine methodological advances with satellite validation efforts (Gray et al., 2018; Iizuka et al., 2018; Martin et al., 2018;

Riihimäki et al., 2019; Topouzelis et al., 2019). As a result, this technology reduces challenges associated with validation and ground-truthing of Landsat and has significant potential to help validate areal estimates and understand the pixel-scale variability observed in long-term timeseries of kelp canopy area and biomass.

The number of studies utilizing Landsat derived timeseries of kelp canopy in the northeast Pacific region and beyond (Butler et al., 2020; Friedlander et al., 2020) has risen over the last decade, resulting in an increased understanding of spatial variability in the environmental and biological processes driving kelp dynamics. On the California coastline, El Niño Southern Oscillation (ENSO) was previously thought to be the dominant large-scale driver of kelp (Zimmerman and Kremer, 1984; Tegner and Dayton, 1987), but appears to be more coupled with anomalously low kelp years rather than dynamical annual fluctuations, particularly for bull kelp (*Nereocystis leutkeana*) in northern California (McPherson et al., 2021) and Oregon (Hamilton et al., 2020). Rather, the North Pacific Gyre Oscillation (NPGO; Di Lorenzo et al., 2008), is consistently a strong correlate with kelp canopy area and biomass (Cavanaugh et al., 2011; Bell et al., 2015; McPherson et al., 2021). Wave disturbance influences giant kelp (*Macrocystis pyrifera*) negatively (Cavanaugh et al., 2011; Bell et al., 2015) and bull kelp positively (Hamilton et al., 2020; McPherson et al., 2021), while spatial variability in wave exposure along the central and southern California coastline drive giant kelp canopy biomass (Bell et al., 2015) and persistence (Young et al., 2015) patterns. Long-term satellite records from Landsat have also been used to observe regional and genera-specific patterns of kelp canopy in response to discrete

climatological events, such as marine heatwaves (MHWs), which are increasing in frequency, duration, and intensity (Oliver et al., 2018; Laufkötter et al., 2020). Kelp response to MHW events in the northeast Pacific has been variable and Landsat has provided evidence of (1) a wide-spread phase-shift between healthy bull kelp forest and urchin barren along 350 km of the northern CA coastline (McPherson et al., 2021), (2) stability to MHW perturbations in Oregon kelp forests (Hamilton et al., 2020), and (3) spatial variability in the resistance and resilience in southern and Baja California, (Arafteh-Dalmau et al., 2019; Cavanaugh et al., 2019), likely because it is near the southern tip of giant kelp's range in the northern hemisphere where temperature crosses giant kelp's physiological threshold.

Given the importance of satellite-derived estimates for understanding spatio-temporal dynamics of kelp canopy area and biomass, it is necessary to validate the methodological approaches and findings of these datasets as they grow and become widely available for use by managers and scientists (e.g., <https://kelp.codefornature.org/> from The Nature Conservancy) and improved spaceborne sensors become available (September 2021: Landsat 9 will become the fifth 30 m resolution sensor in the Landsat suite). In essence, the evolution of quality control measures must be a continuum as the dataset evolves and changes. Though an automated approach for classifying giant kelp canopy has been developed (Bell et al., 2020b) and quality control for imagery contamination (clouds, glint, and Landsat 7 ETM+ scan line error) has sufficiently improved the data product since its origin, ground truthing and validation of satellite imagery at the pixel scale has continued to

be challenging. The availability of sUAS technology provides a useful approach to determining performance of classification schemes for Landsat relative to very high resolution (10 cm) imagery. In this study, we addressed questions geared towards understanding specific methodological behavior and results from the established automated classification (Bell et al. 2020b) and spectral unmixing approach (Multiple Endmember Spectral Mixture Analysis; MESMA; Roberts et al., 1998). Utilizing a unique four-year dataset of near-simultaneous matchups of color imagery from an inexpensive sUAS platform and multispectral Landsat 7 ETM+ and 8 OLI imagery from two kelp beds in the Santa Barbara Channel we specifically asked:

1. How does high spatio-temporal variability in ocean conditions (tides, wave height, and current magnitude) influence kelp canopy characteristics and matchup performance between sUAS and Landsat kelp canopy fraction?
2. What are the pixel and site scale patterns in matchup performance between the sUAS and Landsat kelp canopy fraction? Are these patterns a function of sensor or seasonal impacts on Landsat?
3. How does the Landsat binary decision tree pre-classification method influence kelp detection at the pixel and site scale? How do we use this information to inform the scales at which the classification methods might influence patterns of regional or local scale kelp patterns and dynamics?

Methods

Study sites and imagery acquisition – A multi-year timeseries of matchups for giant kelp canopy was developed using near-simultaneously collected aerial 3-band (blue, green, red) color and satellite multispectral imagery between 2017 and 2020 at two naturally occurring kelp beds in the Santa Barbara Channel (Arroyo Quemado and Mohawk Reef; Table 3.1; Figure 3.1). The dataset consisted of 19 days of overlapping sUAS and Landsat imagery (11 days at Arroyo Quemado and 8 days at Mohawk Reef) where imagery acquisition from the two different platforms was no more than approximately 3 hours apart. Color imagery was acquired using a sUAS, the DJI Phantom 4 Pro equipped with a 20 MP (1” CMOS sensor, 84° FOV) camera. All camera settings were set to automatic, and no spectral calibration was conducted. Flights were conducted between 8:30 a.m. and 12 p.m local time during clear sky conditions at an altitude of 120 m above ground level. Georeferenced orthomosaics of color imagery were created using the photogrammetric software Agisoft Metashape Pro Version 1.5.0 (Figure 3.2A). Land and breaking waves were masked in the imagery prior to classification of the kelp canopy (Figure 3.2B). Landsat 7 ETM+ and Landsat 8 OLI satellite imagery corresponding to each sUAS flight was downloaded from the USGS Earth Explorer website (earthexplorer.usgs.gov) as Collection 1 Level-2 atmospherically corrected surface reflectance. Six of the 19 Landsat images were ETM+ and 13 were OLI (Table 3.1). Prior to kelp canopy classification, each Landsat image was subset to the appropriate site bounding box based on sUAS imagery collected for that corresponding day. Additional Landsat imagery for Arroyo Quemado,

beyond matchups with the sUAS imagery, were collected for January 2018 to July 2018 and used to investigate the impact of current magnitude on kelp canopy dynamics.

Table 3.1. Landsat overflight/sensor and sUAS flight times for each date and site.

Site	Date	sUAS Flight Time (Local)	Landsat Overflight Time (Local)	Landsat Sensor
Arroyo Quemado (34.467°N 120.118°W)	May 31, 2017	10:30	11:34	OLI
	June 16, 2017	8:30	11:34	OLI
	October 6, 2017	11:00	11:35	OLI
	December 1, 2017	10:00	10:37	ETM+
	May 10, 2018	10:30	11:35	ETM+
	December 12, 2018	10:00	10:34	OLI
	January 29, 2019	10:30	10:34	OLI
	June 30, 2019	10:00	11:24	ETM+
	July 24, 2019	10:00	11:34	OLI
	March 4, 2020	11:30	10:34	OLI
	April 21, 2020	11:00	11:34	OLI
Mohawk Reef (34.934°N 119.73°W)	June 16, 2017	10:30	11:34	OLI
	August 3, 2017	11:30	11:34	OLI
	October 6, 2017	12:00	11:35	OLI
	February 3, 2018	11:00	10:36	ETM+
	March 18, 2019	11:00	11:34	OLI
	June 22, 2019	11:30	11:34	OLI
	March 12, 2020	10:30	11:12	ETM+
	November 23, 2020	9:30	9:59	ETM+

Environmental conditions influencing canopy dynamics – Tidal height, wave height, and current velocity were collected for each site, date, and imagery acquisition time across the study period. Tidal height (m) was acquired for each Arroyo Quemado and Mohawk Reef survey date using the matlab function t_xtide , which calculates tidal height based on measurements from the Santa Barbara Harbor tidal station. For sUAS flights, which took approximately 30 minutes to complete, data were extracted 30 min on either side of the mean flight time in Table 3.1. For Landsat imagery, which is collected near instantaneously, data were extracted for the specific flyover time (Table 3.1). Hourly significant wave height data for both sites were downloaded from the

Coastal Data Information Program (CDIP; http://cdip.ucsd.edu/MOP_v1.1/) and extracted from the closest hourly increment to each flight time. Current velocity data were acquired from Acoustic Doppler Current Profilers (ADCPs) deployed across the three-year study period at each site (Washburn et al., 2021b, 2021a) by the Santa Barbara Channel Coastal Long Term Ecological Research (SBC LTER) program. ADCP data were available in 15-minute intervals and extracted from the closest data collection interval to the sUAS flight and Landsat overflight times.

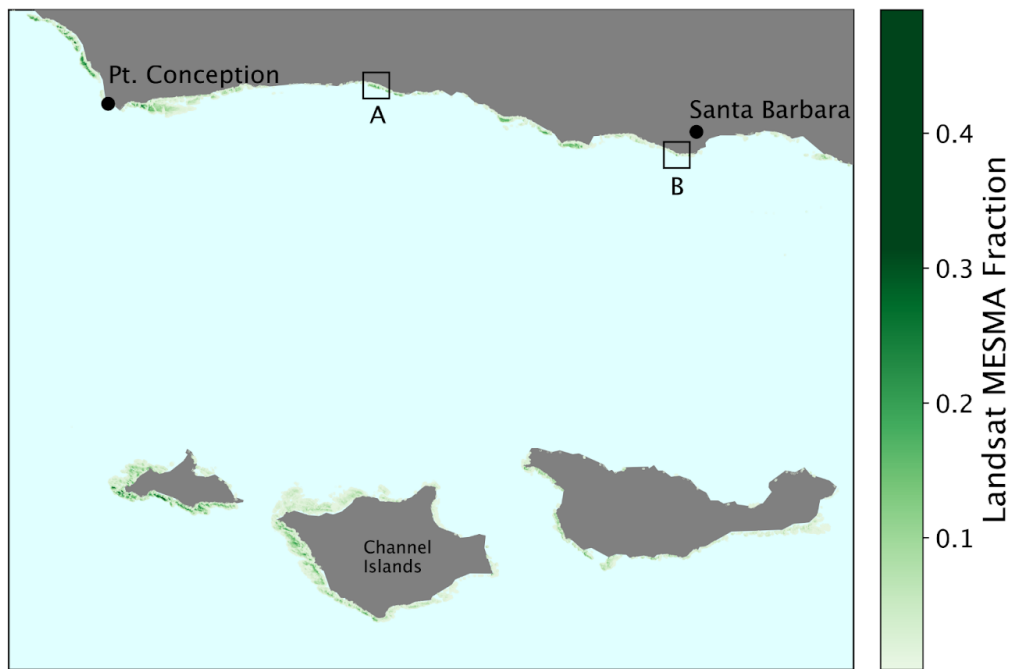


Figure 3.1. Regional map of the Santa Barbara Channel including the study sites Arroyo Quemado (A) and Mohawk Reef (B) overlaid with historical mean Landsat MESMA kelp fraction from 1984 – 2020.

Estimating kelp canopy fraction from sUAS color imagery – Floating kelp canopy was classified in high resolution (10 cm) aerial color imagery using a band ratio of the red band to blue band (Bell et al., 2020a). Pixel values greater than or equal to 1 were classified as kelp canopy, and values less than 1 were classified as seawater. This

simple band ratio showed superior separability of kelp canopy and water compared to other commonly used color band indices (Cavanaugh et al., 2021) and areal estimates from this method were nearly identical to those from calibrated multispectral imagery

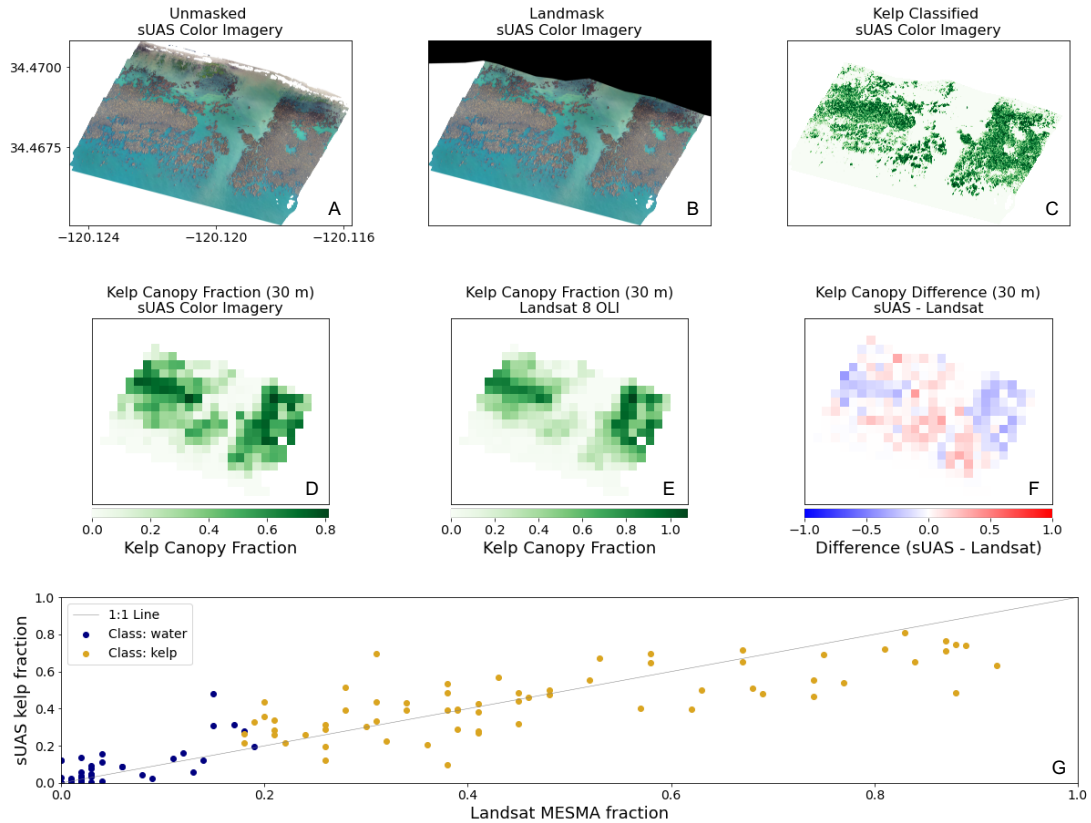


Figure 3.2. Example processing steps for comparing sUAS and Landsat imagery to kelp canopy fraction from imagery collected on May 10th, 2018 at Arroyo Quemado. The unmasked stitched sUAS color imagery (A) is masked for land and waves (B) and classified for kelp canopy (C) using a simple band ratio classification approach. The sUAS imagery is degraded to 30 m resolution (D) and compared to 30 m resolution Landsat MESMA kelp fraction (E). A matchup analysis was conducted at the site and pixel scales using the difference between sUAS and Landsat canopy fractions (F) and direct correlation (G).

(Bell et al., 2020a). Following canopy classification, color imagery was spatially degraded from 10 cm to 30 m pixel resolution using a ‘nearest neighbors’ approach (Matlab function *knnsearch*) to identify color imagery pixels within each Landsat pixel coordinate (Figure 3.2D).

Estimating kelp canopy fraction from Landsat multispectral imagery – Giant kelp canopy was identified using a two-step processing scheme based on Cavanaugh et al., 2011 and Bell et al., 2020b that, first, identified kelp canopy pixels based on a binary decision tree classification and, second, determined the fractional cover of kelp canopy inside each pixel using Multiple Endmember Spectral Mixture Analysis (MESMA; Roberts et al., 1998). The binary decision tree classifier used ETM+ bands 1-5 and 7 and OLI bands 2-7 to classify each pixel as one of four categories: seawater, cloud, land, and kelp (Bell et al., 2020b). The classifier was trained by clustering pixels containing variable cloud, seawater, and kelp conditions using a k-means clustering algorithm. Each pixel within a cluster was then manually classified into one of the four classes and used to train the decision tree classifier. MESMA estimated kelp canopy fraction by modeling each pixel as a linear combination of two spectral endmembers, kelp and seawater (Cavanaugh et al., 2011). Images that contained cloud cover or ETM+ scan line errors inside the sUAS flight area were not included in this analysis. A single static kelp endmember was used across each image, while 30 dynamic seawater endmembers were selected from consistently non-kelp covered areas for each Landsat image to account for changing seawater conditions. The final modeled kelp fraction was selected for each pixel based on the minimum root mean square error (RMSE) out of 30 seawater endmembers (Figure 3.2E). Kelp canopy fraction was determined for each pixel, regardless of the binary decision tree classification. We explored the influence of both the binary decision tree classifier and MESMA on

matchup performance with pixel kelp fraction estimated with sUAS color imagery (Figure 3.2G).

Kelp canopy matchup analysis – A matchup analysis between sUAS and Landsat kelp canopy coverage was conducted using two approaches. The first approach compared total kelp canopy area using 1) only pixels in the image that were pre-classified as kelp using the binary decision tree classification scheme and 2) all pixels in the image regardless of whether they were pre-classified as kelp or seawater. Kelp canopy area was calculated by summing the individual pixel areas (kelp canopy fraction times the 900 m² pixel area) within each image. The second approach compared pixel-specific kelp canopy fractions between the sUAS and Landsat imagery (Figure 3.2F). Matchups of location (pixel) specific kelp canopy fractions were investigated by calculating the difference between the sUAS and Landsat (Figure 3.2F) or directly correlating values for a given site and date (Figure 3.2G). Reduced major axis (RMA) regression was used to determine individual correlations between pixel-based Landsat MESMA fraction and sUAS kelp fraction.

A RMA regression was selected because this model accounts for the error in both sUAS and Landsat kelp fractions. This linear regression approach minimizes the sum of the areas (using both the horizontal and vertical distances to the resulting line), rather than minimizing error in only the vertical direction. As such, neither the kelp canopy fractional values from the sUAS or Landsat are considered independent or dependent and the algebraic solution of x or y from the resulting regression equation is reliable. A general additive model (GAM) was used to determine the overall

relationship between pixel-based Landsat MESMA fraction and sUAS across all dates and sites. GAM is ideal when the relationship between x and y are not assumed to be linear, while allowing regularization of the predictor function to avoid overfitting the data. A one-term power model was used to model the relationship between site level RMA regression slopes and mean Landsat MESMA fraction.

Results

Environmental conditions influencing canopy dynamics – In general, environmental conditions (waves, tidal height, or current velocity) at Arroyo Quemado and Mohawk Reef did not appear to consistently explain differences in pixel level kelp canopy fractions or site level kelp canopy area between the sUAS and Landsat. Environmental conditions present between sUAS and Landsat flight times at each site were relatively consistent (Figure 3.3). Differences between the environmental conditions were generally between 0.2 and -0.2 m for tidal height, and 0.05 to -0.05 for current velocity (m s^{-1}) and wave height (m), with tidal height showing the largest difference range and more notably at Arroyo Quemado (Figure 3.3A) than Mohawk Reef (Figure 3.3B). Wave height conditions were the least variable environmental factor at both sites.

Variability in east current magnitude and direction did, however, appear to influence kelp canopy detection from the satellite at the bed scale and variations in seasonal trends in kelp canopy area were apparent in Landsat canopy area at Arroyo Quemado (Figure 3.4). Though the general trend in canopy area increased through the winter and into spring of 2018 and declined into late summer (Figure 3.4A),

fluctuations were inversely related to the (along shore) east current magnitude, in particular, rather than the (cross shore) north current magnitude. Relatively high

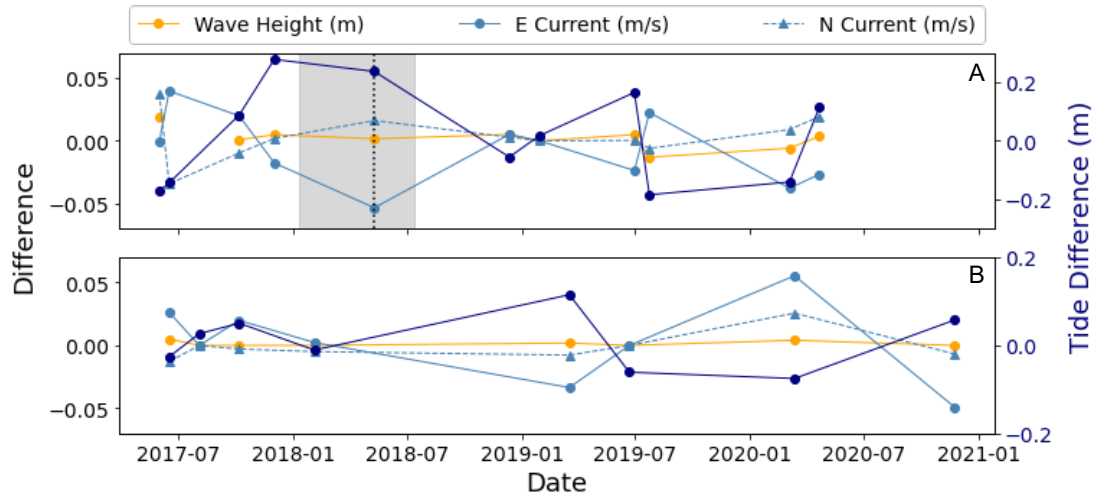


Figure 3.3. Differences between environmental conditions (tidal height, wave height, east current velocity, and north current velocity) between the sUAS and Landsat flight times for Arroyo Quemado (A) and Mohawk Reef (B) on all matchup dates through time. Wave height and current velocity difference are shown on the left y-axis. Tidal difference is shown on the right y-axis. The shaded grey area corresponds with the current magnitude case study shown in Figure 3.4 and the dotted black line to the only Arroyo Quemado sUAS flight within that date range (May 10, 2018). Lines connecting data points do not imply a continuous dataset.

magnitude east current velocities corresponded to dips in canopy area and relatively low current velocities with peaks in canopy area (Figure 3.4A). The result of this effect is apparent in an Arroyo Quemado sUAS image (Figure 3.4B) and the differences in pixel-based kelp canopy area between the two sets of imagery (Figure 3.4C) collected on May 10, 2018. Current velocities around the southern (outer) edge of the kelp bed drag surface fronds below the water surface (Figure 3.4B inset) and kelp canopy fraction differences between the sUAS and Landsat were obvious in the same region (Figure 3.4C). The sUAS estimates of kelp canopy fraction were under-predicted relative to the Landsat imagery across almost the entire bed (indicated by the blue

pixels), but the influence of current is more apparent on the edge of the kelp bed in this particular example.

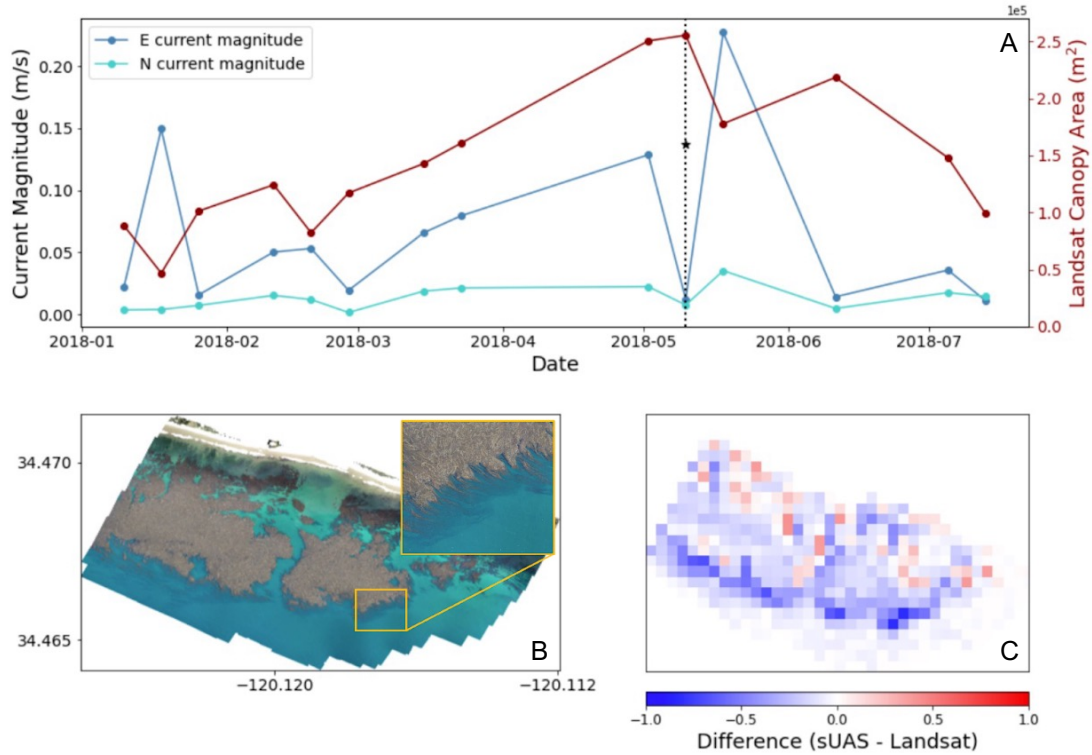


Figure 3.4. (A) Landsat MESMA kelp canopy for each ETM+ or OLI satellite overpass at Arroyo Quemado between January and July 2018 with the corresponding day/time east (E) and (N) current magnitude. The dotted black line represents the day of the only available sUAS and Landsat matchup for this time period (May 10, 2018). The black star indicates the sUAS kelp canopy area referenced on the right y-axis scale. (B) Stitched sUAS imagery from Arroyo Quemado on May 10, 2018. (C) Pixel-based difference in kelp canopy fraction between the sUAS and Landsat for the May 10, 2018 matchup.

Kelp Canopy Matchup Analysis – Slight differences in the response to specific seasonal (spring/summer and fall/winter) and sensor (Landsat 7 ETM+ and Landsat 8 OLI) specifications were observed across Arroyo Quemado and Mohawk Reef (Figure 3.5). At Arroyo Quemado, Landsat overpredicted kelp canopy fraction relative to the sUAS (negative values) for spring/summer (Figure 3.5A) and Landsat 7 (Figure 3.5C) matchups, and conversely, the sUAS over predicted kelp canopy fraction (positive

values) relative to Landsat for fall/winter (Figure 3.5A) and Landsat 8 (Figure 3.5C). Pixel differences of kelp canopy fraction for both seasons and Landsat sensors at Mohawk Reef were generally centered around zero (Figure 3.5B) and didn't appear to show strong bias towards either the sUAS or Landsat data.

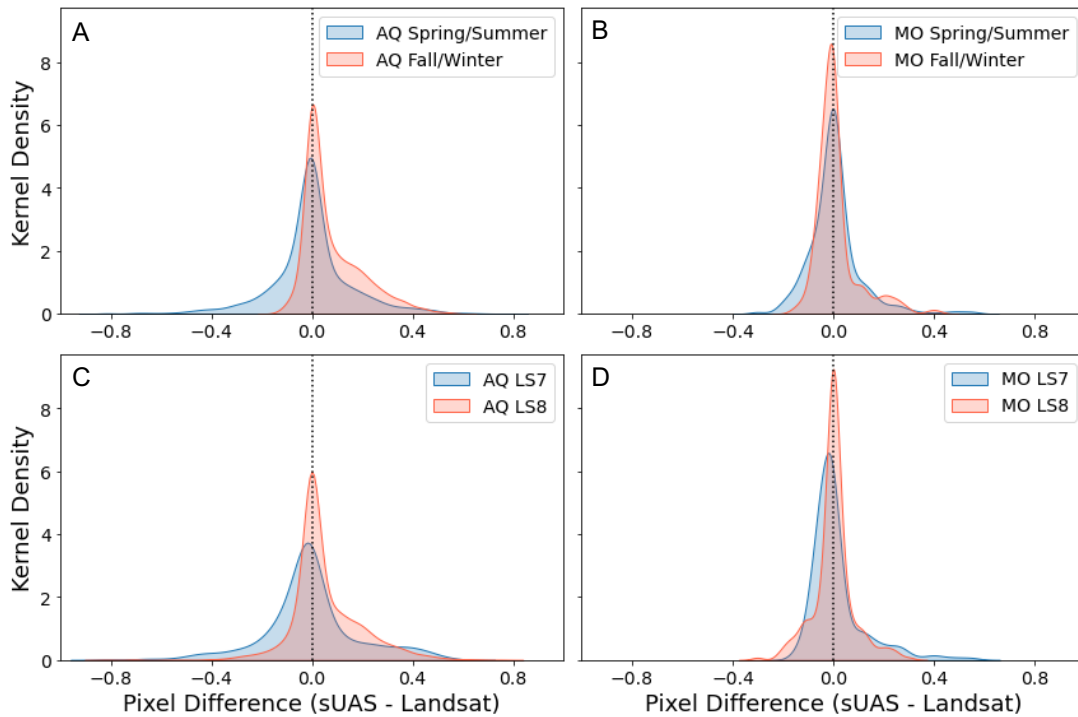


Figure 3.5. Seasonal and Landsat sensor specific kernel density distributions of pixel-based differences between sUAS and Landsat at Arroyo Quemado (A and C) and Mohawk Reef (B and D).

Correlation strength between Landsat MESMA fraction and sUAS kelp fraction were linked to patterns in the site and date specific RMA regressions slopes (Figure 3.6). Slope values close to one corresponded with higher mean Landsat MESMA fractions (Figure 3.6A and B; Table S3.1). Steeper RMA regression slopes, to the left of the 1:1 line, corresponded to mean Landsat MESMA fractions closer to zero.

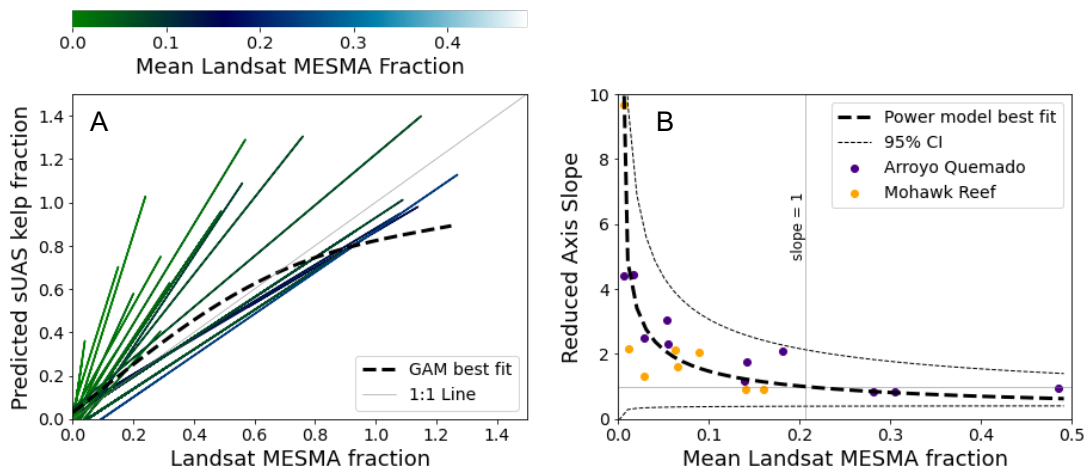


Figure 3.6. (A) Predicted sUAS kelp fraction values based on the Reduced Major Axis (RMA) regressions plotted as a function of Landsat MESMA fraction for each matchup date (regression information shown in Table S3.1), regardless of the binary decision tree classification. Regression lines are color coded by the mean Landsat MESMA fraction and overlaid with the results of a general additive model (GAM) for all pixels across all dates/sites ($r^2 = 0.727$, $p < 2e-16$). The grey line represents the 1:1 line between sUAS and Landsat kelp fractions. (B) RMA regression slope values as a function of the mean Landsat MESMA fraction overlaid with a power model fit ($r^2 = 0.638$; RMSE: 1.281). The horizontal grey line represents a regression slope of 1. The vertical grey line indicates the power model's estimated mean Landsat MESMA fraction where RMA regression slope equals 1.

Although each individual date was modeled using a RMA regression, the overall relationship between Landsat and sUAS kelp fraction displayed a non-linear trend (Figure 3.6A; Figure S3.1; GAM fit: $r^2 = 0.727$, $p < 2e-16$) where Landsat MESMA fractions exceeded 1.2. Both sites displayed a steep drop off in the RMA regression slope between mean Landsat MESMA fractions of approximately 0 to 0.1 and stabilized around 1 for mean fractions greater than 0.1. A power model fit indicated that a slopes greater than 1 corresponded to mean Landsat fractions of less than 0.2 and slopes of approximately 1 generally corresponded to mean Landsat fractions greater than 0.2 (Figure 3.6B).

The influence of site-level characteristics of matchup performance and kelp canopy area was observed between Arroyo Quemado and Mohawk Reef when

investigating the performance of the Landsat binary decision tree classifier and MESMA against the sUAS (Figure 3.7 ‘classified Landsat’ vs. ‘all Landsat’). The relationships between Landsat and sUAS kelp canopy area at Arroyo Quemado followed a similar trend regardless of whether seawater classified pixels were included in the calculation of kelp area or not and estimates of Landsat area were slightly larger than the sUAS in high biomass/density conditions (Figure 3.7A). Increases in canopy cover are associated with seasonal increases in density and canopy biomass (Cavanaugh et al., 2011; Bell et al., 2015), which leads to higher reflectance in the NIR and the effect of these increases on MESMA kelp fraction become apparent in our matchup analysis at MESMA fractions of approximately 0.6 where the GAM best fit line begins to curve towards the right and away from a linear relationship between the two detection methods (Figure 3.6A; Figure S3.1). Kelp canopy area at Mohawk Reef was approximately one order of magnitude lower than Arroyo Quemado, with significantly more scatter around RMA regression lines (Figure 3.7B). Similar trends were observed in the individual timeseries at each site, with little deviation between canopy area determined by Landsat and the sUAS at Arroyo Quemado (Figure 3.7C) and more spread between each individual approach at Mohawk Reef (Figure 3.7D).

Case studies of the pre-classification – Three case study examples from Arroyo Quemado and Mohawk Reef highlighted how the binary decision tree classification scheme presented challenges and limitations in retrieving kelp canopy area from Landsat (Figure 3.8). The Arroyo Quemado Oct. 6, 2017 image was characterized by

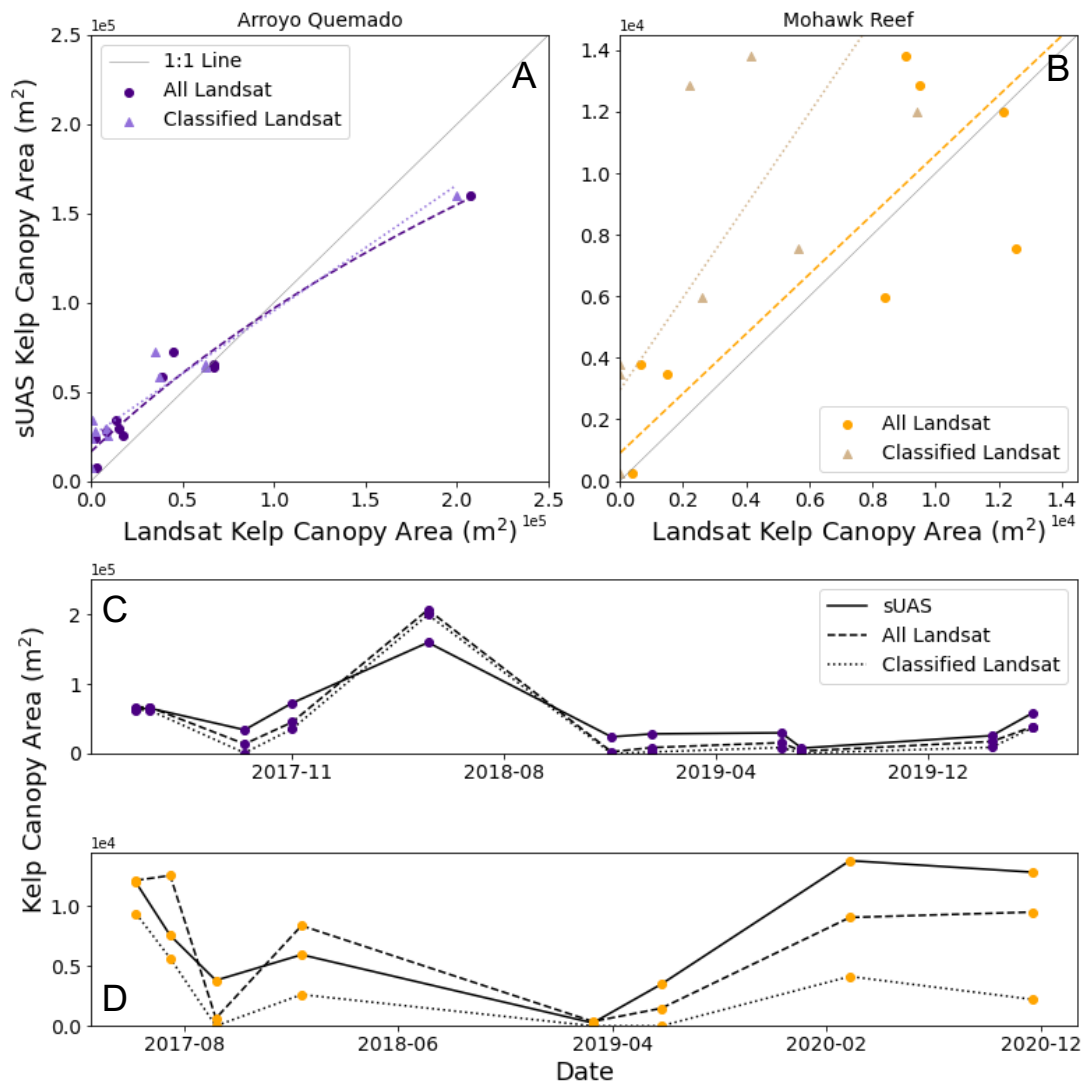


Figure 3.7. Site sUAS kelp canopy area plotted as a function of Landsat kelp canopy area for (A) Arroyo Quemado and (B) Mohawk Reef including all pixels regardless of the binary decision tree classification (circles) and only including pixels that were pre-classified as kelp (triangles). Site kelp canopy area through time for (C) Arroyo Quemado and (D) Mohawk Reef for the sUAS (solid line), including all pixels regardless of the binary decision tree classification (dashed line), and only including pixels that were pre-classified as kelp (dotted line). Regression statistics shown in Table S3.2.

relatively sparse floating canopy (Figure 3.8A; sUAS area = 34000 m²; mean sUAS kelp fraction = 0.13) and Landsat MESMA kelp fractions of less than 0.2 across the entire kelp bed (Figure 3.8B and C). Most pixels were classified as water by the binary decision tree classifier (Figure 3.8C), though visually there was significant kelp canopy

present in the sUAS image (Figure 3.8A). Landsat MESMA also significantly underpredicted kelp fraction relative to the sUAS (Figure 3.8C; slope = 3.03 ± 0.07). The March 18, 2019 Mohawk Reef imagery was characterized by a very sparse floating canopy and small kelp patch (Figure 3.8D and E; sUAS area = 256 m²; mean sUAS kelp fraction = 0.02). All Landsat pixels were classified as water by the binary decision tree classification method, but good agreement between MESMA and the sUAS indicated that MESMA detected very sparse kelp coverage (Figure 3.8F), though visually Landsat appears to miss kelp canopy on the eastern and northern portions of the bed. The June 16, 2017 Mohawk Reef imagery was characterized by dense floating canopy (Figure 3.8G and H; sUAS area = 12000 m²; mean sUAS kelp fraction = 0.23). The relationship between Landsat MESMA fraction and sUAS kelp fraction fell along the 1:1 line (Figure 3.8I), showing strong agreement between the two. Landsat MESMA fraction slightly overestimated sUAS fractions above values between 0.8 – 1.1. In general, pixels less than 0.2 are classified as seawater by the binary decision tree classification method (Figure 3.8; Figure S3.1), but the three case studies presented here show kelp being detected by the sUAS at fractions well below 0.2.

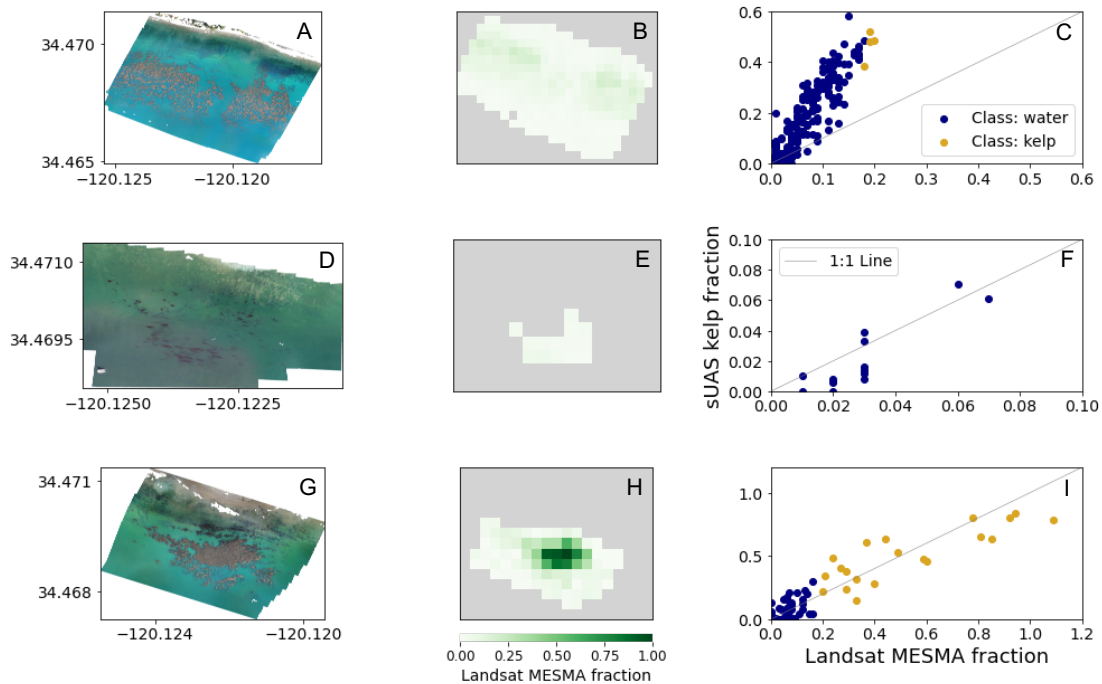


Figure 3.8. sUAS color imagery (A, D, and G), Landsat MESMA fraction (B, E, and H), and sUAS kelp fraction as a function of Landsat MESMA fraction (C, F, and I) for three different case studies. Top row (A - C): October 6, 2017 Arroyo Quemado. Middle row (D - F): March 18, 2019 Mohawk Reef. Bottom row (G - I): June 16, 2017 Mohawk Reef.

Discussion

Influence of Environmental conditions on canopy dynamics – Arroyo Quemado and Mohawk Reef are two relatively protected sites in the Santa Barbara Channel. This region of the southern California coastline is generally defined by lower tidal ranges, currents, and wave height than more northerly and exposed regions within giant kelp’s geographical distribution (i.e., central California; Bell et al., 2015). Despite the fact that this study was conducted for a relatively protected region and designed specifically to reduce environmental variability between Landsat flyovers and sUAS flights (Figure 3.3), the impacts of current velocity were observed on matchups of kelp canopy fraction. These impacts were most apparent on the edge of the kelp bed (Figure 3.4B

and C), and the patterns we observed were spatially similar to previous findings from Arroyo Quemado sUAS imagery where increases in tidal height submerged the sparse edge of the bed, but not the dense center (Cavanaugh et al., 2021).

The temporal offset between the matchups in this study was not long enough to find significant differences between the two sensors at the bed scale, and changes in kelp canopy were only apparent when comparing pixel scale kelp canopy fraction (Figure 3.4). We attributed much of the spatial dynamics of the bed to current velocity, but it's likely that tidal height and current velocity are coupled in this region, and the timescales at which our matchups occur limit our ability to detect changes as a result of tidal height. This indicates that spatial scales, temporal scales, and study design are important when investigating the influence of environmental conditions, especially tides, on kelp canopy area. It is challenging to detect fine-scale spatial dynamics with Landsat canopy cover alone, even across 8 to 16 day repeat flyover timescales. Previous findings indicate that differences in patch/bed scale canopy biomass reflected offsets in tidal state between the eight-day gap between Landsat 5 TM and 7 ETM+ sensors, which led to biases in kelp canopy biomass across Landsat tiles for giant kelp (Bell et al., 2020b). The influence of tides on bull kelp canopy area across annual timescales was not apparent (Finger et al., 2021), but become significant when observed over higher temporal and spatial resolutions (every 10 minutes: Britton-Simmons et al., 2008; every 1 hour: Cavanaugh et al., 2021).

When we compared Landsat MESMA kelp canopy area over a growth season at Arroyo Quemado (January to July 2018) to simultaneous measurements of current

magnitude (Figure 3.4A), reductions in canopy area were associated with increases in east current magnitude. This was especially obvious between mid-May and mid-June when strong current magnitudes corresponded with a dip in canopy area and subsequent recovery that coincided with weak current magnitudes in mid-June. The single sUAS flight during this time period was collected on the day Landsat measured peak canopy area and was 40% lower than Landsat. Differences in canopy detection on the edge of the kelp (Figure 3.4B inset and 3.4C) may be a result of rapidly changing conditions along the edge of the bed from tidal and current conditions across the timescale the two images were collected. The effects of the environmental conditions on kelp at the edge of the bed on May 10, 2018 (Figure 3.4B) represented the largest difference in current magnitude between the Landsat and sUAS imagery across the entire dataset. Current magnitudes at the Landsat flyover were close to zero and stronger during the sUAS flight. The difference observed across such a short window of time indicates the influence of high frequency changes in ocean conditions on canopy characteristics.

Influence of MESMA on Kelp Canopy Matchup Analysis – One important distinction between the sUAS and MESMA fractional estimates of kelp canopy is that the sUAS calculation of canopy fraction originates from a binary estimate of kelp or seawater and fractions are limited to a threshold of 1. This results in a measurement of total kelp canopy cover. The linear unmixing approach of MESMA is not limited to an upper threshold value and can exceed a value of 1 because MESMA measures both canopy cover and surface frond density/biomass relative to pre-defined endmember spectra. It is inexact to describe MESMA kelp canopy fractions as an overestimate of the sUAS

because these two methods determine kelp canopy fraction differently. In fact, robust linear relationships between *in situ* canopy biomass and MESMA kelp fraction have been established (Cavanaugh et al., 2011; Bell et al., 2020b) because upper limits on MESMA kelp fraction do not constrain this relationship. Although the fractional threshold value of 1 for both aerial and sUAS methods can't be defined as a perfect MEMSA comparison, the relationships between MESMA and sUAS kelp fraction helps to further validate large scale aerial estimates of canopy area to Landsat using the MESMA method (Hamilton et al., 2020; Finger et al., 2021) because similar to the sUAS approach applied here, plane-based aerial survey estimates of kelp canopy cover generally rely on a binary pixel classification method.

Specific kelp bed features, such as seasonal changes in bed size and canopy density/biomass (Figure 3.5A and B; 3.6A; 3.7C and D), rather than specific Landsat sensors and their associated errors (Figure 3.5C and D), were more important for driving matchup performance and error across the two sites. Arroyo Quemado, which is a larger, denser kelp bed than Mohawk Reef, had good matchup between the sUAS and Landsat MESMA (Figure 3.7A and C). Mohawk Reef, which is relatively small and sparse showed more scatter between the matchups (Figure 3.7B and D). As a result, we can expect more error in Landsat MESMA estimates when observing low canopy biomass or fringing kelp bed conditions. These conditions commonly occur in regions where benthic substrate conditions are not suitable for continuous kelp colonization (Young and Carr, 2015; Nijland et al., 2019) or biological and environmental

disruptions have resulted in a kelp ecosystem collapse (Johnson et al., 2011; Butler et al., 2020; McPherson et al., 2021).

Verification of pixel classification on Kelp Canopy Matchup Analysis – The binary decision tree classification method is an important step in the automated processing scheme to develop long-term timeseries of kelp canopy area and biomass for the northeast Pacific region because it shortens processing time and computation demand. However, it is important to understand how this approach influences the overall timeseries product and local/regional estimates of canopy area and biomass. We found that the classifier generally classified MESMA kelp fractions of < 0.2 as seawater (Figure 3.8; Figure S3.1) and, therefore, is conservative. This resulted in low kelp densities commonly being classified as seawater across both sites. Similar to site differences in performance of MEMSA, the implications of the pre-classification step on Mohawk Reef were greater than Arroyo Quemado (Figure 3.7B and D) because it's generally a smaller kelp bed with lower biomass kelp pixel fractions. This resulted in larger errors between the sUAS and MESMA (for pixels classified as kelp) and a strong deviation from the 1:1 line between total canopy area (Figure 3.7B). Despite these challenges, the classifier is necessary from a quality control perspective because MESMA can be noisy across Landsat sensors (especially Landsat 5 TM and 7 ETM+) and is unpredictable at a regional scale beyond the spatial scales used in this study. Problems with image quality/noise (i.e., haze, glint, scattering from turbid pixels) that we did not observe across in the sensor matchups at Arroyo Quemado and Mohawk Reef can dramatically alter the accuracy of both the classifier and MESMA

performance. Together, these uncertainties ultimately influence the accuracy of canopy area cover and biomass estimates.

Conclusions

This study provides broader context for validation approaches to satellite derived timeseries by utilizing a unique multiyear dataset of near-simultaneous matchups between sUAS color imagery and multispectral Landsat data, and helps work towards developing approaches to improve a regional northeast Pacific kelp canopy timeseries. By exploring pixel and bed scale uncertainties with regard to environmental processes, pre-classification, and MESMA methods, we have a more nuanced perspective on factors influencing the timeseries results. Though we observed changes in pixel-scale kelp canopy fraction and bed-scale area due to environmental fluctuations of currents and tides, the quarterly (3 month) means used in the current kelp canopy Landsat product likely reduces these effects by averaging out temporal variability (Bell et al., 2020b). Furthermore, since nearly all Landsat pixels below a MESMA fraction of 0.2 are removed by the automated pre-classification step, end-users can have high confidence in the Landsat dataset for regional scales trends in kelp canopy cover. However, defining exact error based on bed size is difficult because the study was only conducted for two kelp beds in the Santa Barbara Channel and kelp canopy fractions can vary significantly across seasons (regardless of bed size) and within a bed. Rather, pixel scale uncertainty appears to be more relevant to end-users studying local kelp patterns in sparse and/or fringing kelp beds.

Future applications of the Landsat kelp canopy dataset should take into account the particular use cases where this knowledge is relevant, such as kelp restoration efforts and metapopulation studies. Due to the high spatio-temporal resolution at which imagery is collected and its cost-effective nature, large-scale satellite mapping approaches are playing a vital role in observing the effectiveness of restoration programs and detecting recovery from widespread urchin barrens to kelp forest in the northeast Pacific region (Hohman et al., 2019). It would be beneficial for early and accurate detection of kelp recovery to inspect the MESMA outputs of all pixels (regardless of whether a pixel is defined as kelp or seawater by the binary decision tree classification step) since recovering kelp beds may be below fractions of 0.2. Additionally, metapopulation studies should apply a conservative temporal period of absence/presence (over 1 year) before classifying patches as empty or extinct (needing recolonization) since kelp canopy can be present at very low densities and avoid detection by Landsat. This approach will likely improve estimates of connectivity and likelihood of persistence through more accurate estimates of patch size, and extinct/extant status (Castorani et al., 2015).

Acknowledgements

We are grateful to Jordan Snyder, Libe Washburn, and all the SBC LTER scientific divers, field technicians, and student volunteers for their assistance with field data collection. We are grateful to Dave Siegel (University of California Santa Cruz) and Raphael Kudela (University of California Santa Cruz) for their helpful guidance and

feedback on the manuscript's scientific goals and data analysis. This work was supported by the US Department of Energy's Advanced Research Projects Agency–Energy (ARPA-E; DE-AR0000922), the US National Science Foundation (OCE 1831937), and by the National Aeronautics and Space Administration (NNX14AR62A).

References

- Alvain, S., Moulin, C., Dandonneau, Y., and Bréon, F. M. (2005). Remote sensing of phytoplankton groups in case 1 waters from global SeaWiFS imagery. *Deep. Res. Part I Oceanogr. Res. Pap.* 52, 1989–2004. doi:10.1016/j.dsr.2005.06.015.
- Arafeh-Dalmau, N., Montaña-moctezuma, G., Martínez, J. A., and Smale, D. A. (2019). Extreme Marine Heatwaves Alter Kelp Forest Community Near Its Equatorward Distribution Limit. *Front. Mar. Sci.* 6, 1–18. doi:10.3389/fmars.2019.00499.
- Banerjee, B. P., Raval, S., and Cullen, P. J. (2020). UAV-hyperspectral imaging of spectrally complex environments. *Int. J. Remote Sens.* 41, 4136–4159. doi:10.1080/01431161.2020.1714771.
- Behrenfeld, M. J., Boss, E., Siegel, D. A., and Shea, D. M. (2005). Carbon-based ocean productivity and phytoplankton physiology from space. *Global Biogeochem. Cycles* 19, 1–14. doi:10.1029/2004GB002299.
- Bell, T., Nidzieko, N. J., Siegel, D. A., Miller, R. J., Cavanaugh, K. C., Nelson, N. B., et al. (2020a). The Utility of Satellites and Autonomous Remote Sensing Platforms for Monitoring Offshore Aquaculture Farms: A Case Study for Canopy Forming Kelps. *Front. Mar. Sci.* doi:10.3389/fmars.2020.520223.
- Bell, T. W., Allen, J. G., Cavanaugh, K. C., and Siegel, D. A. (2020b). Three decades of variability in California's giant kelp forests from the Landsat satellites. *Remote Sens. Environ.* 238. doi:10.1016/j.rse.2018.06.039.
- Bell, T. W., Cavanaugh, K. C., Reed, D. C., and Siegel, D. A. (2015). Geographical variability in the controls of giant kelp biomass dynamics. *J. Biogeogr.* 42, 2010–2021. doi:10.1111/jbi.12550.
- Britton-Simmons, K., Eckman, J. E., and Duggins, D. O. (2008). Effect of tidal currents and tidal stage on estimates of bed size in the kelp *Nereocystis luetkeana*. *Mar. Ecol. Prog. Ser.* 355, 95–105. doi:10.3354/meps07209.

- Butler, C. L., Lucieer, V. L., Wotherspoon, S. J., and Johnson, C. R. (2020). Multi-decadal decline in cover of giant kelp *Macrocystis pyrifera* at the southern limit of its Australian range. *Mar. Ecol. Prog. Ser.* 653, 1–18. doi:10.3354/meps13510.
- Castorani, M. C. N., Reed, D. C., Alberto, F., Bell, T. W., Simons, R. D., Cavanaugh, K. C., et al. (2015). Connectivity structures local population dynamics: A long-term empirical test in a large metapopulation system. *Ecology* 96, 3141–3152. doi:10.1890/15-0283.1.
- Cavanaugh, K. C., Cavanaugh, K. C., Bell, T. W., and Hockridge, E. G. (2021). An Automated Method for Mapping Giant Kelp Canopy Dynamics from UAV. *Front. Environ. Sci.* 8:587354, 1–16. doi:10.3389/fenvs.2020.587354.
- Cavanaugh, K. C., Reed, D. C., Bell, T. W., Castorani, M. C. N., Beas-luna, R., and Barrett, N. S. (2019). Spatial Variability in the Resistance and Resilience of Giant Kelp in Southern and Baja California to a Multiyear Heatwave. *Front. Mar. Sci.* 6, 1–14. doi:10.3389/fmars.2019.00413.
- Cavanaugh, K. C., Siegel, D. A., Reed, D. C., and Dennison, P. E. (2011). Environmental controls of giant-kelp biomass in the Santa Barbara Channel, California. *Mar. Ecol. Prog. Ser.* 429, 1–17. doi:10.3354/meps09141.
- Cheng, K. H., Chan, S. N., and Lee, J. H. W. (2020). Remote sensing of coastal algal blooms using unmanned aerial vehicles (UAVs). *Mar. Pollut. Bull.* 152, 110889. doi:10.1016/j.marpolbul.2020.110889.
- Collins, M., Sutherland, M., Bouwer, L., Cheong, S.-M., Frölicher, T., Combes, H. J. Des, et al. (2019). “Extremes, Abrupt Changes and Managing Risks,” in *IPCC Special Report on the Ocean and Cryosphere in a Changing Climate*, eds. H.-O. Pörtner, D. C. Roberts, V. Masson-Delmotte, P. Zhai, M. Tignor, E. Poloczanska, et al., 589–656.
- Di Lorenzo, E., Schneider, N., Cobb, K. M., Franks, P. J. S., Chhak, K., Miller, A. J., et al. (2008). North Pacific Gyre Oscillation links ocean climate and ecosystem change. *Geophys. Res. Lett.* 35, 2–7. doi:10.1029/2007GL032838.

- Doney, S. C., Ruckelshaus, M., Emmett Duffy, J., Barry, J. P., Chan, F., English, C. A., et al. (2012). Climate change impacts on marine ecosystems. *Ann. Rev. Mar. Sci.* 4, 11–37. doi:10.1146/annurev-marine-041911-111611.
- Finger, D. J. I., McPherson, M. L., Houskeeper, H. F., and Kudela, R. M. (2021). Mapping bull kelp canopy in northern California using Landsat to enable long-term monitoring. *Remote Sens. Environ.* 254, 112243. doi:10.1016/j.rse.2020.112243.
- Fraser, R. H., Olthof, I., Carrière, M., Deschamps, A., and Pouliot, D. (2011). Detecting long-term changes to vegetation in northern Canada using the Landsat satellite image archive. *Environ. Res. Lett.* 6. doi:10.1088/1748-9326/6/4/045502.
- Friedlander, A. M., Ballesteros, E., Bell, T. W., Caselle, J. E., Campagna, C., Goodell, W., et al. (2020). Kelp forests at the end of the earth: 45 years later. *PLoS One* 15, 1–23. doi:10.1371/journal.pone.0229259.
- Giri, C., Ochieng, E., Tieszen, L. L., Zhu, Z., Singh, A., Loveland, T., et al. (2011). Status and distribution of mangrove forests of the world using earth observation satellite data. *Glob. Ecol. Biogeogr.* 20, 154–159. doi:10.1111/j.1466-8238.2010.00584.x.
- Gray, P. C., Ridge, J. T., Poulin, S. K., Seymour, A. C., Schwantes, A. M., Swenson, J. J., et al. (2018). Integrating drone imagery into high resolution satellite remote sensing assessments of estuarine environments. *Remote Sens.* 10. doi:10.3390/rs10081257.
- Hamilton, S. L., Bell, T. W., Watson, J. R., Grorun-Colvert, K. A., and Menge, B. A. (2020). Remote sensing: generation of long-term kelp bed data sets for evaluation of impacts of climatic variation. *Ecology* 0, 1–13. doi:10.1002/ecy.3031.
- Haskins, J., Endris, C., Thomsen, A. S., Gerbl, F., Fountain, M. C., Wasson, K., et al. (2021). UAV to Inform Restoration : A Case Study From a California Tidal Marsh. *Front. Environmental Sci.* 9, 1–20. doi:10.3389/fenvs.2021.642906.

- Hermosilla, T., Wulder, M. A., White, J. C., Coops, N. C., and Hobart, G. W. (2018). Disturbance-Informed Annual Land Cover Classification Maps of Canada's Forested Ecosystems for a 29-Year Landsat Time Series. *Can. J. Remote Sens.* 44, 67–87. doi:10.1080/07038992.2018.1437719.
- Hohman, R., Hutto, S., Catton, C. A., and Koe, F. (2019). Sonoma-Mendocino Bull Kelp Recovery Plan. Plan for the Greater Farallones National Marine Sanctuary and the California Department of Fish and Wildlife. San Francisco, CA.
- Iizuka, K., Itoh, M., Shiodera, S., Matsubara, T., Dohar, M., and Watanabe, K. (2018). Advantages of unmanned aerial vehicle (UAV) photogrammetry for landscape analysis compared with satellite data: A case study of postmining sites in Indonesia. *Cogent Geosci.* 4, 1–15. doi:10.1080/23312041.2018.1498180.
- Johnson, C. R., Banks, S. C., Barrett, N. S., Cazassus, F., Dunstan, P. K., Edgar, G. J., et al. (2011). Climate change cascades: Shifts in oceanography, species' ranges and subtidal marine community dynamics in eastern Tasmania. *J. Exp. Mar. Bio. Ecol.* 400, 17–32. doi:10.1016/j.jembe.2011.02.032.
- Kahru, M., Kudela, R. M., Manzano-Sarabia, M., and Greg Mitchell, B. (2012). Trends in the surface chlorophyll of the California Current: Merging data from multiple ocean color satellites. *Deep. Res. Part II Top. Stud. Oceanogr.* 77–80, 89–98. doi:10.1016/j.dsr2.2012.04.007.
- Kislik, C., and Dronova, I. (2018). UAVs in Support of Algal Bloom Research : A Review of Current Applications and Future Opportunities. *Drones* 2, 1–14. doi:10.3390/drones2040035.
- Kudela, R. M., Hooker, S. B., Houskeeper, H. F., and McPherson, M. L. (2019). The Influence of Signal to Noise Ratio of Legacy Airborne and Satellite Sensors for Simulating Next-Generation Coastal and Inland Water Products. *Remote Sens.* 11.
- Larrinaga, A. R., and Brotons, L. (2019). Greenness indices from a low-cost UAV imagery as tools for monitoring post-fire forest recovery. *Drones* 3, 1–16. doi:10.3390/drones3010006.

- Laufkötter, C., Zscheischler, J., and Frolicher, T. L. (2020). High-impact marine heatwaves attributable to human-induced global warming. *Science* (80-.). 369, 1621–1625.
- Mackas, D. L., Greve, W., Edwards, M., Chiba, S., Tadokoro, K., Eloire, D., et al. (2012). Changing zooplankton seasonality in a changing ocean: Comparing time series of zooplankton phenology. *Prog. Oceanogr.* 97–100, 31–62. doi:10.1016/j.pocean.2011.11.005.
- Margono, B. A., Turubanova, S., Zhuravleva, I., Potapov, P., Tyukavina, A., Baccini, A., et al. (2012). Mapping and monitoring deforestation and forest degradation in Sumatra (Indonesia) using Landsat time series data sets from 1990 to 2010. *Environ. Res. Lett.* 7, 2000–2010. doi:10.1088/1748-9326/7/3/034010.
- Martin, F. M., Müllerová, J., Borgniet, L., Dommange, F., Breton, V., and Evette, A. (2018). Using single- and multi-date UAV and satellite imagery to accurately monitor invasive knotweed species. *Remote Sens.* 10. doi:10.3390/rs10101662.
- Masek, J. G., Goward, S. N., Kennedy, R. E., Cohen, W. B., Moisen, G. G., Schlee, W., et al. (2013). United States Forest Disturbance Trends Observed Using Landsat Time Series. *Ecosystems* 16, 1087–1104. doi:10.1007/s10021-013-9669-9.
- McPherson, M. L., Finger, D. J. I., Houskeeper, H. F., Bell, T. W., Carr, M. H., Rogers-Bennett, L., et al. (2021). Large-scale shift in the structure of a kelp forest ecosystem co-occurs with an epizootic and marine heatwave. *Commun. Biol.* 4, 1–9. doi:10.1038/s42003-021-01827-6.
- Mieszkowska, N., Sugden, H., Firth, L. B., and Hawkins, S. J. (2014). The role of sustained observations in tracking impacts of environmental change on marine biodiversity and ecosystems. *Philos. Trans. R. Soc. A Math. Phys. Eng. Sci.* 372. doi:10.1098/rsta.2013.0339.
- Müllerová, J., Brůna, J., Bartaloš, T., Dvořák, P., Vítková, M., and Pyšek, P. (2017). Timing is important: Unmanned aircraft vs. Satellite imagery in plant invasion monitoring. *Front. Plant Sci.* 8, 1–13. doi:10.3389/fpls.2017.00887.

- Nguyen, L. H., Joshi, D. R., Clay, D. E., and Henebry, G. M. (2020). Characterizing land cover/land use from multiple years of Landsat and MODIS time series: A novel approach using land surface phenology modeling and random forest classifier. *Remote Sens. Environ.* 238, 111017. doi:10.1016/j.rse.2018.12.016.
- Nijland, W., Reshitnyk, L., and Rubidge, E. (2019). Remote Sensing of Environment Satellite remote sensing of canopy-forming kelp on a complex coastline: A novel procedure using the Landsat image archive. *Remote Sens. Environ.* 220, 41–50. doi:10.1016/j.rse.2018.10.032.
- Nowak, M. M., Dziób, K., and Bogawski, P. (2019). Unmanned Aerial Vehicles (UAVs) in environmental biology: A review. *Eur. J. Ecol.* 4, 56–74. doi:10.2478/eje-2018-0012.
- Oliver, E. C. J., Donat, M. G., Burrows, M. T., Moore, P. J., Smale, D. A., Alexander, L. V, et al. (2018). Longer and more frequent marine heatwaves over the past century. *Nat. Commun.* 9, 1–12. doi:10.1038/s41467-018-03732-9.
- Riihimäki, H., Luoto, M., and Heiskanen, J. (2019). Estimating fractional cover of tundra vegetation at multiple scales using unmanned aerial systems and optical satellite data. *Remote Sens. Environ.* 224, 119–132. doi:10.1016/j.rse.2019.01.030.
- Roberts, D. A., Gardner, M., Church, R., Ustin, S., Scheer, G., and Green, R. O. (1998). Mapping chaparral in the Santa Monica Mountains using multiple endmember spectral mixture models. *Remote Sens. Environ.* 65, 267–279. doi:10.1016/S0034-4257(98)00037-6.
- Ryan, J. P., Fischer, A. M., Kudela, R. M., Gower, J. F. R., King, S. A., Marin, R., et al. (2009). Influences of upwelling and downwelling winds on red tide bloom dynamics in Monterey Bay, California. *Cont. Shelf Res.* 29, 785–795. doi:10.1016/j.csr.2008.11.006.
- Stenseth, N. C., Mysterud, A., Ottersen, G., Hurrell, J. W., Chan, K. S., and Lima, M. (2002). Ecological effects of climate fluctuations. *Science (80-)*. 297, 1292–1296. doi:10.1126/science.1071281.

- Tegner, M. J. M., and Dayton, P. K. P. (1987). El Nino effects on southern California kelp forest communities. *Adv. Ecol. Res.* 17, 243–279. doi:10.1016/S0065-2504(08)60247-0.
- Topouzelis, K., Papakonstantinou, A., and Garaba, S. P. (2019). Detection of floating plastics from satellite and unmanned aerial systems (Plastic Litter Project 2018). *Int. J. Appl. Earth Obs. Geoinf.* 79, 175–183. doi:10.1016/j.jag.2019.03.011.
- Ventura, D., Bonifaze, A., Gravina, M. F., Belluscio, A., and Ardizzone, G. (2018). Marine Habitats Using Unmanned Aerial Vehicle. *Remote Sens.* 10, 1–23. doi:10.3390/rs10091331.
- Washburn, L., Gotschalk, C., and Salazar, D. (2021a). SBC LTER: Ocean: Currents and Biogeochemistry: Moored CTD and ADCP data from Arroyo Quemado Reef Mooring (ARQ), ongoing since 2004 ver 22. *Environ. Data Initiat.* doi:<https://doi.org/10.6073/pasta/2ec9f1ad16a8675704b926364ac8f2a3>. Accessed 2021-04-18.
- Washburn, L., Gotschalk, C., and Salazar, D. (2021b). SBC LTER: Ocean: Currents and Biogeochemistry: Moored CTD and ADCP data from Mohawk Outside Spar (MKO), ongoing since 2005 ver 14. *Environ. Data Initiat.* doi:<https://doi.org/10.6073/pasta/73056be98f1f4482940908cf5786d742>. Accessed 2021-04-18.
- Westberry, T., Behrenfeld, M. J., Siegel, D. A., and Boss, E. S. (2008). Carbon-based primary productivity modeling with vertically resolved photoacclimation. *Global Biogeochem. Cycles* 22, 1–18. doi:10.1029/2007GB003078.
- Wu, T., Zheng, W., Yin, W., and Zhang, H. (2021). Development and Performance Evaluation of a Very Low-Cost UAV-Lidar system for Forestry Applications. *Remote Sens.* 13, 1–19. doi:10.3390/rs13010077.
- Young, M. A., Cavanaugh, K. C., Bell, T. W., Raimondi, P. T., Edwards, C. A., Drake, P. T., et al. (2015). Environmental controls on spatial patterns in the long-term persistence of giant kelp in central California. *Ecology* 86, 45–60. doi:10.1890/15-0267.1.

Young, M., and Carr, M. (2015). Assessment of Habitat Representation across a Network of Marine Protected Areas with Implications for the Spatial Design of Monitoring. *PLoS One* 10, 1–23. doi:10.1371/journal.pone.0116200.

Zimmerman, R. C., and Kremer, J. N. (1984). Episodic nutrient supply to a kelp forest ecosystem in Southern California. *J. Mar. Res.* 42, 591–604. doi:10.1357/002224084788506031.

Supplemental Material

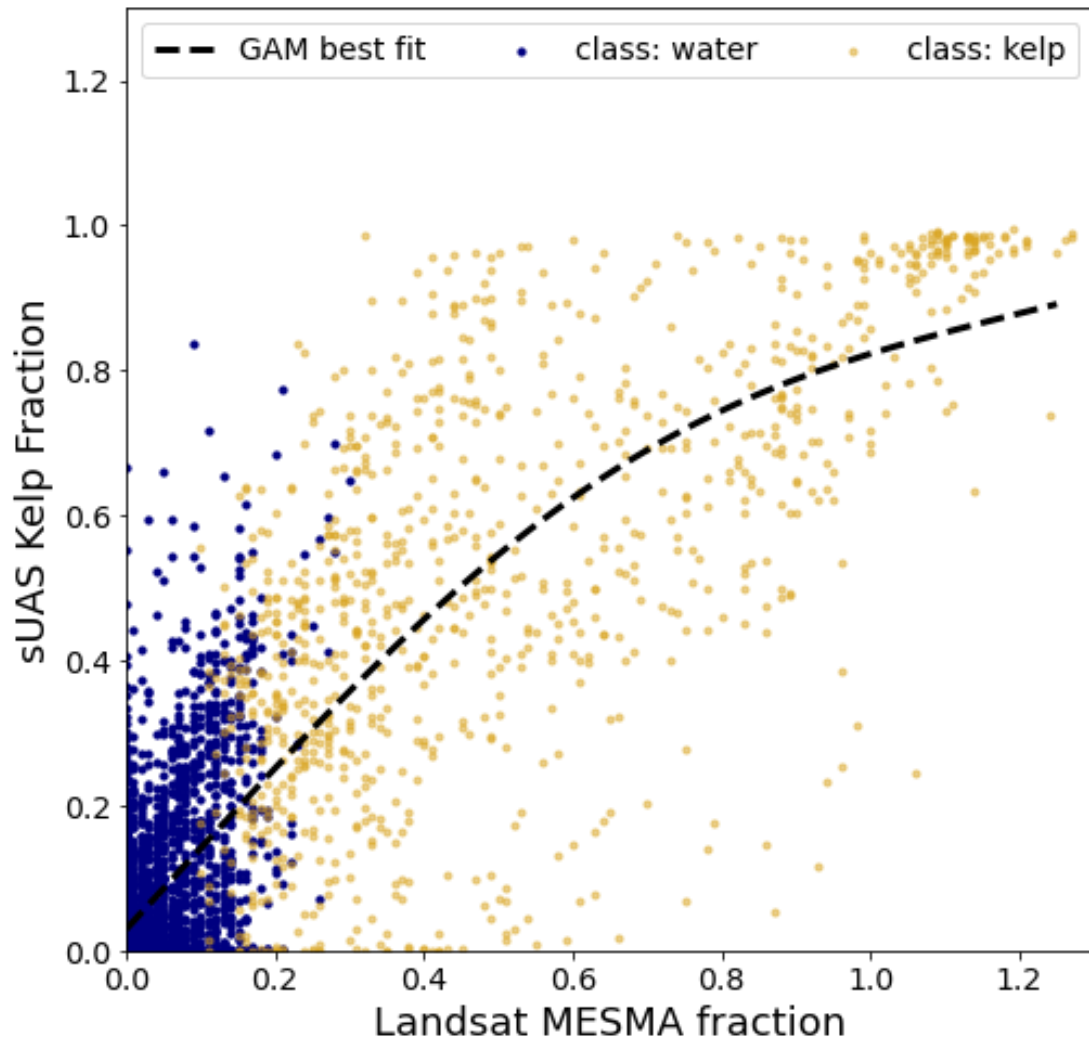
Supplemental Table 1 (Table S3.1). RMA regression statistics corresponding to each matchup date across both sites in Figure 3.6. Standard deviations for RMA regression slopes and intercepts are included.

Site	Date	Slope	Intercept	r
Arroyo Quemado (34.467°N 120.118°W)	May 31, 2017	0.826 ± 0.031	0.039 ± 0.013	0.828
	June 16, 2017	0.842 ± 0.023	0.038 ± 0.009	0.906
	October 6, 2017	3.032 ± 0.068	-0.029 ± 0.005	0.931
	December 1, 2017	2.103 ± 0.046	-0.089 ± 0.011	0.934
	May 10, 2018	0.960 ± 0.020	-0.091 ± 0.013	0.901
	December 12, 2018	4.417 ± 0.214	0.040 ± 0.005	0.556
	January 29, 2019	2.500 ± 0.066	0.024 ± 0.004	0.887
	June 30, 2019	2.301 ± 0.076	-0.021 ± 0.008	0.832
	July 24, 2019	4.429 ± 0.325	-0.035 ± 0.009	0.451
	March 4, 2020	1.770 ± 0.097	-0.040 ± 0.021	0.804
	April 21, 2020	1.175 ± 0.033	0.047 ± 0.010	0.877
Mohawk Reef (34.934°N 119.73°W)	June 16, 2017	0.918 ± 0.038	0.011 ± 0.011	0.930
	August 3, 2017	0.912 ± 0.052	-0.044 ± 0.012	0.844
	October 6, 2017	9.672 ± 1.089	-0.026 ± 0.011	0.367
	February 3, 2018	1.595 ± 0.081	-0.058 ± 0.007	0.819
	March 18, 2019	1.319 ± 0.177	-0.018 ± 0.006	0.892
	June 22, 2019	2.148 ± 0.120	0.003 ± 0.004	0.785
	March 12, 2020	2.053 ± 0.113	-0.048 ± 0.016	0.835
	November 23, 2020	2.113 ± 0.098	-0.048 ± 0.009	0.820

Supplemental Table 2 (Table S3.2). Logarithmic and RMA regression statistics corresponding to Figure 3.7 where sUAS kelp canopy area is plotted as a function of Landsat kelp canopy area for Arroyo Quemado (AQ) and Mohawk Reef (MO). ‘All Landsat’ indicates that all pixels (regardless of the binary decision tree classification) were included in the calculation of kelp canopy area. ‘Classified Landsat’ indicates that only pixels identified as kelp via the binary decision tree classification were included in the calculation of kelp canopy area. For AQ ‘All Landsat’ a logarithmic regression (shown on Figure 3.7) was used to optimize curve fitting. We have also included RMA regression statistics for that category below for comparison and reference to the ‘Classified Landsat’ RMA regression fits but are not displayed on Figure 3.7 in the main text. Standard deviations for logarithmic coefficients (‘Coef’) and RMA regression slopes and intercepts are included.

Site	Group	Coef 1 (a)	Coef 2 (b)	Coef 3 (c)	Type	Python function
AQ	All Landsat	146628.0 ± 103230.3	216352.1 ± 206543.3	-2582271.2 ± 2027032.4	logarithmic regression: $a * \log_2(x + b) + c$	scipy.optimize curve_fit
Site	Group	Slope	Intercept	r	Type	Python function
AQ	All Landsat	0.7042 ± 0.0535	20651.3 ± 3816.6	0.9741	RMA regression	pylr2 regress2
AQ	Classified Landsat	0.7053 ± 0.0583	24891.4 ± 3955.05	0.9692	RMA regression	pylr2 regress2
MO	All Landsat	0.9684 ± 0.2556	905.8 ± 2121.02	0.7911	RMA regression	pylr2 regress2
MO	Classified Landsat	1.4995 ± 0.498	2961.5 ± 2149.6	0.669	RMA regression	pylr2 regress2

Supplemental Figure 1 (Figure S3.1). General additive model (GAM) best fit line for all pixels across all dates/sites ($r^2 = 0.727$, $p < 2e-16$).



CONCLUSION

Remote sensing data are highly advantageous for mapping kelp canopy and have evolved through time from simple photogrammetric collection for estimating harvestable biomass¹ to complex hyperspectral imaging for canopy physiological condition^{2,3}. Plane-based aerial surveys were historically, and continue to be, important for mapping kelp canopy area^{4,5}. However, our (1) access to continuous, moderate-resolution multispectral imagery and (2) understanding of the spatio-temporal patterns and drivers of kelp canopy dynamics were greatly improved after the development and expansion of a satellite-derived timeseries of kelp canopy from 30 m resolution Landsat across the last decade⁶⁻⁸. Despite continued technological improvements, data gaps continue to exist, especially for specific regional (i.e. northern California), kelp genera (i.e. bull kelp), and methodological (i.e. MESMA) observations and validations. Due to the importance of these satellite-derived data in applications from kelp ecology⁹, to management¹⁰, monitoring, and restoration¹¹, this dissertation prioritized investigating those data gaps and the improvement of kelp mapping efforts.

The new observational and methodological perspectives presented in this dissertation improve the overall science of kelp canopy ecosystem dynamics and the quality of data accessible to end-users across multiple fields. However, I include recommendations for future efforts in the kelp remote sensing sphere, especially as technological advances, including improved spaceborne sensors, UASs, and processing

schemes/platforms (i.e. Google Earth Engine and TNC Kelp Watch) continue to become more widely available.

First, Landsat imagery has proved to be valuable for assessing regional-scale trends in kelp canopy coverage and has greatly increased the understanding of spatial variability in the environmental and biological processes driving kelp canopy dynamics in the northeast Pacific region (Chapter 1). This long-term timeseries is now available from Baja California, Mexico to the Washington, USA - Canadian border. As a result of this increased data availability and collaboration, the number of studies utilizing Landsat derived timeseries of kelp canopy in the northeast Pacific region has risen over the last decade^{6,8,9,12-16}. Since application of the Landsat dataset to other temperate regions has been sluggish (only two studies exist in the literature^{17,18}), expanding beyond the northeast Pacific to other temperate regions will be highly advantageous for studying global variability in processes that drive kelp canopy dynamics and ecology.

Second, the development of similar regional-scale datasets for emerging spaceborne sensors with higher spatial resolutions should be prioritized. These sensors can help to account for low biomass and sparse kelp patches/pixels that are difficult and labor intensive to detect using Landsat 30 m resolution imagery (Chapter 3). Additionally, higher resolution satellite imagery may be more advantageous and provide better matchup to aerial survey data than Landsat, which has been shown to underestimate kelp area relative to state-funded, plane-based imagery^{14,19}. Obvious platforms for future development of kelp timeseries include Planet Scope (3 m resolution; available from 2016) and ESA Sentinel 2 (10 m resolution; available from

2105). State agencies are increasingly interested in using spaceborne imagery to replace the costly aerial surveys, especially with imagery of comparable pixel resolutions (< 3 m). Despite the appealing spatial resolution of Planet Scope, significant hurdles are associated with the data processing pipeline, imagery quality (radiometric calibration and georeferencing), and cost of imagery acquisition at large spatial scales. However, progress to produce a reliable kelp canopy dataset has been made by scientists at UC Los Angeles (pers. comm. K. Cavanaugh).

A global timeseries dataset of kelp canopy exists from Sentinel 2 imagery²⁰, but authors note that it's not reliable for kelp beds smaller than 1 hectare (10,000 m²). Therefore, the particular methodological approaches might present similar challenges as Landsat (Chapter 3), but Sentinel 2 may, in some ways, be advantageous to Planet Scope data because imagery is high-quality and freely available. Ultimately, it would be valuable to directly compare the kelp canopy estimates from each sensor (Planet Scope, Sentinel 2, and Landsat) to assess the caveats and benefits of each platform and, therefore, provide thorough recommendations to agencies looking to implement/fund development of these datasets.

Third, there are several opportunities to implement localized studies and validation efforts using UAS platforms. Targeted improvement and validation of the Landsat kelp canopy timeseries using high resolution, multispectral UAS datasets will help improve uncertainty estimates of MESMA kelp canopy fraction and allows for a more direction comparison to Landsat data than 3-band color imagery (Chapter 3).

However, there are barriers associated with obtaining expensive multispectral sensors and the appropriate UAS platforms that might limit this data collection.

The flexibility of UAS platforms are practical tools for validation of canopy biomass estimates (even in long-term validation studies) because *in situ* diver or canopy surveys can be conducted simultaneously with imagery acquisition rather than coordinating dive efforts with clear sky satellite overpasses (Chapter 2). Furthermore, the collection of these data can be combined with citizen science efforts that overlap with *in situ* surveys (i.e. Reef Check California) or expand likelihood for data collection in remote regions of the coastline.

Beyond the practical applications of UASs for validation, these tools can be used to investigate seasonal to annual fluctuations in kelp canopy physiology and kelp bed phenology. Existing studies of kelp canopy physiology using hyperspectral imagery have demonstrated within patch variability of Chl:C and nitrogen content (metrics for blade health and senescence)^{2,3}. Hyperspectral sensors, and 10-band multispectral sensors (MicaSense Blue-Edge) mounted to UASs provide an opportunity to assess these physiological dynamics at local scales, with applications to kelp ecology, aquaculture, and restoration.

Satellites have thus far been used to investigate seasonal fluctuations in kelp canopy dynamics², but UASs allow for higher frequency observations that may help refine observations and timeseries of localized kelp response to discrete events, such as storms and marine heatwaves, without relying on satellite imagery. Moreover, timing of spring canopy emergence can be correlated to specific temporal and spatial

environmental conditions, offering insight into phenological changes associated with climate change and other discrete events.

Beyond specific science recommendation for future research using existing and emerging remote sensing techniques, this dissertation provides targeted suggestions for management and restoration strategies. Overall, time series measurements of remotely sensed and *in situ* data for biological and environmental parameters relevant to kelp forest ecosystems should be prioritized as they are relevant to development of adaptive management strategies (quantifying historical baselines, setting thresholds for monitoring criteria, developing restoration targets, tracking ecosystem recovery, and implementing environmental forecasting models; Chapter 1). If management agencies continue to prioritize blue carbon as a worthwhile climate change related policy, long-term monitoring programs for biomass validation across the northeast Pacific region should be established beyond a small number of existing well-characterized sites to understand sub-regional to regional canopy characteristics and matchups (Chapter 2). Finally, though an automated processing scheme for Landsat kelp canopy timeseries⁷ has sufficiently improved the data product quality since its origin, future applications of the Landsat kelp canopy dataset should take into account particular use cases, such as kelp restoration efforts and metapopulation studies, where kelp pixels in sparse and/or fringing kelp beds are removed by (Chapter 3).

References

1. North, W. J., James, D. E. & Jones, L. G. History of kelp beds (*Macrocystis*) in Orange and San Diego Counties, California. *Dev. Hydrobiol.* **85**, 277–283 (1993).
2. Bell, T. W., Cavanaugh, K. C. & Siegel, D. A. Remote monitoring of giant kelp biomass and physiological condition: An evaluation of the potential for the Hyperspectral Infrared Imager (HyspIRI) mission. *Remote Sens. Environ.* **167**, 218–228 (2015).
3. Bell, T. *et al.* The Utility of Satellites and Autonomous Remote Sensing Platforms for Monitoring Offshore Aquaculture Farms: A Case Study for Canopy Forming Kelps. *Front. Mar. Sci.* (2020). doi:10.3389/fmars.2020.520223
4. Pfister, C. A., Berry, H. D. & Mumford, T. The dynamics of Kelp Forests in the Northeast Pacific Ocean and the relationship with environmental drivers. *J. Ecol.* 1–14 (2017). doi:10.1111/1365-2745.12908
5. Rogers-Bennett, L. & Catton, C. A. Marine heat wave and multiple stressors tip bull kelp forest to sea urchin barrens. *Sci. Rep.* **9**, 1–9 (2019).
6. Cavanaugh, K. C., Siegel, D. A., Reed, D. C. & Dennison, P. E. Environmental controls of giant-kelp biomass in the Santa Barbara Channel, California. *Mar. Ecol. Prog. Ser.* **429**, 1–17 (2011).
7. Bell, T. W., Allen, J. G., Cavanaugh, K. C. & Siegel, D. A. Three decades of variability in California’s giant kelp forests from the Landsat satellites. *Remote Sens. Environ.* **238**, (2020).
8. Bell, T. W., Cavanaugh, K. C., Reed, D. C. & Siegel, D. A. Geographical variability in the controls of giant kelp biomass dynamics. *J. Biogeogr.* **42**, 2010–2021 (2015).
9. Castorani, M. C. N. *et al.* Connectivity structures local population dynamics: A

- long-term empirical test in a large metapopulation system. *Ecology* **96**, 3141–3152 (2015).
10. Esgro, M. & Ray, J. *Interim Action Plan for Protecting and Restoring California's Kelp Forests*. (2021).
 11. Hohman, R., Hutto, S., Catton, C. A. & Koe, F. *Sonoma-Mendocino Bull Kelp Recovery Plan. Plan for the Greater Farallones National Marine Sanctuary and the California Department of Fish and Wildlife*. (2019).
 12. Young, M. A. *et al.* Environmental controls on spatial patterns in the long-term persistence of giant kelp in central California. *Ecology* **86**, 45–60 (2015).
 13. McPherson, M. L. *et al.* Large-scale shift in the structure of a kelp forest ecosystem co-occurs with an epizootic and marine heatwave. *Commun. Biol.* **4**, 1–9 (2021).
 14. Hamilton, S. L., Bell, T. W., Watson, J. R., Grorun-Colvert, K. A. & Menge, B. A. Remote sensing: generation of long-term kelp bed data sets for evaluation of impacts of climatic variation. *Ecology* **0**, 1–13 (2020).
 15. Cavanaugh, K. C. *et al.* Synchrony in dynamics of California giant kelp forests is driven by a combination of local recruitment and regional environmental controls. *Ecology* **94**, 1–33 (2013).
 16. Cavanaugh, K. C. *et al.* Spatial Variability in the Resistance and Resilience of Giant Kelp in Southern and Baja California to a Multiyear Heatwave. *Front. Mar. Sci.* **6**, 1–14 (2019).
 17. Friedlander, A. M. *et al.* Kelp forests at the end of the earth: 45 years later. *PLoS One* **15**, 1–23 (2020).
 18. Butler, C. L., Lucieer, V. L., Wotherspoon, S. J. & Johnson, C. R. Multi-decadal decline in cover of giant kelp *Macrocystis pyrifera* at the southern limit of its Australian range. *Mar. Ecol. Prog. Ser.* **653**, 1–18 (2020).

19. Finger, D. J. I., McPherson, M. L., Houskeeper, H. F. & Kudela, R. M. Mapping bull kelp canopy in northern California using Landsat to enable long-term monitoring. *Remote Sens. Environ.* **254**, 112243 (2021).

20. Mora-Soto, A. *et al.* A High-Resolution Global Map of Giant Kelp (*Macrocystis pyrifera*) Forests and Intertidal Green. *Remote Sens.* **12**, 1–20 (2020).